UNIVERSIDAD MICHOACANA DE SAN NICOLÁS DE HIDALGO

"SECURITY IMPROVEMENT OF POWER SYSTEMS BY USING TRAJECTORY SENSITIVITY APPROACHES"

by

ENRIQUE ARNOLDO ZAMORA CÁRDENAS

THESIS

REQUIREMENT FOR THE DEGREE OF

DOCTOR IN SCIENCES IN ELECTRICAL ENGINEERING

División de Estudios de Posgrado
Facultad de Ingeniería Eléctrica

ADVISOR:
CLAUDIO RUBÉN FUERTE ESQUIVEL, Ph.D.

MORELIA, MICHOACÁN NOVEMBER 2010

SECURITY IMPROVEMENT OF POWER SYSTEMS BY USING TRAJECTORY SENSITIVITY APPROACHES

by

ENRIQUE ARNOLDO ZAMORA CÁRDENAS

THESIS

Requirement for the degree of
DOCTOR IN SCIENCES IN ELECTRICAL ENGINEERING

Universidad Michoacana de San Nicolás de Hidalgo
División de Estudios de Posgrado
Facultad de Ingeniería Eléctrica

Advisor:
CLAUDIO RUBÉN FUERTE ESQUIVEL, Ph.D.

November 2010

Abstract

The security assessment of power systems represents one of the principal studies that must be carried out in energy control centers. The major computational burden on security assessment is spent in the security evaluation of the critical contingencies. In this research several approaches are proposed to improve the dynamic security of power systems. These approaches are based on quantifying the parameters influence on the angular stability of the power systems via the trajectory sensitivities obtained with respect to the system parameters.

In order to implement these approaches a digital program of transient stability was developed in language C++ by following an Object Oriented Programming philosophy (OOP). The power system is represented by means of Differential-Algebraic Equation (DAE) systems, and the angular stability model is based on the power balance formulation. The transient stability solution uses the Simultaneous Implicit method (SI) of integration, which consists of implicitly integrating the differential equations, so that the resulting algebraized set of equations is solved together with the existent algebraic set of equations under a unified frame of reference. Furthermore, sparsity and pre-ordering techniques were considered in order to achieve a very important reduction in the computational burden. The efficient assessment of the parameter influence is accomplished by implementing the Staggered Direct Method (SDM), which consists of the analytical computation of the linear Trajectory Sensitivities (TS) at each time step of integration. The solution then requires only one forward/backward substitution at each integration step. This method is straightforwardly extended in order to compute a sensitivity function matrix obtained with respect to multiple system parameters at the same simulation.

By using the developed program several approaches for improving the dynamic security of power systems have been proposed. Results of applications in small signal and transient stability have tested the successful performance of such proposed approaches. From a multi-contingency point of view, the best location for series compensation to increase the transient

stability limits was achieved by improving the critical clearing times of all possible faults in weak power systems areas. Also, in order to identify the best load shedding directions to improve the voltage profile due to loss of generation, a voltage sensitivity based approach has been proposed. Indices of voltage sensitivity quantification and load participation have been also proposed in order to obtain the best distribution of load shedding. On the other hand, a TS based approach was proposed to assess the Small Signal Stability (SSS) by using time domain simulation. Indices of loads influence on the stability of an Equilibrium Point (EP) are computed and used to identify and modulate the most sensitive loads in order to improve and even stabilize the EPs of power systems.

Acnowledgements

I would like to express my deepest gratitude to my advisor, Dr. Claudio Fuerte, whose invaluable assistance, support and guidance have considerably improved my graduate experience. Thanks for the confidence and opportunity to be one of your doctoral students, as well as his unconditional friendship.

My acknowledgement is also due to the members of the supervisory committee, for the support they provided to improve the level of this thesis report. Their valuable suggestions were very helpful to finish this thesis.

I must also acknowledge to professors Peter Sauer and Anantha Pai for their technical assistance and great hospitality during my stay at Urbana-Champaign. I must to give a very special acknowledgement to Prof. Pai for accepting me as a visiting student in ECE department in the University of Illinois. I wish to express my gratitude for sharing his time, knowledge and experience with me.

A great acknowledgement for the Consejo Nacional de Ciencia y Tecnología and the Universidad Michoacana de San Nicolás de Hidalgo for providing the financial and academic means to develop this thesis.

There are not words to express my appreciation to my wife Iliana. Her dedication, love and confidence in me, has taken the load off my shoulder. I owe her for being unselfishly and to share my passions and ambitions.

My parents deserve special mention for their constant support and guidance to reach my goals. Thank you father for teach me how a man must to support and care his family. Mother I appreciate your countless prayers for me and my family. I am proud to be your son. God bless you.

I must thank to my in-laws the support and assistance to my wife and my son during my multiple absences due to my doctoral studies. Thank you so much for accepting me as a member of your family.

Finally, I would like to thank everybody who was important to the successful realization of this thesis, as well as expressing my apology that I could not mention personally one by one.

Contents

List of Tables

List of Figures

List of Publications

The publications derived from this research work are

Journal

- A. Zamora-Cárdenas and C. R. Fuerte-Esquivel, “Multi-parameter trajectory sensitivity approach for location of series-connected controllers to enhance power system transient stability,” *Electric Power System Research*, 80, Sept. 2010, pp. 1096-1103.

Conference

- E. A. Zamora-Cárdenas and C. R. Fuerte-Esquivel, “Location of Series-Connected Controllers to Reduce Proximity to Transient Instability based on a Trajectory Sensitivities Approach,” 2010 *IEEE Power Engineering Society General Meeting*, Mineapolis, Minesota, USA.

- E. A. Zamora-Cárdenas, C. R. Fuerte-Esquivel and L. Contreras Aguilar, “Application of Dynamic Sensitivity Theory to Assess the Thyristor-Based FACTS Controllers´ Effect on the Transient Stability of Power Systems,” 2009 *IEEE Power Tech Conference*, Bucharest, Romania, June 28 - July 2.

Nomenclature

$\bar{Y}_{bus}^{0}$: Pre-fault Nodal Admittance matrix

$\bar{Y}_{bus}^{f}$: Fault Nodal Admittance matrix

$\bar{Y}_{fault}$: Fault Admittance

$\bar{Y}_{bus}^{pf}$: Post-fault Nodal Admittance matrix

$\boldsymbol{A}_{sys}$: System Coefficient Matrix

B_{SVC}: SVC Susceptance

n_b: Number of buses

n_g: Number of generators

n_{PQ}: Number of Network Nodes

$SN_i(t)$: Sensitivity Norm

SV_i: Voltage Profile Index

t_{cct}: Fault Critical Clearing Time

t_{cl}: Fault Clearing Time

J: Jacobian Matrix

Np: Number of sensitivity parameters

DAD: Differential Algebraic Discrete

DAE: Differential Algebraic Equations system

EP: Equilibrium Point

FACTS: Flexible Altern Current Transmission Systems

GS: Gauss-Seidel method

HB: Hopf Bifurcation

NR: Newton-Raphson method

ODE: Ordinary Differential Equation

OOP: Object-Oriented Programming

PE: Partitioned Explicit method

PFA: Participation Factors Analysis

SDM: Staggered Direct Method

SI: Simultaneous Implicit method

SIB: Singularity Induced Bifurcation

SMA: Selective Modal Analysis

SMIB: Single-Machine Infinite-Bus system

SNB: Saddle Node Bifurcation

SSS: Small Signal Stability

STATCOM: Static Synchronous Compensator

SVC: Static Var Compensator

TCSC: Thyristor-Controlled Series Compensator

TEF: Transient Energy Function

TS: Trajectory Sensitivities

U.E.P.: Unstable Equilibrium Point

Chapter 1

INTRODUCTION

1.1 Motivation and justification

The operation of modern power systems under stressed conditions has become a more complex task for engineers and operators of energy centers. The complexity has risen because of the increased system size, greater dependence on control devices, more interconnections, heavier transmission loadings, and the concentration of the generation among a few large units at light load. In this sense, the security assessment of power systems is one of the most important analyses that has to be realized in the energy centers. The security assessment of power systems is concerned with the analysis of the system electromechanical dynamics subjected to a disturbance. Disturbances in power systems are classified as small and large according to the required modeling and solution methods. Thus, the security assessment of a power system is conventionally analyzed in separate static and dynamic responses [Vittal, 00]. Although "small disturbances" produce changes in system performance, they are generally analyzed as small signal security [Kundur, 94] [Sauer and Pai, 98]. Then, system security is generally associated with large disturbances, which are called contingencies. Static security defines the adequacy of the system's generation and transmission capacity to meet demand on contingency. Over the years, much research has been reported on the topic of including static security in optimal power flows programs [Huneault and Galiana, 91]. In contrast, the dynamic security term is used to mean " the ability of the bulk power electric system to withstand sudden disturbances such as electric short circuits or unanticipated loss of system components". This means that following the ocurrence of a sudden disturbance, the power system will survive the ensuing transient and move into an acceptable steady state condition, and in this new steady state condition all power system components are operating within established limits.

Besides the already complex operation, deregulation has led existing transmission systems to operate too closely to security limits due to multilateral transactions and inadequate capacity. Despite this, the power systems must be operated and transient stability constraints satisfied for a set of likely critical contingencies. In this context, dynamic security assessment plays a very important role. Conventionally, dynamic security assessment comprises the following main stages [Nguyen, 02-1]: contingency selection-screening, security evaluation, contingency ranking and limit computation. According to the operators experience a list of possible contingencies at specific operating conditions is defined. The contingency screening stage consist of identifying the critical and noncritical contingencies, which are separated in order to assess the effects of the critical ones on the transient stability, whereas the non-critical ones can be discarded for saving computational burden. The security evaluation of each critical contingency consists of performing a time domain simulation in order to assess its effect on transient stability. After this, the critical contingencies are ranked in order of severity to investigate preventive actions to improve the system security. Finally, the stability limits are computed and used in monitoring the system security or as security constraints in economic dispatch studies.

The maximum computational burden in any dynamic security assessment approach is spent at the stage of the security evaluation. There are several methods that can be employed to measure the system stability, of which the most promising are the direct methods based on Transient Energy Function (TEF) [Pai, 89] [Fouad and Vittal, 92] [Padiyar and Ghosh, 89] [Chiang et al., 95], and the time domain simulation [Anderson and Fouad, 94] [Kundur, 94] [Sauer and Pai, 98]. The TEF-based techniques provide a quantitative index of the stability margin from the energy point of view; however, it presents fundamental drawbacks such as model limitation and the need to compute the Unstable Equilibrium Point (UEP), which is quite complicated. The energy functions' determination in analytical form is restricted only for the classical generator model. Furthermore, as the system dimension increases and the modeling detail is more complex, the energy functions are more difficult to obtain. Energy functions of power systems including FACTS controllers are not factible. In this context, the time domain simulation method is a better tool in terms of accuracy, reliability and modeling capability. However, this method has two main disadvantages. The first one is its stressful computation requirement, and the other is its incapability to provide any quantitative stability margin assessment.

In this thesis we propose approaches based on TS in order to improve the power system security, specifically to assess the transient and small signal stability. Such approaches utilize analytical TS, which enable us to compute trajectory sensitivities with respect to (w.r.t) multiple power system parameters at the same time leading to a great saving of computational burden. The method is completely general and does not present any restriction regarding the complexity of system and components modeling, nor the system size. Besides the stability information, the effects of the power system parameters can be studied. Such information provides easy and direct preventive control strategies to improve the system security.

1.2 State of art of the Trajectory Sensitivity applications

Unsuccessful efforts made to extend the application of TEF theory to large scale and detailed modeling of power systems have encouraged the researchers to explore new methodologies applied on transient stability in order to improve the power system security. The TS theory has shown itself to be a powerful method in improving the dynamic security by overcoming the fundamental drawbacks of the TEF method. In [Laufenberg and Pai, 98], the TS application to power systems was proposed as a new approach to dynamic security analysis. In such a paper, the TS were obtained w.r.t. to both generator parameters and initial condition of the power system. In this way, the critical machines for different fault clearing times were identified. The power system was mathematically represented by means of an Ordinary Differential Equation (ODE) system, and the effectiveness of the TS application was tested in a Single-Machine Infinite-Bus (SMIB) system, a 17-machine, an a 162-bus system. In [Laufenberg and Pai, 98], the authors applied the TS theory to DAE systems by mean of a SMIB system, and the TS were used as a measure of system security instead of computing the sensitivity energy margins.

TS analysis was applied to investigate a real mayor disturbance of the Nordel power system which ocurred on January 1, 1997 [Hiskens and Akke, 99]. In this study, the numerical TS provided a measure of the influence of component operation outputs on the system behavior subjected to a large disturbance. The TS theory for continuous and discontinuous behavior was used. The TS identified the effect of the critical line impedances in the largest angular deviation experienced during the disturbance. Besides, sensitivities w.r.t. to the timing of switching events were computed, which allowed to quantify the effect of the tripping of a nuclear unit as more critical than the shunt reactor connection on the disturbance.

In [Hiskens and Pai, 00], the TS theory application was proposed for hybrid systems, which utilize a Differential-Algebraic-Discrete (DAD) structure. Such a system model allows to investigate the sensitivity behavior at discrete events.

In [Hiskens and Pai, 00-2], a review of sensitivity applications were presented in topics like parametric influences on system dynamics like line impedances and switching events. It also addresses the problem of identifying the most sensitive parameters to uncertainty in large scale power systems, which avoids extremely the time consuming in computational burden, optimal control and transient stability assessment by using an index of proximity to instability based on trajectory sensitivities.

In [Nguyen et al., 02], the authors proposed the estimation of critical values of interest parameters such as the fault clearing time and mechanical input power. Such a proposal was conducted via the computation of a TS norm, which provides a global quantification of the transient stability. The proposed technique required a-priory information about the range of the critical parameters, which is generally available to the operators. Considering the linear behavior of the sensitivity norm, the estimation was achieved by the extrapolation of the inverse of the sensitivity norm close to the critical values of the sensitivity parameters.

Taking advantage of the fact that modeling is not a restriction, in [Nguyen and Pai, 03] a TS-based method was provided to reschedule power generation to ensure the system stability, while satisfies its dynamic stability constraints for a set of credible contingencies as well as its economic goal. Due to the application of the TS theory to power system analysis is general, the system modeling issue is not a limiting in the proposed method, and hence, the technique was used as a preventive control scheme.

In [Shubhanga and Kulkarni, 04], TS with respect to the clearing times were applied to determine the effectiveness of changes in parameter values. The approach consists of judging the controllability of the trajectory deviations from the nominal from certain variables. This proposed approach overcomes the need of carrying out many simulations to evaluate sensitivities w.r.t. different parameters. This approach was proposed for preventive generation rescheduling and shunt/series compensation in improving the transient stability.

In [Hiskens and Alseddiqui, 06], TS were used to generate accurate first-order approximations of trajectories required in a computational feasible approach, which was proposed to assess the influence of uncertainty in simulations of power system dynamic behavior.

In [Chatterjee and Ghosh, 07-1], the TS were used to assess the effect of the placement of a Thyristor-Controlled Series Compensator (TCSC) on the transient stability of power systems. The TCSC was modeled as a variable capacitor according to changes of the thyristor firing angle.The sensitivities were computed numerically w.r.t. different values of the firing angle of thyristors, which helps to investigate the best TCSC placement for each fault scenary and allows the assessment of different levels of compensation in the transient stability. Also, the TS allowed to determine the locations where the TCSC deteriorate the stability for a particular disturbance. An extension of this research work was realized in [Chatterjee and Ghosh, 07], for the transient stability assessment of power systems containing shunt and series compensators. The TS determined the best possible locations of a Static Synchronous Compensator (STATCOM) and a TCSC in order to improve the transient stability for particular faults and topologies. For the assessment of each sensitivity parameter two numerical simulations were computed.

In [Chatterjee and Ghosh, 07-2], the authors showed that the TS analysis is an useful tool on assessing the effectiveness of the TCSC, via the choice of the controller parameters. Hence, the selection of the best gains values provided the design of the controller. Such a selection was carried out by using the inverse of the norm of the trajectory sensitivities with respect to different values of the controller gains.

In [Chatterjee et al., 08], the authors used a TS approach in order to assess the impact and location of distributed generation on the transient stability of power systems. The TS and the inverse of the sensitivity norm were used to show the dependence of the system stability on the location of distributed generators. The proposed method was used to choose the location of the distributed generation within a small group of buses located close to each other. Besides, the authors showed the potential of the proposed method to be used in improving the voltage stability and post-fault voltage profile at load buses. The proposal was tested in a SMIB and multi-machine systems.

In [Nguyen and Pai, 08], it is investigated the impact of distributed generation on system stability using the trajectory sensitivity approach, besides the machines that are vulnerable to the addition of distributed generation are identified. The authors also varied the penetration level of distributed generation and evaluated the influence of the modeling. Sensitivity formulation for the differential-algebraic equation model is presented through a SMIB example.

The review of the state of the art abovementioned has been focused on the improvement of the security of electric power systems, by means of the application of the dynamic TS theory.

However, additional references are given in the thesis at the beginning of their corresponding chapter.

1.3 Objectives

The general goal of this research consists on the development and proposal of new approaches based on TS, in order to improve the small signal and the transient stability in power systems. The successful performance of the proposed approaches depends on the implementation on an efficient TS methodology.

The first stage of this general goal consisted on developing an efficient transient stability program based on power balance formulation. The program was built up in language C++ following an OOP philosophy and considering sparsity and pre-ordering techniques.

The second stage consisted of implementing the efficient TS methodology in the transient stability program. The efficiency of the TS method depends on the computational burden saving provided by its analytical computation, which permitted the computation of sensitivities w.r.t. multiple parameters at the same time.

Finally, in the last stage several approaches were set forth and tested in order to improve the power system stability in the transient as well as the small disturbance.

1.4 Methodology

The employed methodology to reach the objectives of this research is described as follows,

1. Review of the transient stability theory on power systems.
2. Review of the state of the art of trajectory sensitivity applications.
3. Development of a transient stability digital program based on the power balance formulation, considering computational efficiency techniques.
4. Implementation of the trajectory sensitivity theory in the digital code via the programming of Staggered Direct Method (SDM).
5. Development of approaches to improve the angular stability.
6. Development of experiments in order to test the proposed approaches.

1.5 Thesis outline

The rest of this thesis is organized into six chapters. A brief overview of each one of these chapters is given below:

Chapter 2 presents the mathematical models of the power system components considered in the developed digital program. The features and solution description of the two existent methodologies for assessing the angular stability of power systems (transient and small signal stability) are given. Also, it provides the methodology employed in calculating the discontinuity conditions used in the fault application and clearance for DAE systems.

Chapter 3 provides the mathematical formulation and application of the TS theory to assess the angular stability of power systems represented via DAE systems. In addition, the features of the analytical sensitivity solution are given, as well as the advantages over the numerical solution are outlined.

Chapter 4 addresses the application of the OOP philosophy used in this thesis, in order to design and to implement the power system model and its components to build up the transient stability program from the programming point of view.

Chapter 5 gives the applications of the TS analysis in order to improve the transient stability of the power systems. An approach is proposed to find the most effective location of series compensation in order to increase the critical clearing times. On the other hand, the shunt and series FACTS controllers' performance and the influence of the controllers parameters were assessed. Lastly, in this chapter an approach to identify and modulate the most influential loads in order to improve the voltage profile of the power system is proposed. Results of numerical examples are reported in tables and figures in order to show the effectiveness of performance of the proposed approaches.

Chapter 6 presents a proposed approach for examining and improving the Small Signal Stability (SSS) of the EPs. The features and results are shown by means of studies realized in the 9-buses and 3-generators system as well as in a reduced equivalent of the Mexican energy system consisting of 190-buses and 46-generators.

Chapter 7 finally draws the overall conclusions of this research and gives suggestions for future research work.

Chapter 2

MODELING AND ANALYSIS OF ANGULAR STABILITY

2.1 Introduction

The stability problem is one of the most important issues in the control and operation of power systems [IEEE, 04] [Kundur, 94]. In order to simplify its study, it has been useful in classifying the kind of stability phenomena according to the dynamic response of power systems and different security aspects that must be monitored by power system operators [Acha et al., 02]. In general, the stability concept is associated with the ability of power systems to maintain the voltage profile, frequency and rotor angles into their respective operative limits. According to the nature of the disturbances, the relative response of the power system components will be completely different, which requires modeling these components according to the time response. Then, the stability assessment of the mentioned security aspects requires modeling the power systems according to the system response. Thus, different solution methods will be required in order to analyze the different forms of power system stability [IEEE, 04].

The rotor angle stability can be studied when the system is subjected to either a large or a small disturbance. The rotor angle stability can be defined as ”the ability of interconnected synchronous machines of a power system to remain in synchronism”, [Kundur, 94] [IEEE, 04]. When a large disturbance is applied, nonlinear dynamical analysis must be performed in the time domain in order to assess the angular stability of the power system. This form of stability is called the transient stability, and its assessment consists of observing the rotor angle excursions during the first oscillation [Sauer and Pai, 98] [Kundur, 94] [Stagg and El-Abiad, 68]. If during the transient period all generators maintain synchronism, the power system is said to be transiently stable. However, the system will be unstable if at least one generator loses synchronism with respect to the rest. On the other hand, when a power system is subjected to small disturbances, the system equations can be linearized in order to assess the EP stability by using the linear system theory and the Lyapunov criterion [Lyapunov, 67].

Realistic models of large scale power systems generally are represented by DAE systems. The set of differential equations represents the dynamics of the equipment as generators and controls. The algebraic equations represent the power transfer relationships between the buses of the transmission network. In a DAE model the dynamic variables are called state variables and are time dependent. They change with respect to time according to the dynamic response of their components (time constants). The algebraic variables are called the algebraic states and are assumed to be changing instantaneously with respect to the dynamic states variables. In this thesis, the same DAE model is used to mathematically represent the power systems in large (transient stability) and small (EP stability) disturbances. Both stability studies use the power flow formulation [Sauer and Pai, 98] [Stagg and El-Abiad, 68]. However, according to the severity of the disturbance, the stability analysis of rotor angle requires a different form of solution consisting of different treatments of the DAEs. In the case of the SSS, the DAE model is linearized and reduced to the generation nodes in order to obtain an equivalent system of differential equations to analyze the equilibrium of the corresponding operating point. In the case of transient stability, the DAE system must be solved for nonlinear oscillations in the time domain. In this thesis the SI method [Sauer and Pai, 98], has been employed in order to implicitly integrate the differential equations, which solves both sets of equations under a unified frame of reference. More details for this numerical method are given in Section 2.10.1.

2.2 General Representation of Electric Power Systems

Since the components are modeled by means of DAEs, an electric power system can be analytically represented by a set of parameter-dependent differential equations constrained by a set of algebraic equations, as given by (2.1), where x is a vector of the dynamic state variables, y is a vector of the algebraic variables, and β is a set of non-time varying system parameters.

$$
\begin{array}{lll}
\dot{x} = f(x,y,\beta) & & f : \Re^{n+m+p} \rightarrow \Re^{n} \\
0 = g(x,y,\beta) & & g : \Re^{n+m+p} \rightarrow \Re^{m} \\
x \in \boldsymbol{X} \subset \Re^{n} & y \in \boldsymbol{Y} \subset \Re^{m} & \beta \in \boldsymbol{\beta} \subset \Re^{p}
\end{array}
\tag{2.1}
$$

Due to the fact that the transmission network dynamics are much faster than dynamics of the equipment, it is considered that the variables y instantaneously change with variations of the x states. Hence, only the dynamics of the equipment, e.g. generators and controls, are explicitly modeled by the set of differential equations in (2.1). The set of algebraic equations express the mismatch power flow equations at each system's bus. If the generator model considers the stator effect, a pair of stator equations at each generator must be included in the set of algebraic equations.

2.3 Two-Axis Generator Model

In the Two-Axis generator model of a salient-pole machine, the rotor is represented via a direct and a quadrature magnetic axis. This model considers a field and a damper winding on the $d-$axis as well as a damper winding on the $q-$axis. Thus, the rotor is said to be in $dq0$ coordinates. On the other hand, the stator is composed of three-phase windings and represented by three-phase voltages and currents. Thus, the stator is in *abc* coordinates. The stator equations contain time varying inductances, which increase the complexity in solving the machine equations. In order to overcome this problem the stator variables are appropriately transformed into new variables in $dq0$ coordinates. The transformed stator equations contain non-time varying inductances. In this thesis, the utilized Two-Axis generator model considers four dynamic equations to represent the generator performance by means of two internal voltage equations on the axes $d-q$ and two swing equations for the rotor angle and speed. Another dynamic equation is added to represent the effect of the controlled field voltage by considering a simple fast excitation loop. Lastly, the stator voltages on the axes $d-q$ are represented via two algebraic equations. The Two-Axis model used in this thesis is a reduction from a complete model based on a linear magnetic circuit [Sauer and Pai, 98]. See Appendix A.1.

Rotor equations

The equations of the two electrical systems of the rotor are

$$\dot{E}'_{qi} = \frac{1}{T'_{doi}} \left(-E'_{qi} - (X_{di} - X'_{di}) I_{di} + E_{fdi} \right) \tag{2.2}$$

$$\dot{E}'_{di} = \frac{1}{T'_{qoi}} \left(-E'_{di} - (X_{qi} - X'_{qi}) I_{qi} \right) \tag{2.3}$$

where E'_{di} and E'_{qi} are the transient internal voltage magnitudes on d and q axis, respectively, I_{di} and I_{qi} are the stator currents on d and q axes, X_{ki} and X'_{ki} are the synchronous steady state and transient state reactances on axes $k = q$ and $k = d$, respectively, T'_{doi} and T'_{qoi} are the constant time on d and q axes, respectively; lastly, E_{fdi} is the constant DC-controlled voltage field.

The rotor mechanical model is given by swing equations. For the *ith* generator, these equations are [Sauer and Pai, 98]

$$\dot{\delta}_i = \omega_i - \omega_0 \tag{2.4}$$

$$\dot{\omega}_i = \frac{\omega_0}{2H_i} \left(P_{Mi} - P_{ei} - D_i(\omega_i - \omega_0) \right) \tag{2.5}$$

$$P_{ei} = E'_{qi} I_{qi} + E'_{di} I_{di} + (X'_{qi} - X'_{di}) I_{di} I_{qi} \tag{2.6}$$

where $2H_i$ is the moment of inertia in seconds (sec), D_i is the damping constant, P_{ei} is the generator's electrical power associated with the internal voltage source, P_{Mi} is the turbine mechanical power injection, δ_i is the generator's rotor angle in electrical radians (rad), ω_0 is the synchronous speed in electrical rad/sec, and ω_i is the actual rotor speed in electrical rad/sec.

Excitation system

The excitation system is considered as shown in Figure 2.1, with its equation given by (2.7)

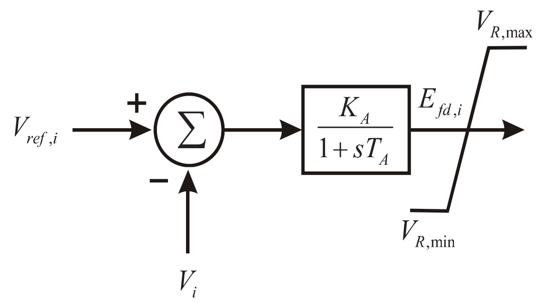

Figure 2.1: Fast exciter (one-gain time constant).

$$\dot{E}_{fdi} = \frac{1}{T_{Ai}} \left(K_{Ai}(V_{ref,i} - V_i) - E_{fdi} \right) \tag{2.7}$$

where E_{fdi} is the DC-controlled field voltage, $V_{ref,i}$ is the reference node voltage, V_i refers to the voltage at the generator terminal, K_{Ai} is the control gain, and T_{Ai} is the excitation system time constant.

Stator equations

Physically the stator represents the coupling point between the generator and the electrical network. The stator algebraic variables are the currents on the $d-q$ axes. Thus, the stator voltage and power expressions depend on generator dynamic variables as well as the stator and network algebraic variables. Applying the Kirchhoff's Voltage Law to the dynamic circuit of the synchronous machine Two-Axis model shown in Figure 2.2 results in the complex equation (2.8), whereas, Eq. (2.9) is the complex power injected at generator terminals. See Appendix A.2.

$$\left[E'_{di} + (X'_{qi} - X'_{di})I_{qi} + jE'_{qi} \right] e^{j(\delta_i - \pi/2)} = (R_{si} + jX'_{di})(I_{di} + jI_{qi})e^{j(\delta_i - \pi/2)} + V_i e^{j\theta_i} \tag{2.8}$$

$$P_{Gi} + jQ_{Gi} = V_i e^{j\theta_i}(I_{di} - jI_{qi})e^{-j(\delta_i - \pi/2)} \tag{2.9}$$

where V_i and θ_i are the voltage magnitude and phase angle at generator terminals on the network side. $(V_{di} + jV_{qi})e^{j(\delta_i - \pi/2)}$ and $(I_{di} + jI_{qi})e^{j(\delta_i - \pi/2)}$ represent the per-unit RMS pha-

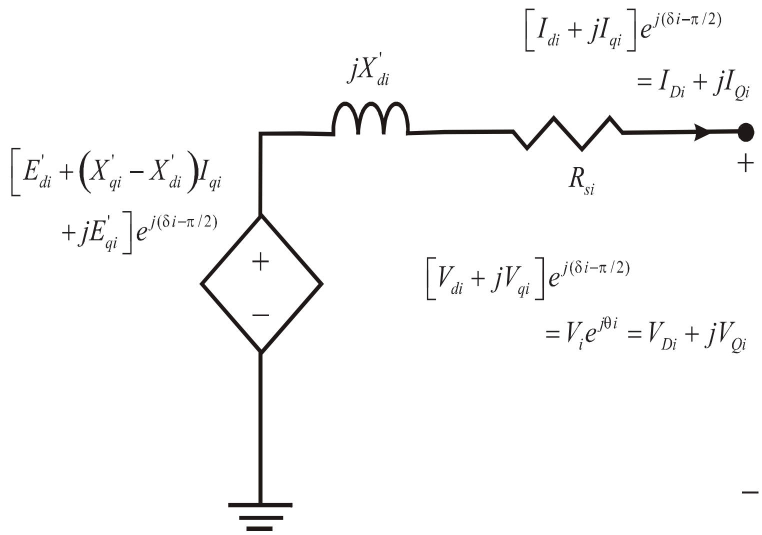

Figure 2.2: Dynamic circuit of the Two-Axis generator model.

sors of voltage and current at generator terminals transformed to coordinates $dq0$. For more details see Appendix A.2.

Separating (2.8) and (2.9) into real equations we obtain the stator voltages (2.10)-(2.11) and power expressions (2.12)-(2.13) for computational purposes [Sauer and Pai, 98]; see Appendix A.2. In this case the armature resistance is neglected.

$$V_{di}^{St} = E_{di}^{'} - V_i sin(\delta_i - \theta_i) + X_{qi}^{'} I_{qi} = 0 \tag{2.10}$$

$$V_{qi}^{St} = E_{qi}^{'} - V_i cos(\delta_i - \theta_i) - X_{di}^{'} I_{di} = 0 \tag{2.11}$$

$$P_{G_i} = I_{di} V_i sin(\delta_i - \theta_i) + I_{qi} V_i cos(\delta_i - \theta_i) \tag{2.12}$$

$$Q_{G_i} = I_{di} V_i cos(\delta_i - \theta_i) - I_{qi} V_i sin(\delta_i - \theta_i) \tag{2.13}$$

2.4 Generator Classical Model

The generator classical model consists of a constant voltage in the generator internal nodes behind the transient reactance as shown in Figure 2.3.

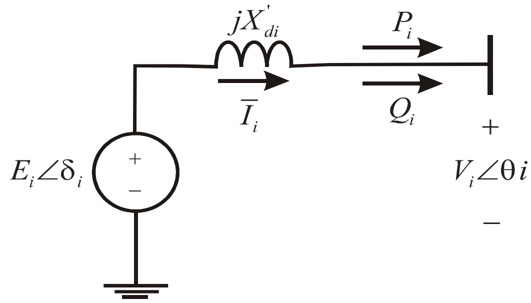

Figure 2.3: Constant voltage behind the transient reactance.

The complex power output at the *ith* internal node is as follows [Sauer and Pai, 98]:

$$\overline{E}_i\overline{I}_i^* = E_i e^{j\delta_i}\left((\overline{E}_i - \overline{V}_i)/jX'_{di}\right)^* \tag{2.14}$$

Developing and separating (2.14) in real and imaginary parts the active and reactive expressions for the electric power injections at generator terminals are shown in (2.15) and (2.16)

$$P_{G_i} = \frac{E_i V_i sin(\delta_i - \theta_i)}{X'_{di}} \tag{2.15}$$

$$Q_{G_i} = \frac{E_i^2}{X'_{di}} - \frac{E_i V_i cos(\delta_i - \theta_i)}{X'_{di}} \tag{2.16}$$

The swing equations for the rotor mechanical model preserving the structure of network are as follows [Sauer and Pai, 98]:

$$\dot{\delta}_i = \omega_i - \omega_0 \tag{2.17}$$

$$\dot{\omega}_i = \frac{\omega_0}{2H_i}\left(P_{Mi} - P_{G_i} - D_i(\omega_i - \omega_0)\right) \tag{2.18}$$

This reduced generator model does not consider the stator; therefore, the generator and network are directly coupled, and the expressions of power injections at generator terminals are the same as the electric power generated at the internal node of generator P_{G_i}.

2.5 Load Models

The load powers generally change with respect to voltage magnitude and frequency. The effect of voltage phase angle on reactive load power disappears after one second of transient behavior [IEEE, 73] [Shackshaft et al., 77], whereas this effect is null on the active load power. There are three highly used static nonlinear load models on the analysis of power systems operation. The general expressions of active and reactive load variation with voltage magnitude may be approximated by [Anderson and Fouad, 94]

$$P_{Li} = P_{Li}^{0}\left(\frac{V_i}{V_i^0}\right)^{\alpha} \tag{2.19}$$

$$Q_{Li} = Q_{Li}^{0}\left(\frac{V_i}{V_i^0}\right)^{\alpha} \tag{2.20}$$

where $\alpha = 0$ represents the constant power load model used for small voltage deviations, $\alpha = 1$ represents the constant current load model, and $\alpha = 2$ models the loads exhibiting constant impedance behavior. P_{Li}^0 and Q_{Li}^0 are the nominal demand of energy in the system loads, and V_i^0 is the nominal voltage magnitude measured at the pre-disturbance condition (t_0). This thesis did not consider the frequency dependency of loads.

2.6 Network Model

The structure preserving model of the electric network considers a power flow balance formulation. This model consists of those equations expressing the active and reactive power balances at every system node.

Transformer

The two-winding transformer was modeled with complex taps on both primary and secondary windings. The magnetizing branch non-linearity under saturated conditions is also considered in the model to account for the core losses. The polynomial equation (2.21) was found to approximate well the non-linearity characteristic [Fuerte and Acha, 97]. However, for purpose of this thesis the transformer's non-linearity is neglected.

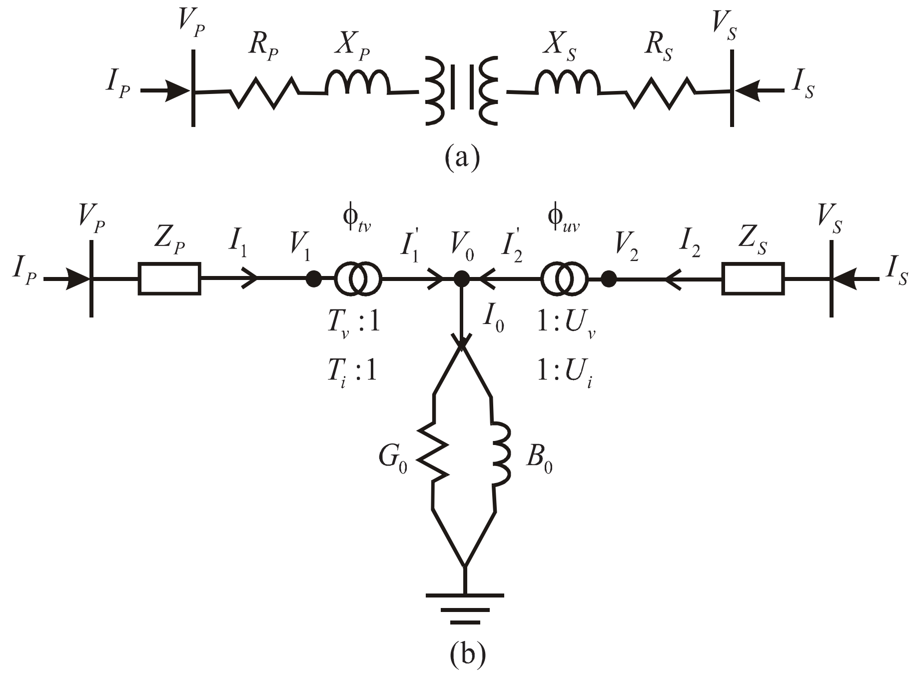

Figure 2.4: Two-winding transformer: (a) Schematic representation. (b) Equivalent circuit.

$$I = 0.0034V + 0.00254V^{19} \tag{2.21}$$

The model is physically represented in Figure 2.4(a) while the schematic equivalent circuit is shown in Figure 2.4(b).

The primary winding is represented as an ideal transformer having complex tap ratios $T_v : 1$ and $T_i : 1$ in series with the impedance Z_p, where $T_v = T_i^* = T_v\angle\phi_{tv}$. The * denotes the conjugate operation. Also, the secondary winding is represented as an ideal transformer having complex tap ratios $U_v : 1$ and $U_i : 1$ in series with the impedance Z_s, where $U_v = U_i^* = U_v\angle\phi_{uv}$.

The transfer admittance matrix relating the primary voltage V_p and current I_p to the secondary voltage V_s and current I_s in the two-winding transformer can be determined by considering the current I_1 across the impedance Z_p and the current I_2 across the impedance Z_s as is shown in (2.22) and (2.23), respectively.

$$I_1 = \frac{(V_p - V_1)}{Z_p} = \frac{(V_p - T_v V_0)}{Z_p} = I_p \tag{2.22}$$

$$I_2 = \frac{(V_s - V_2)}{Z_s} = \frac{(V_s - U_v V_0)}{Z_s} = I_s \tag{2.23}$$

The current I_0 across the iron core as a function of currents I_1' and I_2' is

$$0 = I_1' + I_2' - I_0 = T_i I_1 + U_i I_2 - I_0 \tag{2.24}$$

or

$$0 = -\frac{T_v^* V_p}{Z_p} + \left(\frac{T_v^2}{Z_p} + \frac{U_v^2}{Z_s} + Y_0\right) V_0 - \frac{U_v^* V_s}{Z_s} \tag{2.25}$$

where

$$Y_0 = G_0 + jB_0 \tag{2.26}$$

Arranging (2.22), (2.23) and (2.25) in matrix form,

$$\begin{bmatrix} I_p \\ 0 \\ I_s \end{bmatrix} = \begin{bmatrix} \frac{1}{Z_p} & -\frac{T_v}{Z_p} & 0 \\ -\frac{T_v^*}{Z_p} & \frac{T_v^2}{Z_p} + \frac{U_v^2}{Z_s} + Y_0 & -\frac{U_v^*}{Z_s} \\ 0 & -\frac{U_v}{Z_s} & \frac{1}{Z_s} \end{bmatrix} \begin{bmatrix} V_p \\ V_0 \\ V_s \end{bmatrix} \tag{2.27}$$

Equation (2.27) represents the transformer shown in Figure 2.4. It is possible, however, to find a reduced equivalent matrix that still correctly models the transformer whilst retaining only the external nodes, and this is done by means of a Gaussian elimination,

$$\begin{bmatrix} I_P \\ I_S \end{bmatrix} = \frac{1}{T_v^2 Z_S + U_v^2 Z_P + Z_P Z_S Y_0} \begin{bmatrix} U_v^2 + Z_S Y_0 & -T_v Z_v^* \\ -T_v^* U_v & T_v^2 + Z_P Y_0 \end{bmatrix} \begin{bmatrix} V_P \\ V_S \end{bmatrix} \tag{2.28}$$

Equation (2.28) can be expressed as

$$\begin{bmatrix} I_P \\ I_S \end{bmatrix} = \left[\begin{pmatrix} G_{PP} & G_{PS} \\ G_{SP} & G_{SS} \end{pmatrix} + j \begin{pmatrix} B_{PP} & B_{PS} \\ B_{SP} & B_{SS} \end{pmatrix} \right] \begin{bmatrix} V_P \\ V_S \end{bmatrix} \tag{2.29}$$

The power injection equations of a two-winding transformer are

$$P_P = V_P^2 G_{PP} + V_P V_S \left(G_{PS} cos(\theta_P - \theta_S) + B_{PS} sin(\theta_P - \theta_S)\right) \tag{2.30}$$

$$Q_P = -V_P^2 B_{PP} + V_P V_S \left(G_{PS} sin(\theta_P - \theta_S) - B_{PS} sin(\theta_P - \theta_S)\right) \tag{2.31}$$

$$P_S = V_S^2 G_{SS} + V_S V_P \left(G_{SP} cos(\theta_S - \theta_P) + B_{SP} sin(\theta_S - \theta_P)\right) \tag{2.32}$$

$$Q_S = -V_S^2 B_{SS} + V_S V_P \left(G_{SP} sin(\theta_S - \theta_P) - B_{SP} sin(\theta_S - \theta_P)\right) \tag{2.33}$$

where

$$G_{PP} = \frac{F1(U_v^2 + R1) + F2R2}{A2} \tag{2.34}$$

$$B_{PP} = \frac{F1R2 - F2(U_v^2 + R1)}{A2} \tag{2.35}$$

$$G_{SS} = \frac{F1(T_v^2 + R3) + F2R4}{A2} \tag{2.36}$$

$$B_{SS} = \frac{F1R4 - F2(T_v^2 + R3)}{A2} \tag{2.37}$$

$$G_{PS} = \frac{-T_v U_v (F1cos(\phi 1) + F2sin(\phi 1))}{A2} \tag{2.38}$$

$$B_{PS} = \frac{T_v U_v (F2cos(\phi 1) - F1sin(\phi 1))}{A2} \tag{2.39}$$

$$G_{SP} = \frac{-T_v U_v (F1cos(\phi 2) + F2sin(\phi 2))}{A2} \tag{2.40}$$

$$B_{SP} = \frac{T_v U_v (F2cos(\phi 2) - F1sin(\phi 2))}{A2} \tag{2.41}$$

$$F1 = T_v^2 R_s + U_v^2 R_p + R_{eq1} \tag{2.42}$$

$$F2 = T_v^2 X_s + U_v^2 X_p + X_{eq1} \tag{2.43}$$

$$A2 = F1^2 + F2^2 \tag{2.44}$$

$$R_{eq1} = (R_p R_s - X_p X_s)\, G_0 - (R_p X_s + R_s X_p)\, B_0 \tag{2.45}$$

$$X_{eq1} = (R_p R_s - X_p X_s)\, B_0 + (R_p X_s + R_s X_p)\, G_0 \tag{2.46}$$

$$R1 = R_s G_0 - X_s B_0 \tag{2.47}$$

$$R2 = R_s B_0 + X_s G_0 \tag{2.48}$$

$$R3 = R_p G_0 - X_p B_0 \tag{2.49}$$

$$R4 = R_p B_0 + X_p G_0 \tag{2.50}$$

$$\phi 1 = \phi_{tv} - \phi_{uv} \tag{2.51}$$

$$\phi 2 = \phi_{uv} - \phi_{tv} \tag{2.52}$$

Line

The transmission lines are represented by the π model which considers concentrated parameters as shown in Figure 2.5, where $\overline{y}_{ij}$ and $\overline{y}_{ij}^{sh} = \overline{y}_{ji}^{sh}$ are the series and shunt primitive line admittances, respectively. The losses of the transmission line are considered.

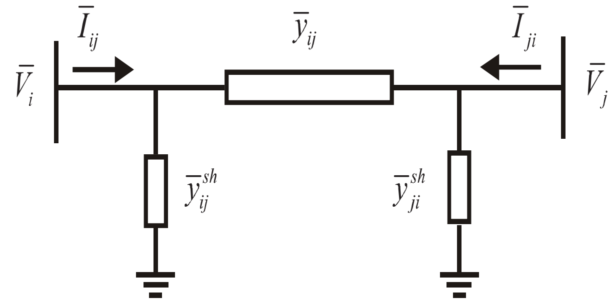

Figure 2.5: Transmission line π model.

By applying Kirchhoff's current law at nodes i and j, the nodal complex currents are obtained as follows:

$$\bar{I}_{ij} = \bar{y}_{ij}\left(\overline{V}_i - \overline{V}_j\right) + \bar{y}_{ij}^{sh}\overline{V}_i \tag{2.53}$$

$$\bar{I}_{ji} = \bar{y}_{ji}\left(\overline{V}_j - \overline{V}_i\right) + \bar{y}_{ji}^{sh}\overline{V}_j \tag{2.54}$$

Equations (2.53) and (2.54) can be expressed as shown in (2.55) and (2.56), respectively

$$\bar{I}_{ij} = \left(\bar{y}_{ij} + \bar{y}_{ij}^{sh}\right)\overline{V}_i - \bar{y}_{ij}\overline{V}_j \tag{2.55}$$

$$\bar{I}_{ji} = -\bar{y}_{ji}\overline{V}_i + \left(\bar{y}_{ji} + \bar{y}_{ji}^{sh}\right)\overline{V}_j \tag{2.56}$$

The nodal complex admittances of the network can be stated by the following conventions:

$$\overline{Y}_{ii} = \bar{y}_{ij}^{sh} + \bar{y}_{ij} = G_{ii} + jB_{ii} \tag{2.57}$$

$$\overline{Y}_{ij} = -\bar{y}_{ij} = G_{ij} + jB_{ij} \tag{2.58}$$

$$\overline{Y}_{ji} = -\bar{y}_{ji} = G_{ji} + jB_{ji} \tag{2.59}$$

$$\overline{Y}_{jj} = \bar{y}_{ji}^{sh} + \bar{y}_{ji} = G_{jj} + jB_{jj} \tag{2.60}$$

Therefore,

$$\overline{I}_{ij} = \overline{Y}_{ii}\overline{V}_i + \overline{Y}_{ij}\overline{V}_j \tag{2.61}$$

$$\overline{I}_{ji} = \overline{Y}_{ji}\overline{V}_i + \overline{Y}_{jj}\overline{V}_j \tag{2.62}$$

The complex power flow equations at both nodes of the transmission line are

$$\overline{S}_{ij} = P_{ij} + jQ_{ij} = \overline{V}_i\overline{I}^*_{ij} \tag{2.63}$$

$$\overline{S}_{ji} = P_{ji} + jQ_{ji} = \overline{V}_j\overline{I}^*_{ji} \tag{2.64}$$

Substituting (2.61) and (2.62) in (2.63) and (2.64) respectively, result in the following equations:

$$P_{ij} + jQ_{ij} = \overline{V}_i^2\overline{Y}^*_{ii} + \overline{V}_i\overline{V}^*_j\overline{Y}^*_{ij} \tag{2.65}$$

$$P_{ji} + jQ_{ji} = \overline{V}_j\overline{V}^*_i\overline{Y}^*_{ji} + \overline{V}_j^2\overline{Y}^*_{jj} \tag{2.66}$$

Lastly, the active and reactive power flows through the line connected between nodes i and j can be obtained by substituting $\overline{V}_i = V_i e^{j\theta_i}$ and $\overline{V}_j = V_j e^{j\theta_j}$ in (2.65) and (2.66), and separating the real and imaginary parts the resulting equations are

$$P_{ij} = V_i^2 G_{ii} + V_i V_j \left(G_{ij}cos(\theta_i - \theta_j) + B_{ij}sin(\theta_i - \theta_j)\right) \tag{2.67}$$

$$Q_{ij} = -V_i^2 B_{ii} + V_i V_j \left(G_{ij}sin(\theta_i - \theta_j) - B_{ij}cos(\theta_i - \theta_j)\right) \tag{2.68}$$

$$P_{ji} = V_j^2 G_{jj} + V_j V_i \left(G_{ji}cos(\theta_j - \theta_i) + B_{ji}sin(\theta_j - \theta_i)\right) \tag{2.69}$$

$$Q_{ji} = -V_j^2 B_{ii} + V_j V_i \left(G_{ji}sin(\theta_j - \theta_i) - B_{ji}cos(\theta_j - \theta_i)\right) \tag{2.70}$$

Assuming n_g generator nodes and n_{PQ} network nodes, V_i and θ_i are the magnitude and phase angle of voltages at network nodes, $i = 1,\ldots,n_g + n_{PQ}$ respectively, and $\overline{Y}_{ij} = G_{ij} + jB_{ij}$ is the admittance of the transmission element connected between nodes i and j.

The mismatch power equations at the network nodes are

$$P_{G_i} = P_{Li} + \sum_{j\in\Omega_i} P_{ij} \qquad \forall i = 1,\ldots,n_g \tag{2.71}$$

$$Q_{G_i} = Q_{Li} + \sum_{j\in\Omega_i} Q_{ij} \qquad \forall i = 1,\ldots,n_g \tag{2.72}$$

$$0 = P_{Li} + \sum_{j\in\Omega_i} P_{ij} \qquad \forall i = 1 + n_g,\ldots,n_{PQ} \tag{2.73}$$

$$0 = Q_{Li} + \sum_{j\in\Omega_i} Q_{ij} \qquad \forall i = 1 + n_g,\ldots,n_{PQ} \tag{2.74}$$

where $\Omega_i = \{j : j \neq i\}$ is the set of nodes adjacent to i, and P_{Li} (Q_{Li}) is the active (reactive) power demanded by the load embedded at the ith node.

2.7 Initial Conditions for the Two-Axis Model of Generator

In order to analyze the transient performance of a power system due to a disturbance, it is necessary to know the EP just before the disturbance occurrence, which provides the required initial conditions to any of the dynamic study. The EP corresponds to an operating point where the power balance between the total load is satisfied by the available generation of the power system and is completely defined by the values of all algebraic and dynamic variables of the system. The algebraic variables are the complex voltages of all system buses as well as the stator currents of generators on the axis d and q; the generator dynamic variables are the internal voltages on the $d-q$ axes , the rotor angle, speed and the field voltage.

The initial conditions for the complex node voltages (angles and magnitudes) are obtained by a power flow study. The initial conditions for the stator currents are computed from the complex power and voltage measured at their corresponding terminals, which were obtained from the power flow study. Since the initial conditions calculation considers the system operating at an EP, the changes of the dynamic variables with respect to time are zero. Thus, the dynamic state variables as well as the fixed inputs (exciter's reference voltages and mechanical powers) are calculated by simple algebraic arrangements as will be shown throughout the following sections.

2.7.1 Stator Currents

After the power flow solution has been obtained the initial conditions for the current flowing in the electrical network can be computed by using the complex power injection and voltages measured at terminals, i.e. as $\bar{I}_{Gi} = I_{Gi}e^{j\gamma_i} = (P_{gei} - jQ_{gei})/\bar{V}_i^*$. Based on equations (2.71) and (2.72), this complex current is computed as

$$I_{Gi}e^{j\gamma_i} = \left((P_{Li} + \sum_{j\in\Omega_i} P_{ij}) - j(Q_{Li} + \sum_{j\in\Omega_i} Q_{ij}) \right) / V_i e^{-j\theta_i} \tag{2.75}$$

The complex current is in the network frame of reference and is equal to the transformed currents flowing out the generator's stator which are in $dq0$ coordinates as shown in Eq. (2.76), which is obtained from the Park's transformation $I_{dq0} = T_{dq0}I_{abc}$. See Appendix A.2.

$$I_{Gi}e^{j\gamma_i} = (I_{di} + jI_{qi})e^{j(\delta_i - \pi/2)} \tag{2.76}$$

2.7.2 Dynamic States

On an EP the derivatives with respect to time are zero, thus equations (2.2)-(2.7) are considered algebraic and can be used for the initial conditions calculation of the dynamic state variables. In this case, once the stator currents have been obtained, the rotor angles at all machines can be calculated. From (2.3), the initial condition for the transient internal voltage magnitude on $d-$axis is given by,

$$E'_{di} = (X_{qi} - X'_{qi})I_{qi} \tag{2.77}$$

With the substitution of (2.77) in the voltage variable source of Figure 2.2 and the application of Kirchhoff 's Voltages Law, the stator complex voltages are

$$0 = V_i e^{j\theta_i} + (R_{si} + jX'_{di})(I_{di} + jI_{qi})e^{j(\delta_i - \pi/2)} - \left[(X_{qi} - X'_{qi})I_{qi} + (X'_{qi} - X'_{di})I_{qi} + jE'_{qi} \right] e^{j(\delta_i - \pi/2)} \tag{2.78}$$

Simplifying (2.78) and replacing $(I_{di} + jI_{qi})e^{j(\delta_i - \pi/2)}$ by $I_{Gi}e^{j\gamma_i}$ we have

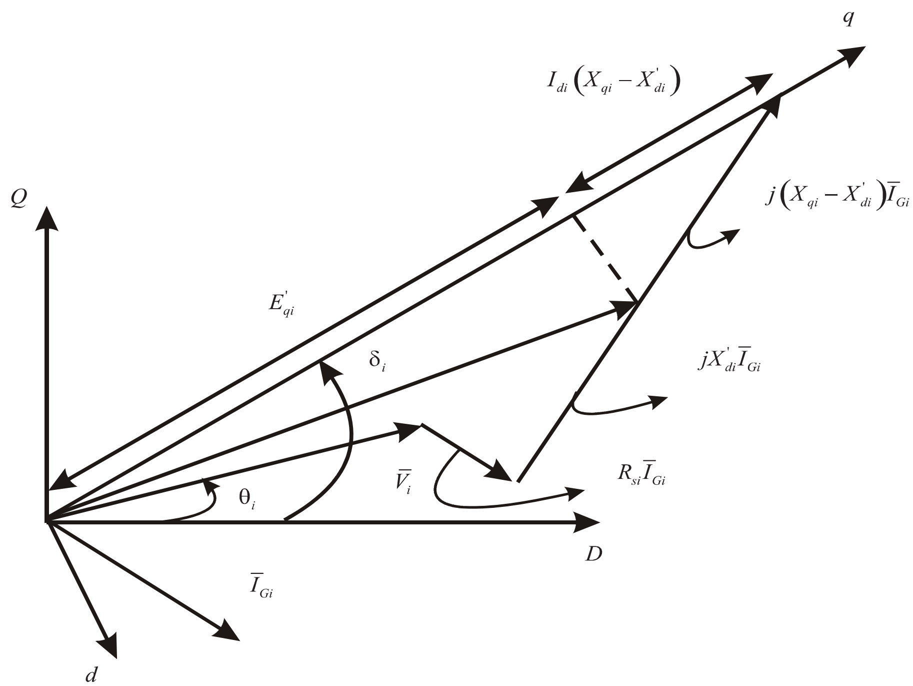

Figure 2.6: Phasor representation of stator voltage.

$$V_i e^{j\theta_i} + (R_{si} + jX_{qi}) I_{Gi} e^{j\gamma_i} = \left((X_{qi} - X'_{di}) I_{di} + E'_{qi}\right) e^{j\delta_i} \tag{2.79}$$

It is clear from (2.79) that the right-hand side represents a voltage behind the impedance $(R_{si} + jX_{qi})$ with a magnitude $\left((X_{qi} - X'_{di}) I_{di} + E'_{qi}\right)$ and an angle δ_i. Since in the left-hand side of (2.79) all variables are already calculated (known), the rotor angle will be calculated as

$$\delta_i = \text{angle of } \left(V_i e^{j\theta_i} + (R_{si} + jX_{qi}) I_{Gi} e^{j\gamma_i}\right) \tag{2.80}$$

The phasor representation of the stator equations (2.79) is shown in Figure 2.6, where $d-q$ axes and $D-Q$ axes are frame of references for the rotor and stator quantities, respectively.

From Eq. (2.76) the stator currents of the $d-q$ axes are

$$I_{di} + jI_{qi} = I_{Gi} e^{j\gamma_i} e^{-j(\delta_i - \pi/2)} \tag{2.81}$$

Based on Figure 2.2, the stator complex voltages in $dq0$ coordinates at the generator terminals can be expressed as

$$V_{di} + jV_{qi} = V_i e^{j\theta_i} e^{-j(\delta_i - \pi/2)} = (V_{Di} + jV_{Qi})(sin\delta_i + jcos\delta_i) \tag{2.82}$$

where V_{Di} and V_{Qi} are the real and imaginary parts of the complex voltage at the generator terminals, i.e.

$$\overline{V}_i = V_{Di} + jV_{Qi} = V_i e^{j\theta_i} = V_i cos\theta_i + jV_i sin\theta_i \tag{2.83}$$

Separating (2.82) in the real and imaginary parts results in

$$V_{di} = V_{Di} sin\delta_i - V_{Qi} cos\delta_i \tag{2.84}$$

$$V_{qi} = V_{Di} cos\delta_i + V_{Qi} sin\delta_i \tag{2.85}$$

In order to compute the initial values of the internal voltages on the rotor $d-q$ axes, Eqs. (2.10) and (2.11) can be expanded as

$$E'_{di} - V_{Di} sin\delta_i + V_{Qi} cos\delta_i + X'_{qi} I_{qi} = 0 \tag{2.86}$$

$$E'_{qi} - V_{Di} cos\delta_i - V_{Qi} sin\delta_i - X'_{di} I_{di} = 0 \tag{2.87}$$

By substituting (2.84) and (2.85) in (2.86) and (2.87), respectively, the initial values of internal voltages on the $d-q$ axes can be calculated as

$$E'_{di} = V_{di} - X'_{qi} I_{qi} \tag{2.88}$$

$$E'_{qi} = V_{qi} + X'_{di} I_{di} \tag{2.89}$$

The DC field voltage is known from Eq. (2.2) as

$$E_{fdi} = E'_{qi} + (X_{di} - X'_{di}) I_{di} \tag{2.90}$$

Finally the voltage reference used as input in the excitation system is calculated from Eq. (2.7)

$$V_{ref,i} = \frac{E_{fdi}}{K_{Ai}} + V_i \tag{2.91}$$

The fixed values as $V_{ref,i}$ and P_{Mi} are calculated in steady state when the system operates at the synchronous speed, thus $\omega_i = \omega_0$. The mechanical power of the generator is equal to the electrical active power associated with the internal node $P_{Mi} = P_{ei}$, see Eq. (2.6).

2.8 Initial Conditions for the Generator Classical Model

For the case of the classical generator model, the computation of initial conditions is very simple. Such a model only requires obtaining the rotor angle δ_i and speed ω_i of the power generators. In this model the internal voltage behind the transient reactance E_i and the mechanical power P_{Mi} are considered constant [Sauer and Pai, 98]. In the pre-transient condition t_0, the state changes are $\dot{\delta}_i = 0$ and $\dot{\omega}_i = 0$. Bearing this in mind, rearranging equations (2.17) and (2.18) the initial conditions for speed and mechanical power are calculated as $\omega_i = \omega_0$ and $P_{Mi} = P_{G_i}$. The internal voltages $E_i \angle \delta_i$ are calculated from the pre-disturbance terminal voltages which resulted from the power flow study [Anderson and Fouad, 94]. Applying the Kirchhoff's Voltages Law in the circuit shown in Figure 2.3, the resulting internal voltages are

$$E_i \angle \delta_i = \overline{V}_i + jX'_{di}\bar{I}_i \tag{2.92}$$

In order to temporarily employ the terminal voltage as the reference we use $\bar{V}_i = V_i \angle 0°$. Considering the complex power in terminals $P_i + jQ_i = \overline{V}_i \bar{I}_i^*$ the current injection is

$$\overline{I}_i = \frac{P_i - jQ_i}{V_i} \tag{2.93}$$

Substituting (2.93) in (2.92) and rearranging the internal voltages result in the following:

$$E_i \angle \delta'_i = \left(V_i + \frac{Q_i X'_{di}}{V_i} \right) + j \left(\frac{P_i X'_{di}}{V_i} \right) \tag{2.94}$$

where δ'_i represents the rotor angle obtained by using the phase angle of terminal voltage as $\theta_i = 0°$, which is taken as the temporal reference.

Finally, the initial rotor angle $\delta_i(t_0)$ from (2.92) is calculated by adding the terminal phase angle θ_i obtained from the previous power flow study

$$\delta_i = \delta_i^{'} + \theta_i \tag{2.95}$$

2.9 Small Signal Stability Analysis (SSS)

SSS is the ability of a power system to maintain synchronism when subjected to small disturbances such as small load and/or generation changes [Kundur, 94] [Sauer and Pai, 98]. The analysis of SSS consists of assessing the stability of an EP, as well as determining those state variables with the most influence on the operating point stability; this can be done by the linearization of the system equations around the operating point, which facilitates applying the theory of linear systems in order to know the SSS [Chen, 99]. The stability of an EP is assessed by eigenvalue analysis (eigen-analysis) according to the Lyapunov criterion [Lyapunov, 67], which states that an EP will be stable in the small signal if all system eigenvalues of the system matrix are located in the left side of the complex plane; the EP will be unstable if at least one eigenvalue is located in the right side of the imaginary axis. In order to have an idea of how stable an EP is, the closest eigenvalue to the imaginary axis is taken as a natural stability index and is called the critical eigenvalue. Even for unstable EPs the eigenvalue with the largest positive real part is defined as the critical one. The critical eigenvalue associated with the state variables is found out by computing a Selective Modal Analysis (SMA) developed in [Pérez et al., 82] and [Verghese et al., 82]. Based on the Participation Factors Analysis (PFA), the SMA provides those state variables having the highest influence in the EP stability by means of their coupling to the critical eigenvalue [Kundur, 94], [Sauer and Pai, 98].

The stability of the EPs can be studied via the bifurcations, which are defined as the stability changes caused by the parameter values of a system. Bifurcations theory is a powerful mathematical tool based on eigen-analysis to assess the stability of EPs in nonlinear systems [Nayfeh and Balachandran, 95]. This theory consists of searching specific eigenvalue structures associated with different unstable behaviors that appear in power systems [Ajjarapu, 06]. The bifurcations that only concern the immediate vicinity of an EP are called local bifurcations. The three most common local bifurcations that can appear in the power system operation are the Hopf Bifurcation (HB) which occurs when the system matrix contains a pair of purely imaginary eigenvalues causing undamped oscillatory behavior [Ajjarapu and Lee, 92] [Kwatny et al., 95] [Wen, 05]; the Singularity Induced Bifurcation (SIB) appears when the operating point lies in the vicinity of an algebraic singularity of the network equations for the DAE models; the Saddle Node Bifurcation (SNB) occurs when there is a simple zero eigenvalue, and the system moves from a stable to an unstable EP [Hill and Mareels, 90] [Venkatasubramanian et al., 92] [IEEE, 02].

Bifurcation points indicate the instability type of an EP. The maximum load in a specific direction that a power system can supply before the appearance of a local bifurcation point states the loading limit in that direction. Thus, limit is directly associated with the system stability margin. The critical eigenvalue of an EP represents a natural index of the stability margin. After a load increase an eigen-analysis computation aids in assessing how near the new EP is from the stability boundary. A small margin indicates closeness to a bifurcation point (to instability). The control of SSS can be provided if it is possible to determine which system parameters and components have the most influence on the dynamic process. In this context, the modal analysis permits us to know the highest coupling of state variables (associated states) of power systems with respect to that critical eigenvalue dominating the EP stability [Kundur, 94] [Sauer and Pai, 98]. In this way, SMA leads to the selection, by means of the associated states to the critical eigenvalue, those components that will provide the best control of EP stability.

Linearization

The solution of Eq. (2.1) corresponds to an equilibrium point where $\dot{\boldsymbol{x}} = 0$; therefore

$$0 = \boldsymbol{f}(\boldsymbol{x}_0, \boldsymbol{y}_0) \tag{2.96}$$

$$0 = \boldsymbol{g}(\boldsymbol{x}_0, \boldsymbol{y}_0) \tag{2.97}$$

The new operating point due to a small disturbance is as follows:

$$\boldsymbol{x} = \boldsymbol{x}_0 + \Delta \boldsymbol{x} \tag{2.98}$$

$$\boldsymbol{y} = \boldsymbol{y}_0 + \Delta \boldsymbol{y} \tag{2.99}$$

Since the new dynamic and algebraic states must satisfy Eq. (2.1), we have

$$\dot{\boldsymbol{x}}_0 + \Delta\dot{\boldsymbol{x}} = \boldsymbol{f}\left[(\boldsymbol{x}_0 + \Delta\boldsymbol{x}), (\boldsymbol{y}_0 + \Delta\boldsymbol{y})\right] \tag{2.100}$$

By expanding in terms of Taylor's series and neglecting the terms involving second and higher order powers of $\Delta\boldsymbol{x}$ and $\Delta\boldsymbol{y}$, Eq. (2.100) can be written as

$$\dot{\boldsymbol{x}}_0 + \Delta\dot{\boldsymbol{x}} = \boldsymbol{f}(\boldsymbol{x}_0, \boldsymbol{y}_0) + \frac{\partial \boldsymbol{f}(\cdot)}{\partial \boldsymbol{x}}\Delta\boldsymbol{x} + \frac{\partial \boldsymbol{f}(\cdot)}{\partial \boldsymbol{y}}\Delta\boldsymbol{y} \tag{2.101}$$

Since $\dot{\boldsymbol{x}}_0 = \boldsymbol{f}(\boldsymbol{x}_0, \boldsymbol{y}_0) = 0$, Eq. (2.101) can be rewritten as

$$\Delta\dot{\boldsymbol{x}} = \frac{\partial \boldsymbol{f}(\cdot)}{\partial \boldsymbol{x}}\Delta\boldsymbol{x} + \frac{\partial \boldsymbol{f}(\cdot)}{\partial \boldsymbol{y}}\Delta\boldsymbol{y} \tag{2.102}$$

In the same form, the linearized approximation of (2.97) is

$$0 = \frac{\partial \boldsymbol{g}(\cdot)}{\partial \boldsymbol{x}}\Delta\boldsymbol{x} + \frac{\partial \boldsymbol{g}(\cdot)}{\partial \boldsymbol{y}}\Delta\boldsymbol{y} \tag{2.103}$$

The matrix representation of the linear equations (2.102) and (2.103) in a conveniently partitioned form for the purposes of this thesis is shown in (2.104). $g(\cdot)$ is associated with the algebraic functions vector of the DAE system, which is composed by two partitions, these are the stator algebraic equations represented by (2.10) and (2.11) for the n_g system generators, as well as the active and reactive power balances defined by (2.71)-(2.74) for the $(n_g + n_{PQ})$ system nodes. Hence, $\Delta\boldsymbol{y} = \begin{bmatrix} \triangle \boldsymbol{I} & \triangle \boldsymbol{V} \end{bmatrix}^T$.

$$\begin{bmatrix} \triangle\,\dot{\boldsymbol{x}} \\ 0 \\ 0 \end{bmatrix} = \begin{bmatrix} \boldsymbol{A}_1 & \boldsymbol{B}_1 & \boldsymbol{B}_2 \\ \boldsymbol{C}_1 & \boldsymbol{D}_1 & \boldsymbol{D}_2 \\ \boldsymbol{C}_2 & \boldsymbol{D}_3 & \boldsymbol{D}_4 \end{bmatrix} \begin{bmatrix} \triangle\,\boldsymbol{x} \\ \triangle\,\boldsymbol{I} \\ \triangle\,\boldsymbol{V} \end{bmatrix} \tag{2.104}$$

where

$$\boldsymbol{x} = \left[x_1, \ldots, x_{n_g}\right]^T \tag{2.105}$$

$$\boldsymbol{x}_i = \begin{bmatrix} E'_{di} & E'_{qi} & \delta_i & \omega_i & E_{fdi} \end{bmatrix}^T \tag{2.106}$$

$$\boldsymbol{I} = \begin{bmatrix} I_{d1,\ldots,}I_{dn_g}, & I_{q1,\ldots,}I_{qn_g} \end{bmatrix}^T \tag{2.107}$$

$$\boldsymbol{V} = \begin{bmatrix} \theta_1, \dots \theta_{n_b}, & V_1, \dots, V_{n_b} \end{bmatrix}^T \tag{2.108}$$

$$\begin{array}{llll} \boldsymbol{A}_1 = \left[\frac{\partial \boldsymbol{f}}{\partial \boldsymbol{x}}\right]_{(5n_g)(5n_g)} & \boldsymbol{B}_1 \quad \boldsymbol{B}_2 & = \left[\frac{\partial \boldsymbol{f}}{\partial \boldsymbol{I}}\right]_{(5n_g)(2n_g)} & \left[\frac{\partial \boldsymbol{f}}{\partial \boldsymbol{V}}\right]_{(5n_g)(2n_b)} \\ \begin{matrix} \boldsymbol{C}_1 \\ \boldsymbol{C}_2 \end{matrix} = \left[\frac{\partial \boldsymbol{g}}{\partial \boldsymbol{x}}\right]_{2(n_g+n_b)(5n_g)} & \begin{matrix} \boldsymbol{D}_1 & \boldsymbol{D}_2 \\ \boldsymbol{D}_3 & \boldsymbol{D}_4 \end{matrix} & = \left[\frac{\partial \boldsymbol{g}}{\partial \boldsymbol{I}}\right]_{2(n_g+n_b)(2n_g)} & \left[\frac{\partial \boldsymbol{g}}{\partial \boldsymbol{V}}\right]_{2(n_g+n_b)(2n_b)} \end{array} \tag{2.109}$$

and where n_g and n_b are the number of machines and buses in a power system, respectively.

By reducing the linearized equation (2.104), the following equivalent system is obtained in the state space:

$$\triangle\, \dot{\boldsymbol{x}} = \boldsymbol{A}_{sys} \triangle\, \boldsymbol{x} \tag{2.110}$$

where

$$\boldsymbol{A}_{sys} = \boldsymbol{K}_1 - \boldsymbol{K}_2 \boldsymbol{K}_4^{-1} \boldsymbol{K}_3 \tag{2.111}$$

$$\boldsymbol{K}_1 = \boldsymbol{A}_1 - \boldsymbol{B}_1 \boldsymbol{D}_1^{-1} \boldsymbol{C}_1 \tag{2.112}$$

$$\boldsymbol{K}_2 = \boldsymbol{B}_2 - \boldsymbol{B}_1 \boldsymbol{D}_1^{-1} \boldsymbol{D}_2 \tag{2.113}$$

$$\boldsymbol{K}_3 = \boldsymbol{C}_2 - \boldsymbol{D}_3 \boldsymbol{D}_1^{-1} \boldsymbol{C}_1 \tag{2.114}$$

$$\boldsymbol{K}_4 = \boldsymbol{D}_4 - \boldsymbol{D}_3 \boldsymbol{D}_1^{-1} \boldsymbol{D}_2 \tag{2.115}$$

Eq. (2.110) is valid as long as $\boldsymbol{K}_4$ and $\boldsymbol{D}_1$ are not singular.

Eigenvectors and participation factors

For any eigenvalue λ_i there exists an associated $n-$column vector $\boldsymbol{\phi}_i$ called the right eigenvector of $\boldsymbol{A}_{sys}$, which satisfies Eq. (2.116) as follows:

$$\boldsymbol{A}_{sys}\boldsymbol{\phi}_i = \lambda_i \boldsymbol{\phi}_i \qquad i = 1,2,\ldots,n \tag{2.116}$$

Also, there exists a $n-$row vector $\boldsymbol{\psi}_i$ associated with the ith eigenvalue λ_i called the left eigenvector which satisfies Eq. (2.117)

$$\boldsymbol{\psi}_i \boldsymbol{A}_{sys} = \lambda_i \boldsymbol{\psi}_i \qquad i = 1,2,\ldots,n \tag{2.117}$$

The participation matrix $\boldsymbol{P}$ is proposed in [Pérez et al., 82] [Verghese et al., 82] as a measure of the association between the state variables and the system modes (eigenvalues). The column vectors making up the participation matrix represent the association of all state variables to the n system eigenvalues as is shown in (2.118). Thus, the element $P_{ki} = \phi_{ki}\psi_{ik}$ measures the relative participation of the kth state to the ith mode of oscillation. The n participation factors composing each vector $\boldsymbol{P}_i$ represent the relative participation of all state variables to the n system eigenvalues, as shown in (2.119)

$$\boldsymbol{P} = \begin{bmatrix} \boldsymbol{P}_1 & \boldsymbol{P}_2 & \ldots & \boldsymbol{P}_n \end{bmatrix} \tag{2.118}$$

$$\boldsymbol{P}_i = \begin{bmatrix} P_{1i} \\ P_{2i} \\ \vdots \\ P_{ni} \end{bmatrix} = \begin{bmatrix} \phi_{1i}\psi_{i1} \\ \phi_{2i}\psi_{i2} \\ \vdots \\ \phi_{ni}\psi_{in} \end{bmatrix} \tag{2.119}$$

Eigen-Analysis (Lyapunov criterion)

The time response of the ith state variable of the linearized system model (2.110) is given by [Kundur, 94],

$$\Delta x_i(t) = \sum_{i=1}^{n} \boldsymbol{\phi}_i \boldsymbol{\psi}_i \boldsymbol{\Delta x}(0) e^{\lambda_i t} \tag{2.120}$$

Knowing the expression (2.120) for the time response of the state variables, the SSS can be judged by directly observing the type of eigenvalues obtained from the system matrix $\boldsymbol{A}_{sys}$. Thus, according to the Lyapunov stability theory, if all eigenvalues of the system matrix in (2.110) have negative real part, the equilibrium point $(\boldsymbol{x}_0, \boldsymbol{y}_0)$ will be stable. However, if any eigenvalue is located on the right-hand of the imaginary axis in the complex plane, the EP will be unstable. A real eigenvalue corresponds to a non oscillatory mode, whilst a conjugate pair of complex eigenvalues ($\lambda = \sigma \pm j\omega$) indicate oscillatory modes of response. If a conjugate pair of eigenvalues has negative real part it corresponds to a damped oscillatory mode (stable EP); otherwise this will be unstable.

As independent system parameters are increased, the system will eventually turn unstable. This loss of stability can be linked with a bifurcation point according to the following relations. The instability due to a real eigenvalue crossing the imaginary axis is called a SNB [Hill and Mareels, 90] [Venkatasubramanian et al., 92] [IEEE, 02]. If a pair of conjugated eigenvalues cross the imaginary axis, the instability will correspond to a Hopf Bifurcation [Ajjarapu and Lee, 92] [Kwatny et al., 95] [Wen, 05]. If matrix $\boldsymbol{K}_4$ in (2.110) turns singular [IEEE, 02], instability will be due to a SIB [Venkatasubramanian et al., 92] [Campbell and Marszalek, 99] [Beardmore and Laister, 78].

2.10 Transient Stability Analysis

The transient stability study consists of the assessment of the power system ability to maintain synchronism when subjected to a severe transient disturbance [Kundur, 94] [IEEE, 04]. The large disturbances in power systems are classified as either the loss of generation or transmission facilities, sudden large changes of load, or short circuit faults. These kinds of disturbances induce large excursions in the system rotor angle trajectories, which require a solution based on nonlinear analysis in the time domain [Sauer and Pai, 98].

Physically, the application and clearing of large disturbances represent changes in the power system topology. This numerically corresponds to solving different dynamic systems of equations at different periods of time during the time domain simulation. According to this, any transient behavior can be assessed from the transient stability viewpoint by solving the different nonlinear dynamical systems at their corresponding three characteristic time periods called pre-disturbance, disturbance and post-disturbance.

The pre-disturbance time period consists of calculating the equilibrium state of the power system, which represents the initial conditions required to start the transient stability analysis. At the time $t = t_0^-$ the system dynamics do not exist, such that the set of DAEs can be treated as algebraic equations as follows:

$$
\begin{aligned}
0 &= f^{pre-dist}(x_0^-, y_0^-, \beta) \\
0 &= g^{pre-dist}(x_0^-, y_0^-, \beta)
\end{aligned}
\tag{2.121}
$$

The fault time period is framed from the disturbance application at the time instant t_0^+ to the disturbance clearing time t_{cl}, as $t_{dist} \in \left[t_0^+, t_{cl}\right]$. During this time period, the nonlinear trajectories of the system states must be obtained by solving the following disturbed DAE system

$$
\begin{aligned}
\dot{x} &= f^{dist}(x, y, \beta) \\
0 &= g^{dist}(x, y, \beta)
\end{aligned}
\tag{2.122}
$$

where the superscript $(dist)$ indicates the disturbed DAE system.

Once the disturbance is cleared, the nonlinear trajectories of the system states will be obtained by solving the post-disturbance DAE system (2.123). The post-disturbance time period is established from the disturbance clearing time t_{cl}^+ to the end of the study time period t_{end}, as $t_{post-dist} \in \left(t_{cl}^+, t_{end}\right]$

$$
\begin{aligned}
\dot{x} &= f^{p-dist}(x, y, \beta) \\
0 &= g^{p-dist}(x, y, \beta)
\end{aligned}
\tag{2.123}
$$

If the disturbance does not require clearing by inducing another change of topology (tripping any faulted transmission or generation facilities), the transient stability assessment will be attained by solving only the system (2.121) at t_0^- and (2.122) in the period concerned from the instant t_0^+ to the end of the study time period t_{end}, i.e. $t_{dist} \in \left(t_0^+, t_{end}\right]$. Thus, the network initial conditions $y_0 = \begin{bmatrix} \theta_i & V_i \end{bmatrix}^T$ for $i = 1, \ldots, n_b$ buses are obtained by computing a load flow study, whereas, the generator initial conditions $x_0 = \begin{bmatrix} I_{di} & I_{qi} & E_{di}^{'} & E_{qi}^{'} & \delta_i & \omega_i & E_{fdi} \end{bmatrix}^T$ for $i = 1, \ldots, n_g$ generators are calculated from simple rearrangements based on algebraic steps.

The first oscillations of the generator rotor angles provide the necessary information to state the multi-machine power system synchronism and assess the transient stability of the power system.

There are two network models to simulate the electric power system for transient stability analysis. The reduced network model consists of obtaining an equivalent set of ODEs from the original set of DAEs. In this case, the DAE reduced to the internal nodes of generators and the resulting equivalent network represents the connectivity between the internal nodes of the system generators [Anderson and Fouad, 94]. Thus, the nonlinear dynamics can be obtained by explicitly integrating the equivalent ODE system. In this case the computational burden is reduced because of the lack of a Jacobian matrix as well as the set of algebraic equations representing the transmission network. However, the validity of this technique is constrained to use only the constant impedance load model [Anderson and Fouad, 94]. On the other hand, the structure preserving model of the network exists, which leads to directly obtaining the voltages and currents along the network during the transient behavior. Besides, in this network model there is no restriction about any type of load model.

Basically there are two general approaches to assess the nonlinear dynamical analysis in the time domain for DAE systems preserving the structure of the network [Sauer and Pai, 98]: The Partitioned Explicit method (PE) is a sequential algorithm where the differential and algebraic sets of equations are solved in separated form. The algebraic variables are kept unchanged while the differential equations are solved by an explicit integration method. Conversely, during the solution of the algebraic equations, the dynamic variables must be kept constant [Stagg and El-Abiad, 68]. Although this method is very easy to implement, it presents some numerical convergence problems [EPRI, 77], whereas, the SI method is a numerically stable method which provides good robustness and accuracy [Alvarado et al., 83]. Such a powerful method implicitly integrates the nonlinear differential equations by considering a linear behavior for a selected small time step. The resulting nonlinear difference equations are solved together with the original algebraic equations of the DAE system, under a unified frame of reference at each time of the study period [Sauer and Pai, 98].

2.10.1 Simultaneous Implicit Method

The SI method based on the trapezoidal rule can be used to simultaneously solve the differential and algebraic sets of equations in a single frame of reference. The trapezoidal rule implicitly integrates the differential equations at a time step. A dynamic linear behavior is assumed at the integration time step $\triangle t = t^{k+1} - t^k$, where t^{k+1} represents the new condition to be known, whereas t^k is the starting condition of the discretization process. For the set of differential equations conforming (2.1)

$$\dot{x} = f(x, y, \beta) \tag{2.124}$$

the integration in the discrete time step from t^k to t^{k+1} is obtained as

$$x^{k+1} = x^k + \int_{t^k}^{t^{k+1}} \dot{x} dt \tag{2.125}$$

Due to the assumed linear behavior at the integration time step, the last term on the right-hand side of (2.125) can be expressed as;

$$\int_{t^k}^{t^{k+1}} \dot{x} dt = \frac{\triangle\, t}{2} \left(\dot{x}^{k+1} + \dot{x}^k \right) \tag{2.126}$$

thus, substituting (2.126) into (2.125), the state variables can be computed by

$$x^{k+1} = x^k + \frac{\triangle\, t}{2} \left(\dot{x}^{k+1} + \dot{x}^k \right) \tag{2.127}$$

or

$$x^{k+1} = x^k + \frac{\triangle\, t}{2} \left(f(x^{k+1}, y^{k+1}, \beta) + f(x^k, y^k, \beta) \right) \tag{2.128}$$

Equation (2.128) can be integrated to the set of algebraic equations by expressing it as

$$x^{k+1} - x^k - \frac{\triangle\, t}{2} \left(f(x^{k+1}, y^{k+1}, \beta) + f(x^k, y^k, \beta) \right) = 0 \tag{2.129}$$

Lastly, the algebraized mathematical model of differential equations (2.129) can be partitioned into two parts corresponding to the time conditions t^{k+1} and t^k as follows:

$$F^{k+1}(x) + F^k(x) = 0 \tag{2.130}$$

where

$$F^{k+1}(x) = x^{k+1} - \frac{\triangle\, t}{2} \left(f(x^{k+1}, y^{k+1}, \beta) \right) \tag{2.131}$$

$$F^k(x) = -x^k - \frac{\triangle\, t}{2} \left(f(x^k, y^k, \beta) \right) \tag{2.132}$$

2.10.2 Newton-Raphson Solution

The trapezoidal rule is applied to algebraize the differential equations, such that the resulting set of difference equations (2.130) is added to the rest of the algebraic equations to be solved under a single frame of reference. Thus, the Newton-Raphson (NR) algorithm provides an approximate solution to the DAE system (2.1) by solving $\begin{bmatrix} \triangle x^k & \triangle y^k \end{bmatrix}^T$ in the linear problem $J^i \triangle X^i = -F(X^i)$, given in expanded form by (2.133) [Sauer and Pai, 98], where J is known as the Jacobian matrix; $\triangle t$ is the integration time step, and the superscript k is an index for the time instant t_k at which variables and functions are evaluated: $x^k = x(t_k)$ and $f^k = f(x^k, y^k)$

$$\underbrace{\begin{bmatrix} I - \frac{\triangle t}{2} f_x^{k+1} & -\frac{\triangle t}{2} f_y^{k+1} \\ g_x^{k+1} & g_y^{k+1} \end{bmatrix}^i}_{J} \underbrace{\begin{bmatrix} \triangle x^k \\ \triangle y^k \end{bmatrix}^i}_{\triangle x^i} = -\underbrace{\begin{bmatrix} F^{k+1}(x) + F^k(x) \\ g^{k+1} \end{bmatrix}^i}_{F(\cdot)} \tag{2.133}$$

For given values $\begin{bmatrix} x^k & y^k \end{bmatrix}^T$, the method starts from an initial guess $x_0^{k+1} = x^k$ and $y_0^{k+1} = y^k$ and updates the solution at each iteration i, i.e. $\begin{bmatrix} x^{k+1} = x^k + \triangle x^k & y^{k+1} = y^k + \triangle y^k \end{bmatrix}^T$, until a convergence criterion is satisfied.

2.10.3 Algebraized Two-Axis Generator Model

This section explains the discretization of the set of differential equations for the Two-axis generator model. The algebraized equations are presented in the partitioned way via the $k+1$ and k stages of evaluation, as was described in (2.130)-(2.132). Also, the corresponding Jacobian elements for the algebraized functions are given. Since the stator equations were already algebraic, only their corresponding Jacobian elements are provided.

The algebraized form of the internal voltages in the axes d and q are

$$F^{k+1}(E'_{di}) = E'^{k+1}_{di} - \frac{\triangle t}{2T'_{q0i}} \left(-E'^{k+1}_{di} + (X_{qi} - X'_{qi}) I^{k+1}_{qi} \right) \tag{2.134}$$

$$F^{k}(E'_{di}) = -E'^{k}_{di} - \frac{\triangle t}{2T'_{q0i}} \left(-E'^{k}_{di} + (X_{qi} - X'_{qi}) I^{k}_{qi} \right) \tag{2.135}$$

$$F^{k+1}(E'_{qi}) = E'^{k+1}_{qi} - \frac{\triangle t}{2T'_{d0i}} \left(-E'^{k+1}_{qi} - (X_{di} - X'_{di}) I^{k+1}_{di} + E^{k+1}_{fdi} \right) \tag{2.136}$$

$$F^k(E_{qi}^{'}) = -E_{qi}^{'k} - \frac{\triangle t}{2T_{d0i}^{'}}\left(-E_{qi}^{'k} - (X_{di} - X_{di}^{'})I_{di}^{k} + E_{fdi}^{k}\right) \tag{2.137}$$

The Jacobian elements for the above algebraized functions are

$$\frac{\partial F(E_{di}^{'})}{\partial I_{qi}} = -\frac{\triangle t}{2T_{q0i}^{'}}(X_{qi} - X_{qi}^{'}) \tag{2.138}$$

$$\frac{\partial F(E_{di}^{'})}{\partial E_{di}^{'}} = 1 + \frac{\triangle t}{2T_{q0i}^{'}} \tag{2.139}$$

$$\frac{\partial F(E_{qi}^{'})}{\partial I_{di}} = \frac{\triangle t}{2T_{d0i}^{'}}(X_{di} - X_{di}^{'}) \tag{2.140}$$

$$\frac{\partial F(E_{qi}^{'})}{\partial E_{qi}^{'}} = 1 + \frac{\triangle t}{2T_{d0i}^{'}} \tag{2.141}$$

$$\frac{\partial F(E_{qi}^{'})}{\partial E_{fdi}} = -\frac{\triangle t}{2T_{d0i}^{'}} \tag{2.142}$$

The algebraized form of the electromechanical swing equations is

$$F^{k+1}(\delta_i) = \delta_i^{k+1} - \frac{\triangle t}{2}(\omega_i^{k+1} - \omega_0) \tag{2.143}$$

$$F^{k}(\delta_i) = -\delta_i^{k} - \frac{\triangle t}{2}(\omega_i^{k} - \omega_0) \tag{2.144}$$

$$\begin{aligned} F^{k+1}(\omega_i) = \omega_i^{k+1} - \tfrac{\triangle t}{2M_i}\Big(P_{Mi} - (E_{qi}^{'k+1}I_{qi}^{k+1} + E_{di}^{'k+1}I_{di}^{k+1} + (X_{qi}^{'} - X_{di}^{'})I_{di}^{k+1}I_{qi}^{k+1}) \\ -D_i(\omega_i^{k+1} - \omega_0)\Big) \end{aligned} \tag{2.145}$$

$$F^{k}(\omega_i) = -\omega_i^{k} - \frac{\triangle t}{2M_i}\left(P_{Mi} - (E_{qi}^{'k}I_{qi}^{k} + E_{di}^{'k}I_{di}^{k} + (X_{qi}^{'} - X_{di}^{'})I_{di}^{k}I_{qi}^{k}) - D_i(\omega_i^{k} - \omega_0)\right) \tag{2.146}$$

Their Jacobian elements are

$$\frac{\partial F(\delta_i)}{\partial \delta_i} = 1 \tag{2.147}$$

$$\frac{\partial F(\delta_i)}{\partial \omega_i} - \frac{\triangle\, t}{2} \tag{2.148}$$

$$\frac{\partial F(\omega_i)}{\partial I_{di}} = \frac{\triangle\, t}{2M_i}\left(E_{di}^{'} + (X_{qi}^{'} - X_{di}^{'})I_{qi}\right) \tag{2.149}$$

$$\frac{\partial F(\omega_i)}{\partial I_{qi}} = \frac{\triangle\, t}{2M_i}\left(E_{qi}^{'} + (X_{qi}^{'} - X_{di}^{'})I_{di}\right) \tag{2.150}$$

$$\frac{\partial F(\omega_i)}{\partial E_{di}^{'}} = \frac{\triangle\, t}{2M_i} I_{di} \tag{2.151}$$

$$\frac{\partial F(\omega_i)}{\partial E_{qi}^{'}} = \frac{\triangle\, t}{2M_i} I_{qi} \tag{2.152}$$

$$\frac{\partial F(\omega_i)}{\partial \omega_i} = 1 + \frac{\triangle\, t}{2M_i} D_i \tag{2.153}$$

The algebraized form of the automatic voltage regulator is the following:

$$F^{k+1}(E_{fdi}) = E_{fdi}^{k+1} - \frac{\triangle\, t}{2T_{Ai}}\left(K_{Ai}(V_{ref,i} - V_i^{k+1}) - E_{fdi}^{k+1}\right) \tag{2.154}$$

$$F^{k}(E_{fdi}) = -E_{fdi}^{k} - \frac{\triangle\, t}{2T_{Ai}}\left(K_{Ai}(V_{ref,i} - V_i^{k}) - E_{fdi}^{k}\right) \tag{2.155}$$

Their corresponding Jacobian elements are the following:

$$\frac{\partial F(E_{fdi})}{\partial V_i} = \frac{\triangle\, t}{2T_{Ai}} K_{Ai} \tag{2.156}$$

$$\frac{\partial F(E_{fdi})}{\partial E_{fdi}} = 1 + \frac{\triangle\, t}{2T_{Ai}} \tag{2.157}$$

Due to their instantaneous behavior, the mathematical expressions for the stator voltages and currents are modeled by means of algebraic equations. Thus, the resulting Jacobian elements for the stator voltage equations (2.10) and (2.11) are

$$\frac{\partial V_{di}^{St}}{\partial \theta_i} = V_i cos(\delta_i - \theta_i) \tag{2.158}$$

$$\frac{\partial V_{di}^{St}}{\partial V_i} = -sin(\delta_i - \theta_i) \tag{2.159}$$

$$\frac{\partial V_{di}^{St}}{\partial I_{qi}} = X_{qi}^{`} \tag{2.160}$$

$$\frac{\partial V_{di}^{St}}{\partial \delta_i} = -V_i cos(\delta_i - \theta_i) \tag{2.161}$$

$$\frac{\partial V_{di}^{St}}{\partial E_{di}^{'}} = 1 \tag{2.162}$$

$$\frac{\partial V_{qi}^{St}}{\partial \theta_i} = -V_i sin(\delta_i - \theta_i) \tag{2.163}$$

$$\frac{\partial V_{qi}^{St}}{\partial V_i} = -cos(\delta_i - \theta_i) \tag{2.164}$$

$$\frac{\partial V_{qi}^{St}}{\partial I_{di}} = -X_{di}^{'} \tag{2.165}$$

$$\frac{\partial V_{qi}^{St}}{\partial \delta_i} = V_i sin(\delta_i - \theta_i) \tag{2.166}$$

$$\frac{\partial V_{qi}^{St}}{\partial E_{qi}^{'}} = 1 \tag{2.167}$$

The Jacobian elements of the stator power injection equations (2.12) and (2.13) are

$$\frac{\partial P_{Gi}}{\partial \theta_i} = -I_{di} V_i cos(\delta_i - \theta_i) + I_{qi} V_i sin(\delta_i - \theta_i) \tag{2.168}$$

$$\frac{\partial P_{Gi}}{\partial V_i} = I_{di} sin(\delta_i - \theta_i) + I_{qi} cos(\delta_i - \theta_i) \tag{2.169}$$

$$\frac{\partial P_{Gi}}{\partial I_{di}} = V_i sin(\delta_i - \theta_i) \tag{2.170}$$

$$\frac{\partial P_{Gi}}{\partial I_{qi}} = V_i cos(\delta_i - \theta_i) \tag{2.171}$$

$$\frac{\partial P_{Gi}}{\partial \delta_i} = I_{di} V_i cos(\delta_i - \theta_i) - I_{qi} V_i sin(\delta_i - \theta_i) \tag{2.172}$$

$$\frac{\partial Q_{Gi}}{\partial \theta_i} = I_{di} V_i sin(\delta_i - \theta_i) + I_{qi} V_i cos(\delta_i - \theta_i) \tag{2.173}$$

$$\frac{\partial Q_{Gi}}{\partial V_i} = I_{di} cos(\delta_i - \theta_i) - I_{qi} sin(\delta_i - \theta_i) \tag{2.174}$$

$$\frac{\partial Q_{Gi}}{\partial I_{di}} = V_i cos(\delta_i - \theta_i) \tag{2.175}$$

$$\frac{\partial Q_{Gi}}{\partial I_{qi}} = -V_i sin(\delta_i - \theta_i) \tag{2.176}$$

$$\frac{\partial Q_{Gi}}{\partial \delta_i} = -I_{di} V_i sin(\delta_i - \theta_i) - I_{qi} V_i cos(\delta_i - \theta_i) \tag{2.177}$$

2.10.4 Algebraized Classical Generator Model

Applying the trapezoidal method (2.131)-(2.132), the swing equations for the classical model of generator result in the following algebraized equations:

$$F^{k+1}(\delta_i) = \delta_i^{k+1} - \frac{\triangle\, t}{2}(\omega_i^{k+1} - \omega_0) \tag{2.178}$$

$$F^{k}(\delta_i) = -\delta_i^{k} - \frac{\triangle\, t}{2}(\omega_i^{k} - \omega_0) \tag{2.179}$$

$$F^{k+1}(\omega_i) = \omega_i^{k+1} - \frac{\triangle\, t}{2M_i}\left(P_{Mi} - \frac{E_i V_i^{k+1} sin(\delta_i^{k+1} - \theta_i^{k+1})}{X_{di}^{'}} - D_i(\omega_i^{k+1} - \omega_0)\right) \tag{2.180}$$

$$F^k(\omega_i) = \omega_i^k - \frac{\triangle\, t}{2M_i}\left(P_{Mi} - \frac{E_i V_i^k sin(\delta_i^k - \theta_i^k)}{X_{di}^{'}} - D_i(\omega_i^k - \omega_0)\right) \tag{2.181}$$

The Jacobian elements added to the Jacobian of the power system are

$$\frac{\partial F(\delta_i)}{\partial \delta_i} = 1 \tag{2.182}$$

$$\frac{\partial F(\delta_i)}{\partial \omega_i} = -\frac{\triangle\, t}{2} \tag{2.183}$$

$$\frac{\partial F(\omega_i)}{\partial \theta_i} = -\frac{\triangle\, t}{2M_i}\left(\frac{E_i V_i cos(\delta_i - \theta_i)}{X_{di}^{'}}\right) \tag{2.184}$$

$$\frac{\partial F(\omega_i)}{\partial V_i} = \frac{\triangle\, t}{2M_i}\left(\frac{E_i sin(\delta_i - \theta_i)}{X_{di}^{'}}\right) \tag{2.185}$$

$$\frac{\partial F(\omega_i)}{\partial \delta_i} = \frac{\triangle\, t}{2M_i}\left(\frac{E_i V_i cos(\delta_i - \theta_i)}{X_{di}^{'}}\right) \tag{2.186}$$

$$\frac{\partial F(\omega_i)}{\partial \omega_i} = 1 + \frac{\triangle\, t}{2M_i} D_i \tag{2.187}$$

The Jacobian elements provided by the power injections (2.15) and (2.16) at generator terminals are

$$\frac{\partial P_{Gi}}{\partial \theta_i} = -\frac{E_i V_i cos(\delta_i - \theta_i)}{X_{di}^{'}} \tag{2.188}$$

$$\frac{\partial P_{Gi}}{\partial V_i} = \frac{E_i sin(\delta_i - \theta_i)}{X_{di}^{'}} \tag{2.189}$$

$$\frac{\partial P_{Gi}}{\partial \delta_i} = \frac{E_i V_i cos(\delta_i - \theta_i)}{X_{di}^{'}} \tag{2.190}$$

$$\frac{\partial Q_{Gi}}{\partial \theta_i} = -\frac{E_i V_i sin(\delta_i - \theta_i)}{X_{di}^{'}} \tag{2.191}$$

$$\frac{\partial Q_{Gi}}{\partial V_i} = -\frac{E_i cos(\delta_i - \theta_i)}{X'_{di}} \tag{2.192}$$

$$\frac{\partial Q_{Gi}}{\partial \delta_i} = \frac{E_i V_i sin(\delta_i - \theta_i)}{X'_{di}} \tag{2.193}$$

2.11 Discontinuity Conditions Calculation (Fault and Post-Fault conditions)

In order to carry out a transient stability analysis, a digital program requires being able to compute the disturbance and post-disturbance conditions of the algebraic system variables. At the instant of either application or clearing of a disturbance the dynamic variables cannot change instantaneously. Therefore, at these two instances of time such variables keep constant and their corresponding changes with respect to time are considered zero. The network and stator algebraic variables suddenly change with respect to the dynamics, thus the algebraic equations must be solved considering the dynamic variables as fixed inputs. In this case we used the Gauss-Seidel (GS) iterative method to solve the network equations, whereas the stator equations are updated in sequential form during the iterative process as will be explained in the next subsection. Since the digital code developed in this thesis only considers the positive sequence of the network (balanced three-phase power systems), uniquely the three-phase fault to ground is considered. Furthermore, in order to simulate a severe fault on transient stability, the fault is applied in one of the two terminal nodes of the transmission lines. This is done by considering the fault occurrence too close to the terminal node. In this context the fault can be solid and applied without fault admittance [Stagg and El-Abiad, 68].

2.11.1 Fault Conditions for the Two-Axis Generator Model

Applying or clearing a fault produces an instantaneous change of all nodal voltages of a power system. The voltage changes at generator terminals $\bar{V}_i$ make the stator currents $\bar{I}_{Gi}$ also change instantaneously; this in turn affects the voltage magnitude behind the impedance jX_{qi} which is given by $(X_{qi} - X'_{di})I_{di} + E'_{qi}$; see Eq. (2.79) which is phasor represented in Figure 2.6. In this thesis the fault conditions for the algebraic network and stator variables are calculated through the following steps:

1. *Building up the* $\bar{Y}^0_{bus}$ *sparse matrix at the pre-transient conditions prior to the moment of the fault application. All system loads must be converted to equivalent admittances and added to the diagonal elements in the* $\bar{Y}^0_{bus}$ *matrix as shown in* [Anderson and Fouad, 94] [Stagg and El-Abiad, 68].

2. *In order to simulate a fault admittance* $\bar{Y}_{fault}$ *should be in the diagonal element of* $\bar{Y}_{bus}$ *corresponding to the faulted node; thus, the new faulted* $\bar{Y}_{bus}$ *will be* $\bar{Y}^f_{bus} = \bar{Y}_{bus} + \bar{Y}_{fault}$. *If a solid three-phase fault to ground is simulated, the fault admittance must consider a very high value to simulate a short circuit. The same result is achieved by setting the voltage in the faulted node to zero.*

3. *Computing the voltage magnitude behind the reactance* jX_{qi} *as*

$$E_{qi} = (X_{qi} - X'_{di})I_{di} + E'_{qi} \tag{2.194}$$

4. *Computing a GS iteration using the magnitudes* E_{qi} *and the unchanged angles* δ_i *as fixed inputs in all generators during such an iteration. The voltage at the faulted node must be kept constant; thus, its corresponding equation must be excluded from the iterative process of the GS as follows:*

$$\bar{V}_i^{k+1} = \frac{1}{\bar{Y^f}_{bus}(i,i)}\left[-\sum_{j\in\Omega_i}\bar{Y^f}_{bus}(i,j)\bar{V}_j^k - \bar{Y}'_{di}\bar{E}_{qi}\right] \quad \forall i \neq (\text{\# faulted node}) \tag{2.195}$$

where $\bar{Y}'_{di}$ *is the inverse of the transient reactance on the* $d-axis$ *of the embedded generators.*

5. *The new calculated voltages at generator terminals* $V_i\angle\theta_i$ *for all* $i = 1,\ldots,n_g$ *will produce the new values for the stator currents, which are computed as*

$$I_{Gi}\angle\gamma_i = \frac{(E_{qi}\angle\delta_i) - (V_i^{k+1}\angle\theta_i^{k+1})}{jX_{qi}} \tag{2.196}$$

where the new values of I_{di} *and* I_{qi} *for* $i = 1,\ldots,n_g$ *are computed from* (2.76) *as follows:*

$$I_{di} + jI_{qi} = I_{Gi}e^{j(\gamma_i - \delta_i + \pi/2)} \tag{2.197}$$

the new values of I_{di} are used to update the new magnitudes E_{qi} in (2.194) to start the next GS iteration. The process is repeated until a specified tolerance is achieved.

6. *Finally, in order to adjust the new discontinuity conditions for algebraic variables with the state variables, a new NR solution as in (2.133) is computed. For this particular case, the digital program does not consider dynamic effects, and the state variables are kept constant during the iterative process by setting $\triangle t = 0$. In order to solve the NR, the initial conditions for the algebraic variables correspond to the discontinuity conditions calculated one instant after the fault application $Y^+ = \begin{bmatrix} I_{di} & I_{qi} & V_i & \theta_i \end{bmatrix}^T$, whereas, for the non-changed dynamic variables correspond to one instant before the fault application $X^- = \begin{bmatrix} E'_{di} & E'_{qi} & \delta_i & \omega_i & E_{fdi} \end{bmatrix}^T$.*

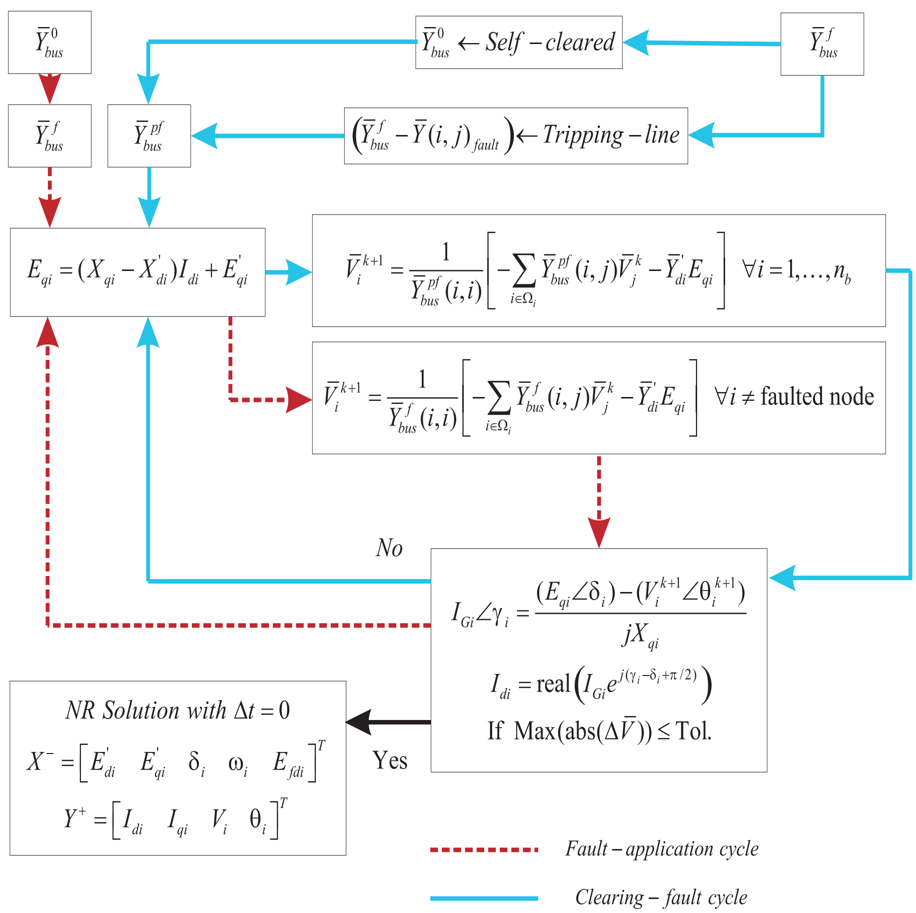

Figure 2.7: Flow diagram: fault-application and clearing-fault circuits.

For the calculation of the post-fault conditions, from step 1 $\bar{Y}^0_{bus}$ is already built up from the process of fault conditions. Instead step 2 the post-fault $\bar{Y}_{bus}$ matrix defined as $\bar{Y}^{pf}_{bus}$ should be calculated. If the fault is going to be self-cleared the pre-transient matrix $\bar{Y}^0_{bus}$ will be used again without changes as post-fault $\bar{Y}^{pf}_{bus} = \bar{Y}^0_{bus}$. However, if the fault is going to be cleared by tripping the faulted transmission line, the corresponding line element $\bar{Y}(i,j)_{fault}$ must be eliminated from the faulted $\bar{Y}^f_{bus}$, as $\bar{Y}^{pf}_{bus} = \bar{Y}^f_{bus} - \bar{Y}(i,j)_{fault}$.

In order to simulate the fault clearing, the voltage at the faulted node must again be a free variable, and its associated equation must be included once more in the GS process, the opposite of step 4, i.e. Eq. (2.195) must be computed for all $i = 1,...,n_b$ as follows:

$$\bar{V}_i^{k+1} = \frac{1}{\bar{Y}^{pf}_{bus}(i,i)}\left[-\sum_{j\in\Omega_i}\bar{Y}^{pf}_{bus}(i,j)\bar{V}_j^k - \bar{Y}'_{di}\bar{E}_{qi}\right] \quad \forall i = 1,...,n_b \tag{2.198}$$

Therefore by taking into account these considerations the post-fault conditions can be calculated by applying in the same way the remaining steps. Figure 2.7 shows the flow diagram according to the steps for the fault-application cycle as well as the clearing-fault cycle.

2.11.2 Fault Conditions for the Classical Generator Model

Since we have neglected the stator effect in the generator classical model, the algebraic fault conditions to be calculated are only the complex voltages in all system buses. Such voltage conditions are obtained by applying the Gauss-Seidel method at the instant that the fault has been applied. In this iterative process the algebraic variables instantaneously change. At this instant the time is considered not changing, thus during this process the dynamic variables δ_i and ω_i are kept constant. For the classical model the fault conditions calculation can be resumed in the following steps:

1. Computing steps 1 and 2 exactly the same as in the case for the Two-Axis model.
2. Computing the Gauss-Seidel iterative process using $E_i\angle\delta_i$ for $i = 1,\ldots,n_g$ as fixed inputs during the whole process. The voltage in the faulted node must be kept constant; thus, its corresponding equation must be excluded from the iterative GS process.
3. After achieving the specified tolerance in the GS process, one NR solution (2.133) is computed with $\triangle t = 0$.

The approach for clearing the fault is the same as the fault application, but the faulted node voltage must return to being a free variable, and its equation must be included again in the GS process. Besides, the self-cleared and line tripping forms of fault clearing are performed the same as in the case of the Two-Axis generator model.

2.12 Conclusions

The mathematical models of the power system components to be considered in this thesis have been described in this Chapter. These models have been developed based on the power-flow formulation and integrated in a single frame of reference by means of a set of differential-algebraic equations, in order to carry out transient and small signal stability analyses. Furthermore, the corresponding solution method for each kind of these studies were also described.

An approach to calculate discontinuity conditions of the system trajectories is proposed to compute the fault and post-fault initial conditions required in the transient stability analysis. This approach is based on a sequential application between the Gauss-Seidel and Newton-Raphson methods.

Chapter 3

DYNAMICAL TRAJECTORY SENSITIVITY THEORY

3.1 Introduction

The sensitivity theory arose from the mathematical interest of investigating the influence of the coefficients of the differential equations used to model the power systems dynamics. In [Bode, 45] Bode introduced a sensitivity definition in the frequency domain as the effect of the parameter changes on the dynamics of a system, which was applied to design feedback control systems. Also in the frequency domain, Horowitz [Horowitz, 63] [Horowitz and Shaked, 75] developed some methods to the design of low sensitivity conventional feedback control systems. Further design methods of electric networks were proposed in [Brogan, 74] [Bikhovsky, 58] [Bikhovsky, 64] in the frequency domain. Thus, the earlier sensitivity applications were done on modern control theory on the basis of the frequency domain. The analysis of sensitivities reached a great peak in applications on the basis of the time domain. At the end of the sixties, due to the development of state space methods in control engineering as well as the availability of the digital computer. This in turn introduced the general sensitivity problem to the automatic control systems [Nuguyen, 71] [Kokotovic and Rutman, 65] [Kokotovic and Sannuti, 68] [Kokotovic and Rutman, 66] [Kokotovic et al., 69] [Kokotovic, 64] [Cruz and Perkins, 64] [Cruz and Perkins, 65] [Cruz and Perkins, 66] [Perkins and Cruz, 66] [Perkins and Cruz, 65] [Perkins, 71] [Perkins et al., 72] and [Kreindler, 68] [Kreindler, 68-1] [Kreindler, 69].

In this thesis the $\beta - variations$ are defined as the parameter variations around a nominal value β_0 that do not affect the order of the mathematical model. Thus, a necessary condition for variations to be $\beta - variations$ is that $\beta_0 \neq 0$. Thus, the β parameters have been used to obtain trajectory sensitivities w.r.t. parameter variations of the electric power systems.

The dynamics of a system are considered a function of changes in the parameters. Such a function is called parameter sensitivity [Frank, 78] and is strictly defined as " the effect of parameter changes on the dynamics of a system, say, the time response, the state, the transfer function, or any other quantity characterizing the system dynamics". In this context, the trajectory sensitivity theory has recently been applied to the dynamical performance assessment of power systems by means of transient stability analysis. This theory has provided a very good qualitative insight of the parameter influence on the state trajectories of interest; by way of example, the trajectory sensitivity of the rotor angles are obtained with respect to any system time-invariant parameter. This allows us to identify not only the critical machines but also the most influential sensitivity parameter. Thus, the transient stability improvement can be considered a problem of controllability of transient trajectories by a change of the most sensitive parameters.

3.2 Trajectory Sensitivity Analysis

A power system can be analytically represented by a set of DAEs, as given by (3.1), where x is the state variable vector, such as rotor angles and speeds of generators, internal voltages on the axes, DC field voltages, etc., and whereas y is a vector of the algebraic variables such as complex nodal voltages and currents at the generator stator. In addition β is a set of non-time varying system parameters. The dynamics of equipment, e.g. generators and controls, are explicitly modeled by the set of differential equations through the function $f(\cdot)$. The set of algebraic equations $g(\cdot)$ expresses the mismatch power flow equations at each network node, as well as initial condition equations for state variables.

$$\begin{array}{lll} \dot{x} = f(x,y,\beta) & & f : \Re^{n+m+p} \rightarrow \Re^{n} \\ 0 = g(x,y,\beta) & & g : \Re^{n+m+p} \rightarrow \Re^{m} \\ x \in \boldsymbol{X} \subset \Re^{n} & y \in \boldsymbol{Y} \subset \Re^{m} & \beta \in \boldsymbol{\beta} \subset \Re^{p} \end{array} \tag{3.1}$$

Nonlinear dynamics due to a fault in the transmission network can be assessed by a transient stability study, which consists of solving Eq. (3.1) from the time t_0 of the disturbance inception to the clearing time t_{cl}, and from this time to the end of the study time period t_{end}, $T = [t_0, t_{cl}] \cup (t_{cl}, t_{end}]$. State trajectories associated with this dynamic behavior will vary with changes in the system parameters or the variables' initial conditions, and these variations can be quantified through a time domain sensitivity analysis. Nevertheless, there are two limitations in this approach which rely on repeated simulations: i) the computational burden required to calculate sensitivities, and ii) no quantitative measure of the proximity to instability of the power system.

It has been demonstrated that it is possible to find out in a rigorous approach how sensitive the trajectories of each state are to changes in system parameters or initial conditions. The theoretical treatment to obtain analytical equations of TS has been reported for both ODEs and DAEs systems [Tomovic and Vucobratovic, 72] [Hiskens and Pai, 00]. The sensitivities of equation (3.1) w.r.t. system parameters can be analytically found for the post-disturbance state $t \in (t_{cl}, t_{end}]$ by perturbing β from its nominal value β_0, and considering that $f(x,y,\beta)$ and $g(x,y,\beta)$ are functions of class C^1, which means that their partial derivatives of first order w.r.t. x, y and β exist and are continuous from the disturbance clearing time t_{cl} to the end of the study time t_{end}, for all $(x,y,\beta) \in (t_{cl}, t_{end}]\, \mathrm{x}\Re^{n\mathrm{x}m\mathrm{x}p}$ and initial conditions $x(t_{cl}) = x_{cl}$, $y(t_{cl}) = y_{cl}$.

3.3 Trajectory Sensitivity Theory for Differential Algebraic Equations Model

3.3.1 Analytical Formulation

Let β_0 be the nominal values of β, and assume that the nominal set of DAEs $\dot{x} = f(x,y,\beta_0)$, $0 = g(x,y,\beta_0)$ has a unique nominal trajectory solution $x(t,x_{cl},y_{cl},\beta_0)$ and $y(t,x_{cl},y_{cl},\beta_0)$ over $t \in (t_{cl}, t_{end}]$. Thus, for all β sufficiently close to β_0, the set of DAEs (3.1) has a unique perturbed trajectory solution $x(t,x_{cl},y_{cl},\beta)$ and $y(t,x_{cl},y_{cl},\beta)$ over $t \in (t_{cl}, t_{end}]$ that is close to the nominal trajectory solution. This perturbed solution is given by [Hiskens and Pai, 00]

$$x(\cdot) = x_{cl} + \int_{t_{cl}}^{t_{end}} f\left(x(\cdot), y(\cdot), \beta\right) ds \tag{3.2}$$

$$0 = g\left(x(\cdot), y(\cdot), \beta\right) \tag{3.3}$$

The sensitivities of dynamic and algebraic state vectors w.r.t. a chosen system parameter, $x_\beta = \partial x(\cdot)/\partial\beta$ and $y_\beta = \partial y(\cdot)/\partial\beta$, at a time t along the trajectory are obtained from the partial derivative of Eqs. (3.2) and (3.3) w.r.t. β:

$$\frac{\partial x(\cdot)}{\partial\beta} = \int_{t_{cl}}^{t_{end}} \left(\frac{\partial f(\cdot)}{\partial x}\frac{\partial x}{\partial\beta} + \frac{\partial f(\cdot)}{\partial y}\frac{\partial y}{\partial\beta} + \frac{\partial f(\cdot)}{\partial\beta} \right) ds \tag{3.4}$$

$$0 = \frac{\partial g(\cdot)}{\partial x}\frac{\partial x}{\partial\beta} + \frac{\partial g(\cdot)}{\partial y}\frac{\partial y}{\partial\beta} + \frac{\partial g(\cdot)}{\partial\beta} \tag{3.5}$$

Lastly, the smooth evolution of the sensitivities along the trajectory is obtained by differentiating Eqs. (3.4) and (3.5) w.r.t. t:

$$\begin{aligned} \dot{x}_\beta &= \tfrac{\partial f(\cdot)}{\partial x}\tfrac{\partial x}{\partial\beta} + \tfrac{\partial f(\cdot)}{\partial y}\tfrac{\partial y}{\partial\beta} + \tfrac{\partial f(\cdot)}{\partial\beta} \\ &\equiv f_x x_\beta + f_y y_\beta + f_\beta \qquad ; x_\beta(t_{cl}) = 0 \end{aligned} \tag{3.6}$$

and

$$\begin{aligned} 0 &= \tfrac{\partial g(\cdot)}{\partial x}\tfrac{\partial x}{\partial\beta} + \tfrac{\partial g(\cdot)}{\partial y}\tfrac{\partial y}{\partial\beta} + \tfrac{\partial g(\cdot)}{\partial\beta} \\ &\equiv g_x x_\beta + g_y y_\beta + g_\beta \qquad ; y_\beta(t_{cl}) = 0 \end{aligned} \tag{3.7}$$

where f_x, f_y, f_β, g_x, g_y and g_β, are time-varying matrices computed along the system trajectories.

3.3.2 Sensitivity Discretization

Once analytical Eqs. (3.6) and (3.7) have been formulated for trajectory sensitivities, the SDM is applied to solve these equations with those representing the power system dynamics (3.1). In this case, the trapezoidal rule is applied to algebraize the differential equations, such that sets of DAEs (3.1), (3.6), and (3.7) are expressed by the following set of algebraic-difference equations

$$F_1(\cdot) = x^{k+1} - x^k - \frac{\triangle t}{2}\left(f^{k+1} + f^k\right) = 0 \tag{3.8}$$

$$F_2(\cdot) = g^{k+1} = 0 \tag{3.9}$$

$$F_3(\cdot) = x_\beta^{k+1} - x_\beta^k - \frac{\triangle\, t}{2}\begin{pmatrix} f_x^{k+1}x_\beta^{k+1} + f_y^{k+1}y_\beta^{k+1} + f_\beta^{k+1} \\ +f_x^k x_\beta^k + f_y^k y_\beta^k + f_\beta^k \end{pmatrix} = 0 \tag{3.10}$$

$$F_4(\cdot) = g_x^{k+1}x_\beta^{k+1} + g_y^{k+1}y_\beta^{k+1} + g_\beta^{k+1} = 0 \tag{3.11}$$

where $\triangle\, t$ is the integration time step, and the superscript k is an index for the time instant t^k at which variables and functions are evaluated, e.g. $x^k = x(t^k)$ and $f^k = f(x^k, y^k)$. Nonlinear Eqs. (3.8) and (3.9) are coupled with the set of nonlinear DAEs given by Eq. (3.1) whereas Eqs. (3.10) and (3.11) correspond to the set of linear time-varying DAEs (3.6) and (3.7).

3.3.3 Linear Sensitivity Computation

The Newton-Raphson algorithm provides an approximate solution to (3.8) and (3.9) by solving for $\begin{bmatrix} \triangle\, x^k & \triangle\, y^k \end{bmatrix}^T$ in the linear problem $J_i \triangle X_i = -F(X_i)$, given in expanded form by Eq. (3.12), where J is known as the Jacobian matrix

$$\underbrace{\begin{bmatrix} I - \frac{\triangle t}{2} f_x^{k+1} & -\frac{\triangle t}{2} f_y^{k+1} \\ g_x^{k+1} & g_y^{k+1} \end{bmatrix}^i}_{J} \underbrace{\begin{bmatrix} \triangle\, x^k \\ \triangle\, y^k \end{bmatrix}^i}_{\triangle\, x^i} = -\underbrace{\begin{bmatrix} F^{k+1} + F^k \\ g^{k+1} \end{bmatrix}^i}_{F(\cdot)} \tag{3.12}$$

For given values $\begin{bmatrix} x^k & y^k \end{bmatrix}^T$, the method starts from an initial guess $x_0^{k+1} = x^k$ and $y_0^{k+1} = y^k$ and updates the solution at each iteration i, i.e. $\begin{bmatrix} x^{k+1} = x^k + \triangle\, x^k & y^{k+1} = y^k + \triangle\, y^k \end{bmatrix}^T$, until a convergence criterion is satisfied.

Once the states have been computed for a new time step, the linear equations (3.10) and (3.11) are rearranged to compute the trajectory sensitivities from the resulting set of linear equations (3.13)

$$\underbrace{\begin{bmatrix} I - \frac{\triangle t}{2} f_x^{k+1} & -\frac{\triangle t}{2} f_y^{k+1} \\ g_x^{k+1} & g_y^{k+1} \end{bmatrix}}_{J} \underbrace{\begin{bmatrix} x_\beta^{k+1} \\ y_\beta^{k+1} \end{bmatrix}}_{\boldsymbol{S}} = \underbrace{\begin{bmatrix} x_\beta^k + \frac{\triangle t}{2}\left(f_x^k x_\beta^k + f_y^k y_\beta^k + f_\beta^k + f_\beta^{k+1}\right) \\ -g_\beta^{k+1} \end{bmatrix}}_{\boldsymbol{B}} \tag{3.13}$$

The coefficient matrix on the left side of Eq. (3.13) corresponds to the Jacobian matrix used in the final NR iteration to solve for x^{k+1} and y^{k+1} at Eq. (3.12). Based on this observation, the computational burden for the calculation of trajectory sensitivities is substantially reduced because the coefficient matrix is already factored, and only a forward/backward substitution is required for the solution of x_β^{k+1} and y_β^{k+1} at each discrete time t^{k+1} of the post-disturbance integration period [Hiskens and Pai, 00].

3.4 Numerical Formulation

If it is considered a very small perturbation $\triangle\,\beta$ over the nominal parameter β_0 such that $\beta = \beta_0 + \triangle\,\beta$, the sensitivities x_β and y_β can also be calculated in a simpler way by assuming that the slope of the tangent line to the nominal trajectory solution $x(t, x_{cl}, y_{cl}, \beta_0)$, $y(t, x_{cl}, y_{cl}, \beta_0)$ at β_0 is well approximated by the slope of the secant line through $x(t, x_{cl}, y_{cl}, \beta_0)$, $y(t, x_{cl}, y_{cl}, \beta_0)$ and the perturbed trajectory solution $x(t, x_{cl}, y_{cl}, \beta)$, $y(t, x_{cl}, y_{cl}, \beta)$. Therefore, the numerical approximation of sensitivities is given as

$$x_\beta = \frac{\partial x(\cdot)}{\partial \beta} \approx \frac{\triangle\, x(\cdot)}{\triangle\,\beta} \equiv \frac{x(t, x_{cl}, y_{cl}, \beta) - x(t, x_{cl}, y_{cl}, \beta_0)}{\beta - \beta_0} \tag{3.14}$$

$$y_\beta = \frac{\partial y(\cdot)}{\partial \beta} \approx \frac{\triangle\, y(\cdot)}{\triangle\,\beta} \equiv \frac{y(t, x_{cl}, y_{cl}, \beta) - y(t, x_{cl}, y_{cl}, \beta_0)}{\beta - \beta_0} \tag{3.15}$$

This formulation is easier to implement than the analytical formulation presented in subsection 3.3.1 because sensitivities are computed at a given time $t \in (t_{cl}, t_{end}]$ by subtracting the perturbed and nominal trajectory solutions obtained from Eq. (3.1) and then by dividing over the parameter change $\triangle\,\beta$. However, this numerical method involves greater computations than the direct calculation of sensitivities using Eqs. (3.12) and (3.13) [Tomovic and Vucobratovic, 72] [Frank, 78]. The computational burden rises as the number of sensitivities to be computed augments.

3.5 Multi-Parameter Sensitivity

For a given fault scenario in a power system, the sensitivities with respect to *Np* suitable parameters can be calculated one at a time. If these sensitivities are calculated based on the numerical formulation described in Section 3.4, it is necessary to carry out *Np*+1 transient stability simulations to find the perturbed and nominal trajectory solutions. Additionally, Np+1 transient stability simulations have to be performed for each different fault scenario considered in the study, resulting in a prohibitive computational effort.

On the other hand, Eq. (3.13) has to be solved Np times at each time of the whole post-disturbance integration period to compute all sensitivities for a given fault scenario. However, the computational effort of this solution is significantly reduced because the Jacobian matrix J is already factorized. Thus it is only necessary to carry out Np forward/backward substitutions to calculate all sensitivities for a fault scenario. Based on this observation, the solution approach described in subsection 3.3.3 is extended to compute multi-parameter trajectory sensitivities associated with Np parameters of the system. In this case Eq. (3.13) is expressed as (3.16), which is solved Np times for the calculation of $x_{\beta i}^{k+1}$ and $y_{\beta i}^{k+1}$ $\forall_i = 1, \ldots, N_P$.

$$\underbrace{J \begin{bmatrix} S_{\beta 1} & S_{\beta 2} & \cdots & S_{\beta N_P} \end{bmatrix}}_{\boldsymbol{S}} = \underbrace{\begin{bmatrix} B_{\beta 1} & B_{\beta 2} & \cdots & B_{\beta N_P} \end{bmatrix}}_{\boldsymbol{B}} \tag{3.16}$$

3.6 Conclusions

This chapter provides a review of the trajectory sensitivity theory from electric power systems viewpoint. In this context, the trajectory sensitivity concept is addressed by means of the description of the trajectory sensitivity analysis, after a large disturbance has taken place in the power system. Furthermore, multi-parameter trajectory sensitivities are formulated mathematically with respect to system parameters from the set of Differential-Algebraic equations representing the power system. Finally, it is highlighted the advantage of using the analytical formulation of the trajectory sensitivities instead of its numerical formulation from the computational efficiency viewpoint.

Chapter 4

APPLICATION OF THE OBJECT ORIENTED PROGRAMMING PHILOSOPHY TO THE ANALYSIS OF ANGULAR STABILITY

4.1 Introduction

The Object Oriented Programming philosophy is arguably one of far reaching developments in the computer industry [Buzzi-Ferraris, 94] [Capper, 94]. It addresses the issue of large-scale software systems such as Data Base Management Systems [Barlow and Bernat, 94] (DBMS) and Graphical User Interfaces [Foley et al., 93] (GUI). Applications of the OOP technology to the solution of 'number-crunching' engineering-type problems are a powerful development. Most engineering systems consist of the interconnection of physical objects and OOP seems the natural approach for conducting the modeling and coding of such systems. C++ is an enhanced version of C. It retains C's efficient programming capabilities while adding the following characteristics: stronger type checking, extensive data abstraction features and support for OOP.

The Electricity Supply Sector has followed these developments very closely and some OOP applications to power systems appeared in open literature [Hakavik and Holen, 94] [Neyer et al., 90] and [Foley and Bose, 95]. The driving force behind these developments is the notion that existing commercial software of power systems is rapidly becoming a liability from both the technical and the economic point of view. Neyer, Wu and Imhof [Neyer et al., 90] argued that the use of conventional computer languages often leads to an inflexible code which is costly to maintain and to adapt to the very specific needs and changing requirements of each utility. In the discussion of that paper, Kirschen and Irisarri agree with the need to use OOP but caution against re-writing 'number crunching' power engineering applications using any OOP language owing to the inherent overheads associated with such computer languages.

Keeping these observations on board but bearing in mind that one of the most difficult problems with power systems software following a top-bottom design is its maintenance and upgrading as new features need to be added; this chapter describes the OOP applied to power systems. It touches on both power plant components and on the design and elaboration of an OOP transient stability program.

4.2 Objective Modeling of Power Networks

This section describes how the various OOP mechanisms are used when modeling the actual power system. In OOP the model is structured in much the same way as the physical network. The plant components that make up the power system consist of the established plant components such as generators, transformers, transmission lines, loads and mechanically-controlled shunt and series compensation.

A fundamental principle in OOP is to represent these real world objects as data objects in the computer program. Using the OOP terminology objects are instances of a class declaration that consist of both data and functions. All these modules can be regarded as methods which manipulate data from the objects that describe the power system. Figure 4.1 shows the global design that led to the implementation of the transient stability program in OOP.

The aggregation and inheritance relationship concepts are used to decompose the electric power system into classes [Foley and Bose, 95] [Manzoni et al., 97]. The aggregation concept refers to supply one component model by aggregating either physical or abstract entities. For instance, an integrated power system is made up of generators, transmission lines, transformers, etc., as shown in Figure 4.1. The inheritance relationship refers to extending the facilities of existing classes, such as data members and member functions, to new classes in order to avoid code duplication.

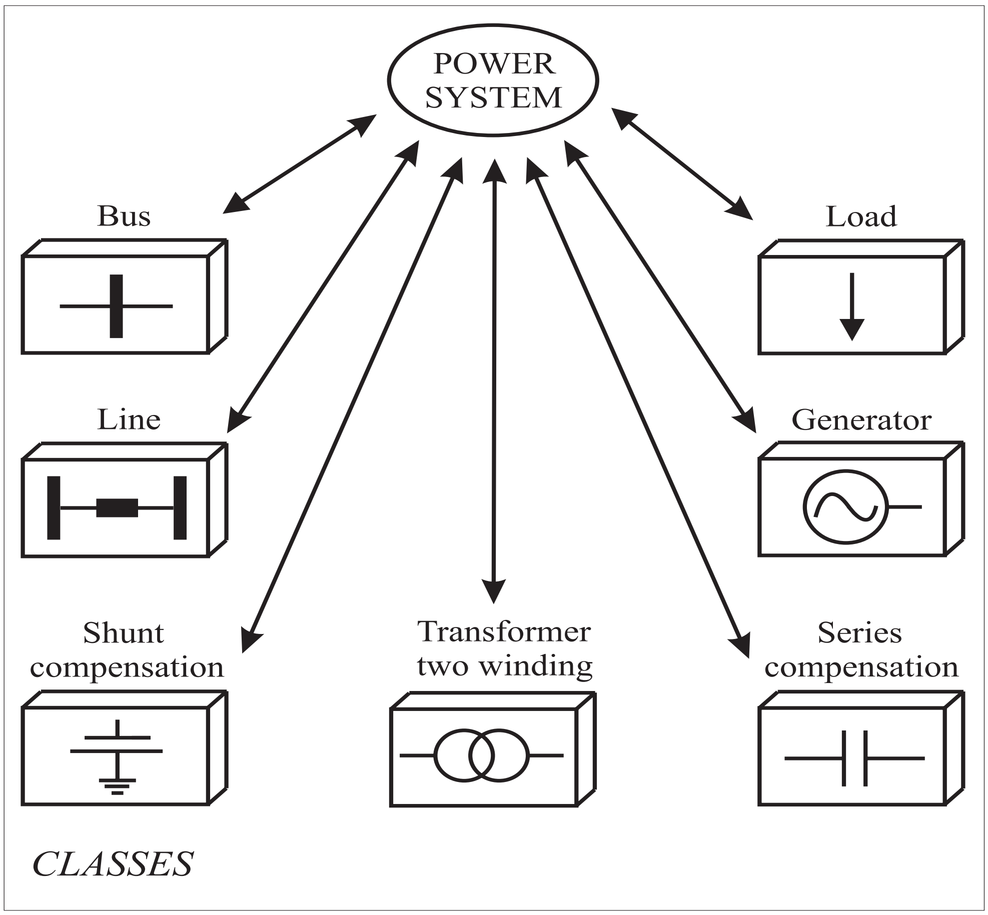

Figure 4.1: Global design of OOP transient stability.

The number of objects (plant components) associated with each class, and their physical and topological attributes, are read from an input file. These objects are stored in an array in order to efficiently handle their common data members and member functions.

Figure 4.2 shows the array of objects associated with the class *Bus* as well as the parameters associated with each object of the array.

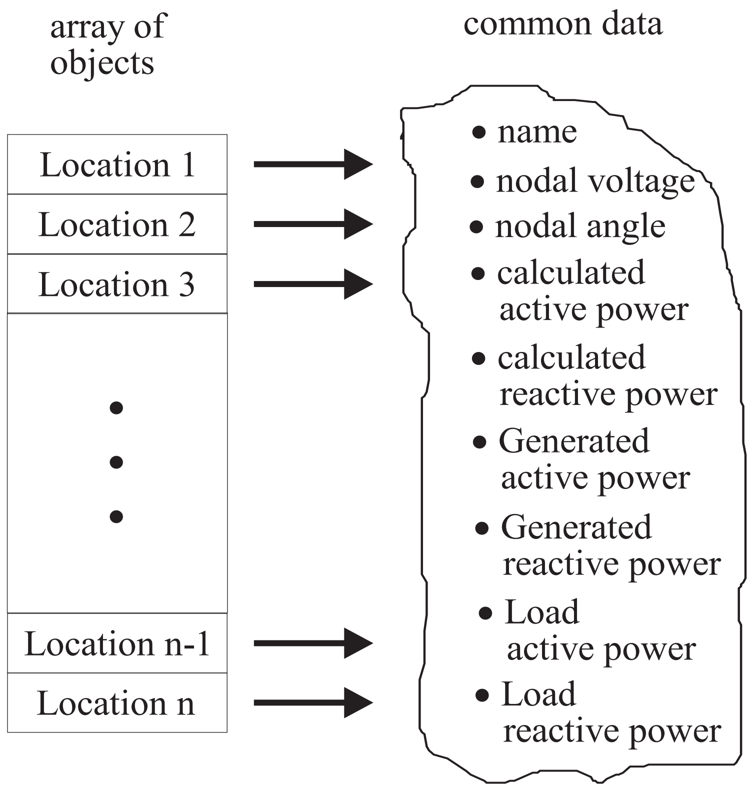

Figure 4.2: Array of objects of class *Bus*.

4.3 Derived types and data abstraction

The first step towards data abstraction is to bring together variables of different kinds into a single user-defined variable. In C++, the type class and the type struct may be used as the starting point for defining objects. These constructs are amenable to data abstraction because they allow for encapsulation of data and functions, using that data, into a single object. Classes are an essential feature of OOP techniques. A class is a user defined type, also called an abstract data type, which has its own collection of data, functions and operators.

The class *Component* has been defined as the base class [Fuerte et al., 98]. It consists of data members and function members that are common to all plant components, such as sending and receiving buses and transfer admittance matrix. The methods may include calculation of the power and mismatch equations, assembling, ordering and decomposition of the sparse Jacobian matrix as well as backward and forward substitutions. This class is illustrated in Figure 4.3 with its more important data and functions. The symbol (..) in Figure 4.3 indicates that the function contains arguments.

One of the central concepts of OOP is that we should deal with objects, such as transmission lines, rather than their circuit representation, such as models of transmission lines; the data associated with an object should be accessible by means of function calls which hide details of the class implementation. However, this encapsulation and data hiding can produce extra function calls, increasing the call-overhead of the program. This results in poorer run-time performance.

When a power formulation-based transient stability program utilizes a Newton-Raphson solution, a large part of the computational burden is associated with the fill-in of the Jacobian matrix, the LU factorization and the forward and backward substitution. In order to avoid a poor run-time performance due to call overhead when elements are assigned to the Jacobian matrix and vector of mismatches, it was found to be more efficient to include the sparse matrix and its associated functions into the class *Component* as shown in Figure 4.3 [Fuerte et al., 98]. It is realized that a OOP design calls for a separate sparse matrix class; however, principle was traded off for numeric efficiency. A Jacobian element is directly assigned to the sparse Jacobian matrix at the point in time in which it is computed with no additional function call. This philosophy contrasts with approaches followed in several other works [Hakavik and Holen, 94],[Manzoni et al., 97], where a Matrix class has been used.

```
class Component {                     //class name.
private:                              //the private part.
        int nse,nre;                  //Sending and receiving buses.
        int *order;                   //Ordering vector.
        int*newcol;                   //Vector of new columns.
        double **pt_G;                //Real and imaginary parts
        double**pt_B;                 // of transfer admittance matrix.
        double *pt_V;                 //Solution vector.
public:                               //the public part.
        Component();                  //Constructor.
        ~Component();                 //Destructor.
        int Sending(..);              //Assignation of sending node.
        int Receiving(..);            //Assignation of receiving node.
        void Power_Cal();             //Calculation of power equations.
        void Mismatch();              //Calculation of mismatch equations.
        void Ordering();              //Symbolic factorisation.
        void  LU();                   //Matrix decomposition.
        void Solve();                 //Backward and forward substitution.
        void set_dimension(..);       //Dimension of sparse jacobian
        Element **pt_J;               //Structure of sparse matrix off-diagonal elements.
        Diagonal_Element *diag;       //Structure of sparse matrix diagonal elements.
        void setdim_Ybus(..);         //Dimension of the sparse Ybus matrix.
        void Gauss_Seidel(..);        //Computation of discontinuity algebraic conditions.
        ElemYbus **pt_Ybus;           //Structure of the off-diagonal elements of the sparse
                                      //Ybus matrix.
        DiagYbus *diag_Ybus;          //Structure of the diagonal elements of the sparse
                                      //Ybus matrix.
        void set_DimSens(..);         //Dimension of the sensitivity functions vector.
        void solve_SMatrix();         //Backward and forward substitution for the
                                      //sensitivity system.
        double **pt_SMatrix;          //Sensitivity functions matrix.
        <additional methods>
        };
```

Figure 4.3: Class *Component*.

4.4 Class hierarchy and inheritance

While subroutines and functions are used in conventional programming in order to avoid code duplication, inheritance is the mechanism used in OOP. Inheritance is a way of creating new classes by extending the facilities of existing classes, such as data members and methods members defined at a certain level in the hierarchy. The facilities of the existing class are automatically available to all subclasses. The extended class is known as base class, and its extensions are known as derived classes. Using the syntax of C++, the class hierarchy is constructed by simply writing a reference to an old class in the header of the new class.

```
class ConTran : public Component{ //Class.
private:                                  //The private part.
        double rtp,xtp;                        //Primary winding data.
        double rts,xts;                   //Secondary winding data.
        double  go,bo;                    //Iron core data.
        double tapp,taps;                 //Taps transformer data.
        double phap,phas;                 //Phase shifter angles data.
public:                                   //The public part.
        ConTran();                        //Constructor.
        ~ConTran();                       //Destructor.
        void tran_par1(..);               //Assignation of electric parameters.
        void tran_par2(..);               //Assignation of controllable parameters.
        double Get_TapP(..);              //Accessing methods
        double Get_TapS(..);              //of taps and phase
        double Get_PhaP(..);              //shifting transformer
        double Get_PhaS(..);              //data.
        void admitance_matrix(..);        //Construction of transformer admittance.
        void Jacelements(..);             //Jacobian due FACTS devices.
        void change_tapp(..);             //Actualisation of primary tap.
        void change_taps(..);             //Actualisation of secondary tap.
        void change_phap(..);             //Actualisation of primary phase angle.
        void change_phas(..);             //actualisation of secondary phase angle.
        <additional  methods>
        };
```

Figure 4.4: Conventional transformer class implementation.

The implementation of the class corresponding to a conventional two winding-transformer is given in Figure 4.4. The newly derived class inherits data members and function members of the class *Component*. It illustrates how classes are implemented in the program. *ConTran* is the user defined name for the class. The private part consists of the parameters which are normally used to describe the electrical behavior of the two-winding transformer. The public part consists of the various methods associated with the class, such as data accessing methods and methods for building its transfer admittance matrix and for placing the individual contributions of the components into the Jacobian matrix. A constructor is invoked whenever an object is created, and a destructor is invoked whenever an object is destroyed.

4.5 Sparsity techniques

In practice the formation of actual matrices is not desirable. Instead, the Jacobian and nodal admittance matrices of the power network are stored and processed in vector form, where only non-zero elements are explicitly handled [Tinney and Walke, 67]. In languages with no linked lists facilities several one-dimensional arrays and complicated programming schemes are required in order to obtain efficient solutions of power system analysis. In C++ the programming efforts are greatly reduced due to the existence of pointers and structures.

In theory, C++ allows sparsity techniques to be implemented by following a rather purist OOP philosophy [Buzzi-Ferraris, 94],[Hakavik and Holen, 94]. However, this approach incurs excessive cpu time overhead and has not been followed in this work. Instead, a more efficient OOP approach has been adopted where sparsity was implemented as an array of pointers pointing to structures. Structures allow the encapsulation, in a single variable, of all the information associated with a sparse coefficient, e.g. value, column and pointer to the next element. Pointers are used to move from one structure to another. This is illustrated in Figure 4.5.

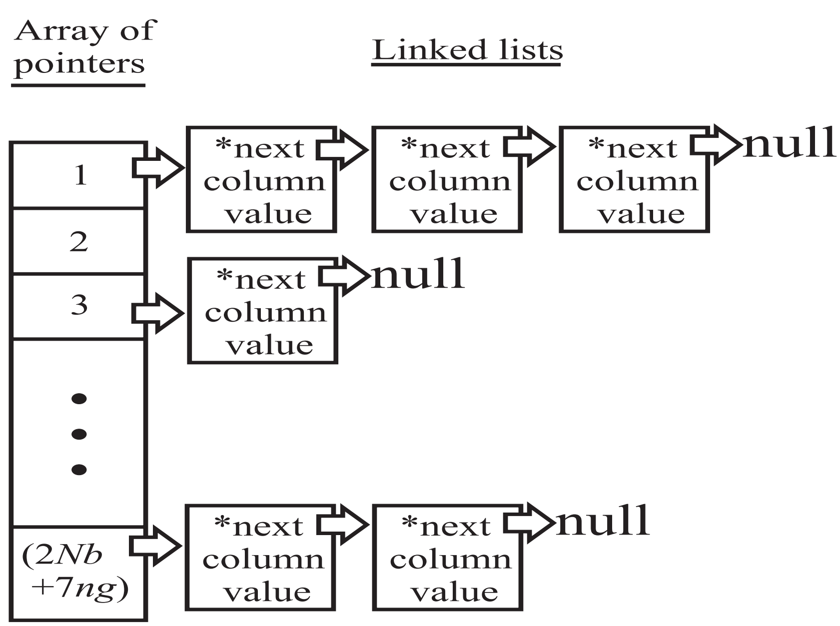

Figure 4.5: Linked lists for storing of sparse Jacobian.

An array of pointers is created with the same size as the number of rows in the matrix. Each element points to the address of the start of a list. Thus, one list is created for each row. In the case of the Jacobian matrix for power formulation-based transient stability, an array of pointers of size equal to $2*n_b+7*n_g$ is created when the Two-Axis generator model is considered, whereas $2*(n_b+n_g)$ for the classical generator model. n_b and n_g are the number of buses and embedded generators in the network, respectively. Each list consists of one or more structures containing information associated with off-diagonal elements only. The information associated with diagonal elements is stored in a separate array of structures. Both structures are shown in Figure 4.6.

```
struct Element
{
  double value;
  int column;
  Element *next;
}

struct Diagonal
{
  double value;
  int new column;
  int elements;
}
```

Figure 4.6: Structures of sparse Jacobian matrix elements.

Struct *Element* contains the column location of the off-diagonal element, as well as its value and a pointer which points to the address of the structure corresponding to the next off-diagonal element in that row. The pointer of the last structure in the list is set equal to zero to indicate the end of the list. The information pertaining to the Jacobian diagonal element in a given row is stored in struct *Diagonal*. It consists of its numeric value, the number of off-diagonal elements in that row, and the elimination order as determined by Tinney's second ordering scheme [Tinney and Walke, 67].

4.6 Time domain solution

The Newton-Raphson solution of the transient stability study requires the calculation of the functions vector and the Jacobian matrix, in factorized form, at each iterative step. The functions vector requires the active and reactive power as well as the dynamic contributions from the generator and the load objects, while the calculated part of the power mismatch vector requires contributions from the line, transformer and shunt objects. Figure 4.7 shows the class *Bus* where data such as nodal voltages, generation power, load power, and the calculated power have been defined as data members to each node in the electric power system.

```
class Bus {                          //class name.
private:                             //the private part.
        char name[NAME];             //Name of node;
        double voltage;              //Nodal voltage magnitude.
        double angle;                //Nodal voltage angle.
        double vnom;                 //Nominal voltage magnitude.
        double anom;                 //Nominal voltage angle.
        double Vre;                  //Real and imaginary parts
        double Vim;                  //of the nodel voltages.
        double PBus;                 // Active power calculated.
        double QBus;                 //Reactive power calculated.
        double Pgen;                 //Active power in generator.
        double QGen;                 //Reactive power in generator.
        double PLoad;                //Active power load.
        double QLoad;                //Reactive power in load.
public:                              //the public part.
        Bus();                       //Constructor.
        ~Bus();                      //Destructor.
        void set_parnod (..)         //Node atributes.
        void set_voltage (double p1=0) {voltage=p1;}
        void set_angle (double p1=0) {angle=p1;}
        void set_PBus (double p1=0){PBus+=p1;}
        void set_QBus (double p1=0) {QBus+=p1;}
        void set_PGen (double p1=0)         {PGen+=p1;}
        void set_QGen (double p1=0) {QGen+=p1;}
        void set_PLoad (double p1=0) {PLoad+=p1;}
        void set_QLoad (double p1=0) {QLoad+=p1;}
        <additional methods>
        };
```

Figure 4.7: Class *Bus.*

Construction of the functions vector and the factorized Jacobian matrix consists of the computation and insertion of all elements corresponding to all class objects in the overall Jacobian structure. The insertion of elements is reached by finding their location in the functions vector and the factorized matrix by considering a superposition approach. For each plant component, the contribution terms of the functions and Jacobian are computed and inserted according to the plant component model and the bus or buses to which the plant component is connected. These buses determine the location of the functions and the individual Jacobian terms in the overall functions vector and Jacobian structure. The contributions of the line, transformer, load, shunt and generator objects to the functions vector and Jacobian are shown in Figure 4.8.

$$\begin{bmatrix} +\partial P_{ij}/\partial\theta_i & +\partial P_{ij}/\partial\theta_j & +\partial P_{ij}/\partial V_i & +\partial P_{ij}/\partial V_j \\ +\partial P_{ji}/\partial\theta_j & +\partial P_{ji}/\partial\theta_i & +\partial P_{ji}/\partial V_j & +\partial P_{ji}/\partial V_i \\ +\partial Q_{ij}/\partial\theta_i & +\partial Q_{ij}/\partial\theta_j & +\partial Q_{ij}/\partial V_i & +\partial Q_{ij}/\partial V_j \\ +\partial Q_{ji}/\partial\theta_j & +\partial Q_{ji}/\partial\theta_i & +\partial Q_{ji}/\partial V_j & +\partial Q_{ji}/\partial V_i \end{bmatrix} \begin{bmatrix} \Delta\theta_i \\ \Delta\theta_j \\ \Delta V_i \\ \Delta V_j \end{bmatrix} = - \begin{bmatrix} +P_{ij}(\theta_i,\theta_j,V_i,V_j) \\ +P_{ji}(\theta_j,\theta_i,V_j,V_i) \\ +Q_{ij}(\theta_i,\theta_j,V_i,V_j) \\ +Q_{ji}(\theta_j,\theta_i,V_j,V_i) \end{bmatrix}$$

(a)

$$\begin{bmatrix} +\partial P_{Li}/\partial V_i \\ +\partial Q_{Li}/\partial V_i \end{bmatrix} \begin{bmatrix} \Delta\theta_i \\ \Delta V_i \end{bmatrix} = - \begin{bmatrix} +P_{Li}(V_i) \\ +Q_{Li}(V_i) \end{bmatrix}$$

$$\left[+\partial Q_{Sh}/\partial V_i\right]\left[\Delta V_i\right] = -\left[+Q_{Sh}(V_i)\right]$$

(b)

$$\begin{bmatrix} +\partial P_{Gi}/\partial\theta_i & +\partial P_{Gi}/\partial V_i & \partial P_{Gi}/\partial I_{di} & \partial P_{Gi}/\partial I_{qi} & \partial P_{Gi}/\partial\delta_i \\ +\partial Q_{Gi}/\partial\theta_i & +\partial Q_{Gi}/\partial V_i & \partial Q_{Gi}/\partial I_{di} & \partial Q_{Gi}/\partial I_{qi} & \partial Q_{Gi}/\partial\delta_i \\ \partial V_{di}^{St}/\partial\theta_i & \partial V_{di}^{St}/\partial V_i & \partial V_{di}^{St}/\partial I_{qi} & \partial V_{di}^{St}/\partial E'_{di} & \partial V_{di}^{St}/\partial\delta_i \\ \partial V_{qi}^{St}/\partial\theta_i & \partial V_{qi}^{St}/\partial V_i & \partial V_{qi}^{St}/\partial I_{di} & \partial V_{qi}^{St}/\partial E'_{qi} & \partial V_{qi}^{St}/\partial\delta_i \\ & \partial FE'_{di}/\partial I_{qi} & & \partial FE'_{di}/\partial E'_{di} & \\ \partial FE'_{qi}/\partial I_{di} & & \partial FE'_{qi}/\partial E'_{qi} & & \partial FE'_{qi}/\partial E_{fdi} \\ & \partial F\delta_i/\partial\delta_i & & \partial F\delta_i/\partial\omega_i & \\ \partial F\omega_i/\partial I_{di} & \partial F\omega_i/\partial I_{qi} & \partial F\omega_i/\partial E'_{di} & \partial F\omega_i/\partial E'_{qi} & \partial F\omega_i/\partial\omega_i \\ & \partial FE_{fdi}/\partial V_i & & \partial FE_{fdi}/\partial E_{fdi} & \end{bmatrix} \begin{bmatrix} \Delta\theta_i \\ \Delta V_i \\ \Delta I_{di} \\ \Delta I_{qi} \\ \Delta E'_{di} \\ \Delta E'_{qi} \\ \Delta\delta_i \\ \Delta\omega_i \\ \Delta E_{fdi} \end{bmatrix} = - \begin{bmatrix} P_{Gi}(\theta_i,V_i,I_{qi},I_{di},\delta_i) \\ Q_{Gi}(\theta_i,V_i,I_{qi},I_{di},\delta_i) \\ V_{di}^{St}(\theta_i,V_i,I_{qi},E'_{di},\delta_i) \\ V_{qi}^{St}(\theta_i,V_i,I_{di},E'_{qi},\delta_i) \\ FE'_{di}(I_{qi},E'_{di}) \\ FE'_{qi}(I_{di},E'_{qi},E_{fdi}) \\ F\delta_i(\delta_i,\omega_i) \\ F\omega_i(I_{di},I_{qi},E'_{di},E'_{qi},\omega_i) \\ FE_{fdi}(V_i,E_{fdi}) \end{bmatrix}$$

(c)

Figure 4.8: Components contribution to the full Jacobian matrix and solution vector: (a) lines and transformers. (b) loads and shunt compensators (c) generators.

Figure 4.8(a) shows the element contributions in both directions from either a line or transformer connected between the buses i and j. The part (b) of the figure gives the load and shunt compensation contributions embedded in the bus i. Lastly, in the part (c) of the figure, both algebraic and dynamic contributions are shown for the Two-Axis generator model embedded in the ith bus. The sign + indicates the element addition to the overall Jacobian matrix and the vector of functions by following the superposition approach.

4.7 Conclusions

This chapter has addressed the computational implementation of the proposed model to analyze the transient stability of power systems. Such an implementation consisted of modeling the physical electric power components as data objects by following an Object Oriented Programing philosophy. Each type of plant component is declared as a class, whereas each instance of such a class is denominated an object. The objects are made up of both data and functions such as system parameters and equations, respectively.

It is also presented the methodology to construct a sparse Jacobian matrix based on linked lists of abstract data, which are the component contributions to the full Jacobian matrix of the power system. The proposed methodology for the computational implementation follows the superposition principle.

Chapter 5

APPLICATIONS OF TS FOR TRANSIENT STABILITY ANALYSIS

5.1 Introduction

Advances in Flexible AC Transmission Systems controllers have led to their application in improving electric power systems' controllability [Acha et al., 04] [Song and Johns, 99]. It has been recognized that the location of these controllers has a large impact on their performance with regard to the control objective to be fulfilled. The best allocation for one objective may be less suitable for another objective. This has motivated the development of several kinds of approaches to find proper locations of FACTS controllers in order to improve the power system static or dynamic performance. Methodologies based on singular value decomposition [Gamm and Golub, 98], bus participation factor [Mansour et al., 94], augmented Lagrange multipliers [Fang and Ngan, 99], heuristic methods [Paterni et al, 99] [Gerbex et al., 03], mixed integer linear programming [Lima et al., 03] and a sensitivity-based approach [Cañizares and Faur, 99] [Singh and David, 01] have been proposed to allocate controllers to satisfy suitable steady-state control objectives. On the other hand, proper locations to improve damping of low-frequency electromechanical oscillations have been determined based on modal analysis [Martins and Lima, 90] [Okamoto et al., 95] [Wang, 99] and residue method [Sadikovic et al., 06] [Magaji and Mustafa, 08].

Transient stability analysis is also an essential study in the operation and planning of an electric power system [Kundur, 94]. If this study determines that a rotor angle transient instability takes place due to large electromechanical oscillations among generation units and lack of synchronizing torque on the system, control actions have to be taken to prevent partial or complete service interruption. Among different preventive control measures, it is possible to apply series compensation in a proper place to regain an acceptable state of equilibrium after the disturbance by improving the system's stability condition [Kundur, 94]. The stability condition can be computed by a time domain simulation, which is applicable for arbitrarily complicated models, and it is feasible for large-scale power system analysis. However, this simulation only provides information about a single scenario, and repeated simulations have to be done to assess the degree of system stability for any change in system operating conditions.

The system stability condition can be examined from the viewpoint of system energy rather than in time domain through the TEF Method [Fouad and Vittal, 92] [Pai, 89]. In this method, the numerical integration of the system dynamic equations is limited to the fault-on period to determine the energy associated with the system at the end of the disturbance. A major advantage of the TEF method is that it can provide a quantitative measure of how stable or unstable a particular case may be in terms of the transient energy margin. This in turn allows sensitivity analysis to give information about the effect of system parameter variation on system stability. In this context, based on the TEF method, a critical energy sensitivity analysis of the post-fault period is proposed in [Zhao et al., 94] to determine the effective location of FACTS devices, where the entire network is reduced to the internal node of the machines. Analytical expressions for energy margin sensitivity are proposed in [Vittal et al., 89] to assess the effect of change of line impedance on the energy margin for a specified contingency scenario, considering the machine internal node formulation. This methodology is extended in [Shubhanga and Kulkarni, 02] to determine the effectiveness of shunt and series FACTS devices by considering structure preserving energy margin sensitivities. Despite that the results presented in [Zhao et al., 94] [Vittal et al., 89] and [Shubhanga and Kulkarni, 02] demonstrate the versatility of the TEF method for both transient stability and sensitivity analysis, its application becomes increasingly complex when detailed models of power system components are considered or when dealing with DAE models of power systems [Laufenberg and Pai, 98], and when a number of parameters have to be taken into account in the sensitivity analysis [Chatterjee and Ghosh, 07].

Recently, TS analysis has been proposed as an alternative to the TEF-based methods in order to obtain information about the power system performance [Laufenberg and Pai, 98].

In this approach, a linearization is carried out around a nominal trajectory rather than around an equilibrium point, such that it is possible to assess variations in the nominal transient trajectory resulting from perturbations in the underlying parameters and/or initial conditions [Laufenberg and Pai, 98]. In addition, the analytical formulation of this approach overcomes the need for repetitive simulations to judge how changes in operating conditions influence the system stability. Applications of TS include the study of parameter uncertainty in system behavior [Hiskens et al., 00-1] [Hiskens and Alseddiqui, 06], determination of well-conditioned parameters for reliable estimation [Sanchez et al., 88] [Benchluch and Chow, 93] [Hiskens, 01], and determination of critical machines which are likely to go unstable for a given loading condition and a specified contingency [Nguyen and Pai, 03], among others [Hiskens and Pai, 00-2].

5.2 Location of series-connected controllers on transient stability

Owing to the fact that TS analysis provides both a qualitative measure on how stable or instable a particular case may be, and valuable insights into the influence of parameters on the nominal transient trajectory of the system, this approach was applied to successfully analyze the Nordel power grid disturbance on January 1, 1997 [Hiskens and Akke, 99]. Sensitivities of relative rotor angle w.r.t. line impedances were used to identify which line was the most sensitive w.r.t. system stability and to indicate the effect of this line w.r.t. different generators in the system. Based on these results, authors suggested that the TS approach could be used to choose effective locations of FACTS devices. This idea is revisited and applied in this study in order to determine the suitable locations of series-connected controllers, from a transient stability viewpoint.

Since the improvement of transient stability can be considered a problem of controlling transient trajectories by a change in parameters, TS can be used to judge the effectiveness of FACTS controllers in improving stability, as was proposed in [Chatterjee and Ghosh, 07] considering static models of a TCSC and a STATCOM. The effects of these compensators were assessed by placing them individually at each transmission line, one at a time, and calculating a post-fault stability condition based on the numerical formulation of the trajectory sensitivity. In this case, sensitivities of state trajectories w.r.t. system parameters are found by perturbing the selected parameter from its nominal value, and making the division of the changes in the state variables over the parameter perturbation: $\Delta x/\Delta\beta$, at each integration time. This approach requires two time-domain simulations for each sensitivity, and the selection of the size of the parameter perturbation. The latter is heuristically selected so that the numerical sensitivity could be very close to the analytically calculated trajectory sensitivity value.

The most effective location of series compensators can be obtained by the approach suggested in [Chatterjee and Ghosh, 07] for a given fault scenario after computing Γ transient stability simulations, where $\Gamma = (1 + \#\text{of lines impedances suitable to be compensated } (Np))$. The best location corresponds to the transmission line that produces the highest sensitivity value of state trajectories. A drawback of this numerical approach is that the computational burden can be significant if sensitivities w.r.t. many parameters are required. Furthermore, as the number of fault scenarios increases by nf times, the required number of time-domain simulations to calculate sensitivities rises to $\Gamma_{total} = nf \times \Gamma$ increasing the computational cost tremendously. A radical approach based on the analytical TS described in Chapter 3 is applied in this case to avoid the problem of performing a large number of time-domain simulations to determine the most effective location of series compensation. This consists on analytically formulating the trajectory sensitivities based on a structure preserving model of the power system, with the following advantages over the computation of multi-parameter sensitivities based on numerical approximations: i) For a given fault scenario, only one transient stability simulation is necessary to determine all sensitivities; ii) The number of transient stability simulations increases in direct proportion to the number of fault scenarios, but it is not a function of the Np parameters considered in the sensitivity study. These two characteristics importantly contribute to the reduction of the computational burden required to find the best location of series-connected controllers from a transient stability viewpoint.

The goal of this section is to determine the best candidate line to be compensated to improve the transient stability for a set of possible faults taking place in a specified system geographic area. This improvement is quantified through a sensitivity index considering the sensitivities w.r.t. the series susceptance of transmission lines. In order to consider a critical fault condition in the network, the applied disturbance consists of a three-phase to ground fault at one end of the transmission element, which is cleared by tripping the faulted element [Sauer and Pai, 98].

5.2.1 Sensitivity quantification

Based on the observation that when the system approaches its stability boundary the trajectory sensitivities approach infinity [Laufenberg and Pai, 98], it is possible to associate sensitivity information with the stability level of the system for a particular system parameter. The line susceptance effect on the system stability is measured by computing sensitivities of rotor angles trajectories w.r.t. transmission line susceptances, and measuring the proximity to instability.

An index of proximity to instability is determined based on the sensitivity norm for a n_g – machines system given by [Nguyen and Pai, 03],

$$SN_i(t) = \sqrt{\sum_{k=1}^{n_g} \left(\left(\frac{\partial \delta_k(t)}{\partial \beta_i} - \frac{\partial \delta_j(t)}{\partial \beta_i} \right)^2 + \left(\frac{\partial \omega_k(t)}{\partial \beta_i} \right)^2 \right)} \qquad \forall i = 1, \ldots, N_P \tag{5.1}$$

where j denotes the reference machine, and β_i represents the ith line susceptance of the power system.

The growth in the peak values of trajectory sensitivities indicates an underlying stability problem, and ideally $SN_i(t)$ should be infinite at the point of the system instability. Bearing this in mind, the index of proximity to instability is defined as the inverse of $SN_i(t)$, $\eta_i = 1/max|SN_i(t)|$, which will approach zero as the system moves toward instability [Nguyen and Pai, 03]. Based on this result, the most effective location of series compensation corresponds to a transmission line whose small perturbations in its susceptance produce the lowest value of η_i.

5.2.2 Comparison of the proposed method with other approaches

The TEF method has been used to determine the effective location of series controllers to improve the transient stability performance of a power system based on energy margin sensitivities. The energy margin is defined as the difference between critical energy W_{cr} and the value of the energy function at the corresponding clearing time W_{cl}. The effective location of FACTS controllers was determined in [Zhao et al., 94] using sensitivity analysis of critical energy. In this approach, the entire network is reduced to the internal node of the machines. Based on the same machine internal node formulation, energy margin sensitivity equations to line impedance changes are derived in [Vittal et al., 89]. The disadvantages of these proposals based on internal node representation are as follows [Fouad and Vittal, 92] [Shubhanga and Kulkarni, 02]: i) The formulation is limited for load models of constant impedance type and classical model for generators. ii) The inclusion of FACTS controllers embedded at network nodes is not feasible. iii) An energy function with a path dependent term cannot be strictly defined for networks reduced to the machine internal node, because it is not possible to test the sign definite properties of energy function. To overcome these difficulties, a Structure Preserving Energy Margin based-sensitivity analysis was proposed in [Shubhanga and Kulkarni, 02] to determine the effectiveness of shunt and series compensations for a specific contingency scenario. In this case, the topology of the network is retained, which allows modeling constant power type loads. The following assumptions are made to derive the structure preserving energy function: i) Generators are represented by the classical model. ii) Transmission losses are neglected. iii) It is assumed that a fixed amount of compensation, determined by the control strategy, is introduced after fault clearing. Analytical expressions for energy margin sensitivity indices are derived in terms of local signals to decide the effective location of controller devices considering the post-fault uncompensated system. Although the TEF-based sensitivity techniques described above offer a quantitative and qualitative description of the change in transient stability behavior due to changes in system parameters, their application becomes increasingly complex when considering detailed models of the power system components. This is because the application of energy function is not mathematically justified for detailed generator models with controllers. In addition, it is difficult to accurately compute an energy margin for all contingencies when the fault-on dynamics contain fast dynamics [Sauer et al., 89]. The motivating factor for the use of the trajectory sensitivity approach is its theoretical robustness, which is independent of unstable equilibrium point calculations and model complexity. The drawback is the need to integrate more equations. As mentioned in Section 3.4, the numerical approach to compute sensitivities can be applied to assess the best location of series compensation from a transient stability viewpoint. However, if the controller location is determined considering nf fault scenarios and Np sensitivity parameters, the required number of time-domain simulations will be $nf(1+Np)$. For the same case, the analytical approach described in this chapter reduces the number of simulations to only nf, therefore the main drawback of a huge number of simulations required to locate a series controller has been eliminated. Details of the number of simulations required for both approaches are given in the study cases presented in upcoming sections.

5.2.3 Study cases

The effectiveness of the proposed approach to identify the best location of series-connected controllers is numerically assessed in this section by analyzing the WSCC 9-buses, 3-generators system [Sauer and Pai, 98] and the New England 39-buses, 10-generators system [Pai, 89]. The diagrams and data of these power systems are given in Appendix C and D, respectively. For the purpose of the studies, the Two-Axis generator model is considered, which includes a simple faster exciter loop containing max/min ceiling limits, a field winding on $d-$axis and a damper winding on both $d-$axis and $q-$axis [Sauer and Pai, 98]. The constant impedance model is considered to represent the loads, whereas, the π model is considered for the transmission line (the transmission system losses are considered). Lastly, a Two-winding model including the magnetizing branch effect is used to represent the conventional transformers [Fuerte et al., 98].

5.2.3.1 WSCC 9-buses, 3-generators system

For this system, faults are applied one at a time at both ends of a selected transmission line, and sensitivity indices are computed for all transmission lines to determine which is the most suitable to be compensated. A stressed scenario is attained by considering the clearance of the kth fault at its critical clearing time (CCT), $t_{cl}^{k} = t_{cct}^{k}$. The results computed by the proposed approach are reported in Table 5.1 as follows: column one indicates the faulted line and column two reports the fault location. Column three indicates the critical clearing time of each fault. Lastly, the transient sensitivity index w.r.t. each transmission element η_{β} is reported for the rest of columns. For a given fault scenario, the indices are reported by row w.r.t. the lines embedded in the system after the fault has been cleared, the empty cell corresponds to the tripped line. The values of these indices are considered base sensitivity indices to assess the impact of the series-connected controllers and are denoted by η_{β}. From a computational burden viewpoint, it is important to point out that 12 simulations are only required to obtain all results based on the proposed approach, whilst 72 simulations are required if the numerical TS method is used.

According to Subsection 5.2.1, the most sensitive line is identified by the column with smallest indices η_{β} the Table 5.1. From results reported in Table 5.1, it is observed that

Table 5.1: η_β for each faulted element for the WSCC system.

Line	Fault near node	t_{cct}(ms)	$7-8$	$8-9$	$7-5$	$9-6$	$5-4$	$6-4$
$7-8$	7	151	-	0.199	0.003	0.103	0.126	0.427
	8	233	-	0.959	0.010	0.128	0.043	0.676
$8-9$	8	254	0.293	-	0.009	0.027	0.036	0.413
	9	208	7.204	-	0.015	0.007	0.728	0.025
$7-5$	7	132	0.002	0.004	-	0.0004	0.014	0.002
	5	252	0.002	0.003	-	0.0003	0.008	0.001
$9-6$	9	180	0.533	0.046	0.004	-	0.022	0.481
	6	310	1.098	0.021	0.002	-	0.010	0.167
$5-4$	5	335	0.197	0.042	0.023	0.006	-	0.038
	4	258	0.177	0.331	0.059	0.016	-	0.094
$6-4$	6	261	1.616	4.580	0.177	4.814	0.663	-
	4	252	4.608	0.231	0.014	0.108	0.079	-

the best candidate line to be compensated varies according to the fault location. By way of example, for a fault in line 6-4 near bus 4, the transient stability of the system is most affected by changes in the susceptance line connecting buses 7-5, B_{7-5}. Therefore, it is the best possible location of the series compensation for this fault scenario. The second option for allocating the compensation is at the line connected between buses 5-4. On the other hand, the best global improvement of the system transient behavior will be achieved by compensating the most sensitive line for the majority of the fault cases, which corresponds to the line connected between buses 7-5. The second option is to apply the compensation at the line connected between buses 9 and 6.

Trajectory sensitivity analysis only indicates which line has to be compensated, but it does not indicate the type and degree of compensation to have a specific improvement on the system transient stability. Although a proper solution of this issue is out of the scope of this thesis, this problem has been addressed by a simple comparison of the system transient behavior with and without a specified level of compensation. This comparison has been used to validate the results obtained by sensitivity analysis.

Numerical validation of the stability index correctness is undertaken by the stability study of a fault taking place on line 6-4 near node 4, which is cleared by tripping the faulted line at the critical clearing time of $t_{cct} = 252$ms. Capacitive compensation with a value of 30% of the line series inductance is located on the two lines with greater global effect on the transient performance: lines 7-5 and 9-6, one at a time. Figure 5.1 shows the transient trajectories of the relative machine angle $\delta_2 - \delta_1$ for these cases as well as for the base case without compensation. A comparison of these results confirms that the compensation on the most critical line 7-5 damps out the first oscillation and improves the overall system transient behavior better than compensation allocated at line 9-6.

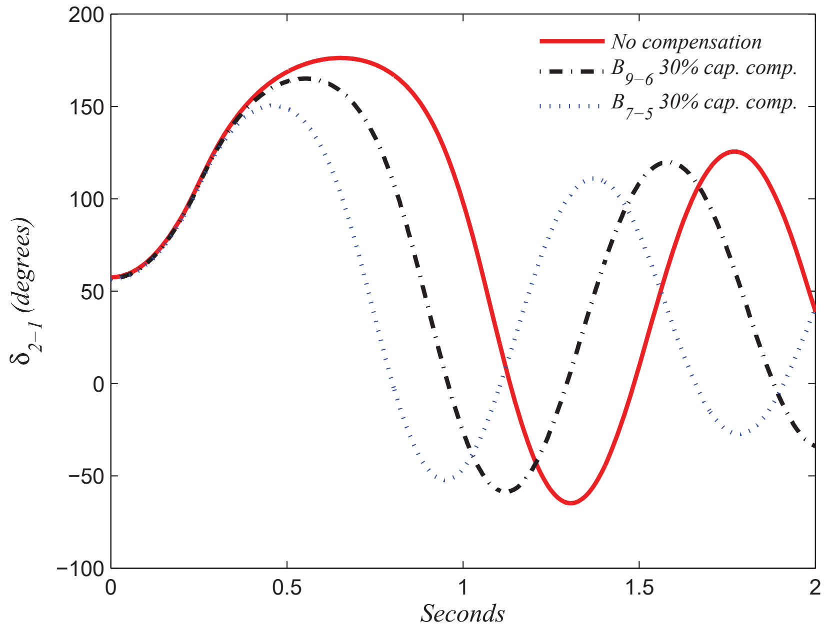

Figure 5.1: Effect of compensation of the lines on transient stability

In order to assess how the system stability changes when the most sensitive line is compensated, all cases reported in Table 5.1 were simulated but considered that transmission line 7-5 has a series capacitive compensation of 30% of its series reactance. The new *CCTs* are shown in Table 5.2 for each fault scenario, as well as the difference between these times and those computed in the base case, which is denoted by Δt_{cct}. Positive values of Δt_{cct} indicate that there was an improvement on the *CCT* and a reduction to the proximity to instability. The opposite applies for negative values of Δt_{cct}.

From Table 5.2, it is observed that in most of the cases the series capacitive compensation improves the *CCT* value; however, when the fault takes place on line 5-4 near bus 5, the compensation worsened stability by reducing the *CCT*. To verify this case numerically, the transient trajectories of the relative rotor angle of machine 2 are computed for a clearing time of 335 ms without compensation as well as series capacitive and series inductive compensation at line 7-5. The results shown in Figure 5.2 demonstrate how the inductive compensation improves the system's stability. This behavior has also been reported in [Shubhanga and Kulkarni, 02], and points out the importance of judging the type of the required compensation to improve the system's stability for a given fault scenario.

Table 5.2: *CCTs* with 30% of series capacitive compensation for the WSCC system.

Line 7 − 5 compensated on 30%							
Line	Fault	t_{cct}(ms)	Δt_{cct}(ms)	Line	Fault	t_{cct}(ms)	Δt_{cct}(ms)
$7-8$	7	172	21	$9-6$	9	205	25
	8	271	38		6	371	61
$8-9$	8	280	26	$5-4$	5	328	-7
	9	210	2		4	261	3
$7-5$	7	-	-	$6-4$	6	413	152
	5	-	-		4	266	14

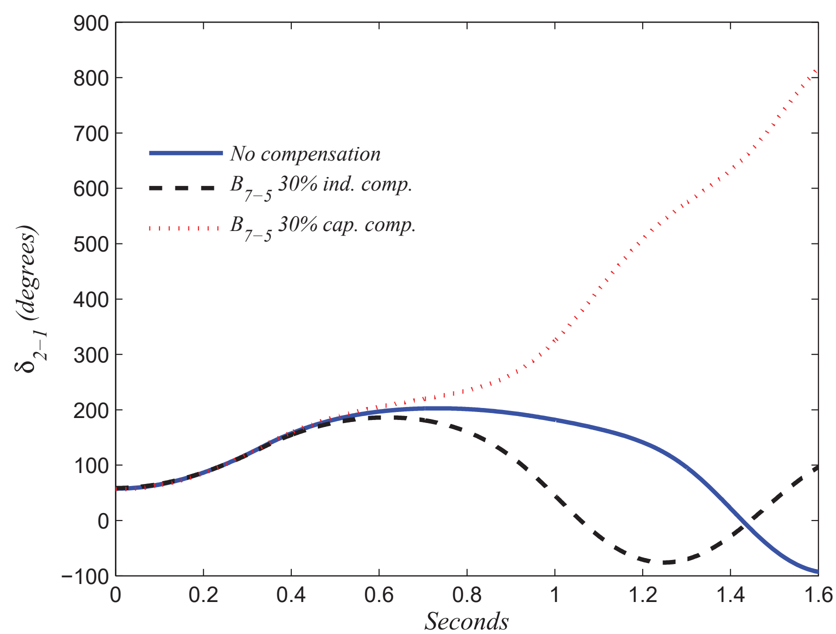

Figure 5.2: Transient stability improvement by series inductive compensation.

In order to show how the location series compensation given by the TS study can substantially improve the system's stability, a three-phase fault is applied on the line connecting buses 9-6 near bus 6 and cleared by tripping the line at a clearing time of 311 ms, without compensation in the system. For this fault scenario, Figure 5.3 shows the unstable trajectories of relative rotor angle of the machines 2 and 3 w.r.t the machine 1. The same case is simulated, but it considered that the most sensitive line B_{7-5} was capacitively compensated in 30% and that the fault was cleared at 371 ms. For this case, the system remains stable as schematically shown in Figure 5.3. Comparing both sets of trajectories, it is observed that the series compensation of the most sensitive line not only makes the system stable for this fault scenario, but also improves the *CCT* by 61 ms, as indicated in Table 5.2.

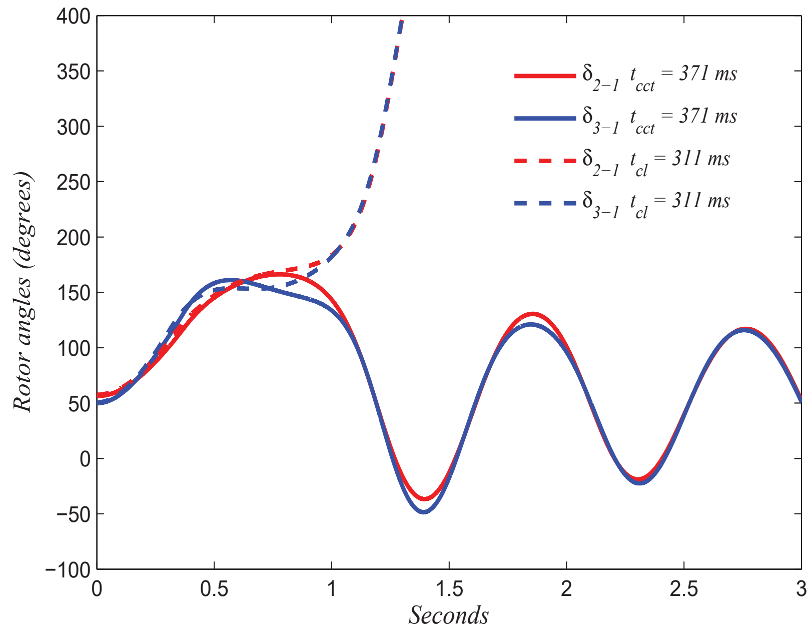

Figure 5.3: *CCT* improved by 61 ms.

5.2.3.2 New England 39-buses, 10-generators system

The multi-parameter sensitivity approach has been applied in the 39-buses, 10-generators power system to find the most suitable location of series compensation within an area considered weak from a transient stability point of view. This area corresponds to the part of the network where faults on transmission lines have the lower clearing time values. For this system, the weak area of interest corresponds to the part of the network bound by buses 25, 26, 27, 28 and 29, which includes the generator embedded at bus 38 that first lose synchronism w.r.t. the rest of system generators, as shown in Figure D.1 of Appendix D. By way of example, Figure 5.4 shows the trajectories of the relative rotor angles w.r.t. the machine connected at bus 39 for a fault on the line connecting buses 26-28, near bus 28, which is cleared by tripping the line at 166 ms after the disturbance takes place. From these trajectories, it is clear that the generator connected at bus 38 is the most advanced w.r.t. the rest of the machines and produces the loss of system synchronism.

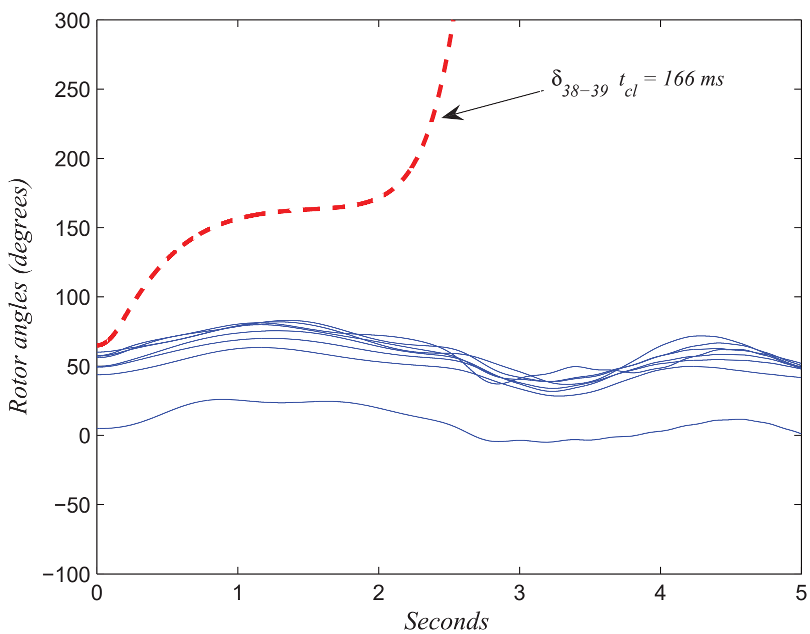

Figure 5.4: Transient stability of first oscillation.

The most effective location of series compensation is assessed by applying a three-phase fault at all transmission lines, one at a time, and by computing sensitivity indices w.r.t. all line susceptances. The study required 68 simulations to identify the most influential line susceptance in the power system. It must be pointed out that if the same study is executed based on computing the trajectory sensitivities with perturbed trajectories [Chatterjee and Ghosh, 07], 2312 (68 base fault simulations plus 33 perturbed trajectories times 68 fault simulations) time-domain simulations are required significantly increasing the computational burden.

Table 5.3 reports the stability indices resulting from the TS analysis as explained by Table 5.1. Lines with the lower values of stability indices are only reported. It is interesting to observe that these indices correspond to faults applied at buses making up the weak area, which indicates that once the weak area has been identified, or an area of interest has been determined, it is only necessary to carry out the study in the set of transmission lines conforming this area. The study in a sub-region of the power system substantially reduces the computational burden (number of operations as well as memory requirements) especially for cases of large-scale systems.

Table 5.3: η_β for each fault for the New England system.

Line	Fault	t_{cct}(ms)	$25-26$	$26-27$	$26-28$	$26-29$	$28-29$
$25-26$	25	296	-	0.113	0.031	0.014	0.137
	26	193	-	0.115	0.033	0.016	0.156
$26-27$	26	208	0.175	-	0.228	0.105	1.032
	27	282	0.108	-	0.140	0.064	0.624
$26-28$	26	158	0.264	2.152	-	0.016	4.042
	28	165	0.452	4.061	-	0.028	7.503
$26-29$	26	136	0.244	1.782	0.025	-	0.164
	29	125	0.143	1.112	0.015	-	0.100
$28-29$	28	119	0.267	1.805	1.572	0.013	-
	29	103	0.370	2.502	2.184	0.017	-

From the results of Table 5.3, it is realized that the most effective location of series compensation is at the line with the most sensitive susceptance for all fault scenarios, i.e. the line connected between buses 26 and 29 because of its corresponding column with the smallest indices η_β in the table. The suitable compensation of this line will reduce the proximity to transient instability by improving the $CCTs$ of faults. This statement is confirmed by results shown in Figure 5.5, which correspond to the relative rotor angle trajectory of the generator connected at bus 38, δ_{38-39}, for cases without compensation, and 30% of capacitive compensation at the most sensitive lines B_{26-29} and B_{25-26}. For the three cases, the fault occurs on line 26-28, near node 28, and is cleared at 166 ms by tripping the line. The fault scenario without compensation is instable whilst cases with series compensation improved the transient stability behavior, achieving the most effective damping when compensation is applied in line 26-29.

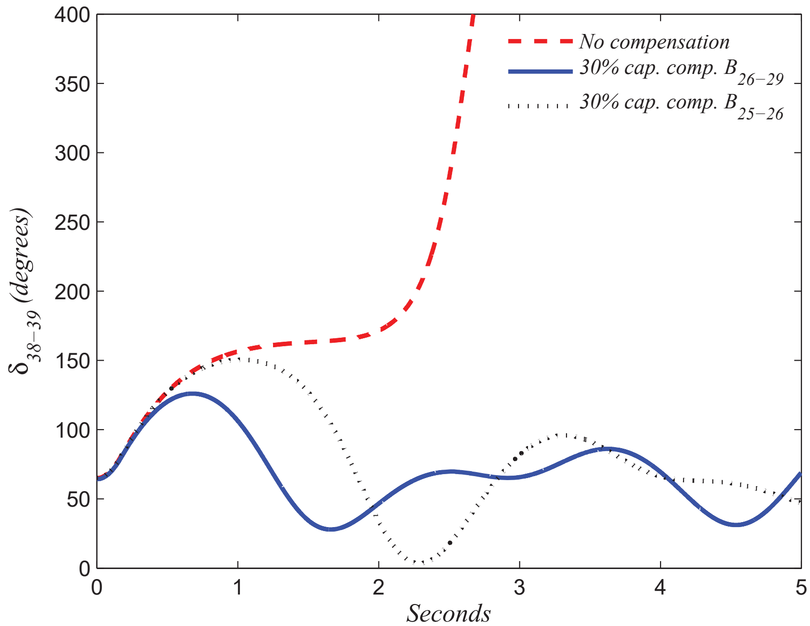

Figure 5.5: Transient trajectories for a fault in the line 26-28.

Finally, Table 5.4 reports *CCTs* when a fault occurs at each one of the transmission lines that constitute the weakest area of the network, and the transmission line 26-29 is capacitively compensated. The improvements of these times over the base *CCTs* given in Table 5.3 are also reported. The best improvement is obtained when the fault is applied on line 28-29 near bus 28, increasing the *CCT* in 75 ms, whereas the *CCT* is marginally improved by 7 ms when the fault is applied on line 25-26 near bus 25.

Table 5.4: *CCTs* with 30% for the New England system.

Line 26-29 compensated on 30%							
Line	Fault	t_{cct}(ms)	Δt_{cct}(ms)	Line	Fault	t_{cct}(ms)	Δt_{cct}(ms)
$25-26$	25	303	7	$26-29$	26	-	-
	26	204	11		29	-	-
$26-27$	26	218	10	$28-29$	28	194	75
	27	295	13		29	161	58
$26-28$	26	200	42				
	28	213	48				

5.3 Thyristor-based FACTS controllers effect

The main idea behind FACTS is to use network parameters as controls to redirect power flow, as well as inject reactive power to the system, increasing the transient stability margin of power systems. In this context, assessment of the system transient stability condition is essential to quantify the effect of FACTS controllers application. The capabilities of TS analysis are used in this section to study the effect of FACTS controllers on the transient stability after the system is subjected to a disturbance. Two FACTS controllers are considered in this study, namely Static Var Compensator SVC and TCSC, whose effectiveness is evaluated by carrying out a TS analysis with and without considering these controllers embedded in the system.

The assessment of FACTS controllers effect on the transient stability based on the application of trajectory sensitivities is carried out by computing the sensitivity of the post-disturbance trajectory for a given clearing time t_{cl} with respect to a chosen parameter. As the t_{cl} increases, the peak of these sensitivities increases such that the system approaches to its boundary stable region of attraction. Since the system stress is related to the scheduled generation, the transient stability assessment is attained via trajectory sensitivities with respect to the modified mechanical input power $P_i = P_{Mi} - E_i^2 G_{ii}$ $i = 1,2,3$, where the sensitivity parameters vector is $\beta = \begin{bmatrix} P_1 & P_2 & P_3 \end{bmatrix}^T$. Also, TS computed w.r.t. the controllers parameters were obtained in order to identify those most sensitive control gains providing the best effect on the power system transient stability. The system under consideration is the WSCC 3-machine, 9-bus system [Sauer and Pai, 98], and the considered generator model is the classical model. The models and controllers data are given in Appendix B. In order to assess the FACTS effect, the system disturbance consisted on the connection of load at bus 7, which is disconnected after a specified clearing time.

5.3.1 Effect of shunt compensation with SVC

A SVC is connected to the system at bus 7. From a given EP corresponding to the base case a load of $P_{L7} = 0.3$pu and $Q_{L7} = 0.9$pu is connected at bus 7 to quantify the performance of the controller. The SVC does not inject reactive power before the load step. The load is disconnected at different clearing times as indicated in Table 5.5. The set of DAEs that represent the system are given by (2.15)-(2.18). The sensitivity matrix is given by (5.3), whereas the state vector is given by (5.2) where x_1, x_2 and B_{SVC} represent the auxiliary variables and the variable susceptance of the SVC. Table 5.5 shows the peak of the sensitivities of machines angles w.r.t. modified mechanical input torque with the controller disconnected and connected to the system.

$$\boldsymbol{x} = \begin{bmatrix} \omega_1 & \omega_2 & \delta_2 & \omega_3 & \delta_3 & x_1 & x_2 & B_{svc} \end{bmatrix}^T \tag{5.2}$$

$$\frac{\partial x}{\partial \beta} = \begin{bmatrix} \frac{\partial \omega_1}{\partial P_1} & \frac{\partial \omega_2}{\partial P_1} & \frac{\partial \delta_2}{\partial P_1} & \frac{\partial \omega_3}{\partial P_1} & \frac{\partial \delta_3}{\partial P_1} & \frac{\partial x_1}{\partial P_1} & \frac{\partial x_2}{\partial P_1} & \frac{\partial Bsvc}{\partial P_1} \\ \frac{\partial \omega_1}{\partial P_2} & \frac{\partial \omega_2}{\partial P_2} & \frac{\partial \delta_2}{\partial P_2} & \frac{\partial \omega_3}{\partial P_2} & \frac{\partial \delta_3}{\partial P_2} & \frac{\partial x_1}{\partial P_2} & \frac{\partial x_2}{\partial P_2} & \frac{\partial Bsvc}{\partial P_2} \\ \frac{\partial \omega_1}{\partial P_3} & \frac{\partial \omega_2}{\partial P_3} & \frac{\partial \delta_2}{\partial P_3} & \frac{\partial \omega_3}{\partial P_3} & \frac{\partial \delta_3}{\partial P_3} & \frac{\partial x_1}{\partial P_3} & \frac{\partial x_2}{\partial P_3} & \frac{\partial Bsvc}{\partial P_3} \end{bmatrix}^T \tag{5.3}$$

Table 5.5: Sensitivities with and without SVC for different clearing times.

Sensitivity	Without SVC		With SVC	
	$\partial\delta_2/\partial P_2$	$\partial\delta_3/\partial P_3$	$\partial\delta_2/\partial P_2$	$\partial\delta_3/\partial P_3$
$t_{cl} = 0.01$s.	11.7576	4.4756	11.6916	4.4558
$t_{cl} = 0.10$s.	23.5407	11.5781	16.1887	8.1623
$t_{cl} = 0.15$s.	201.8799	113.4272	22.7245	11.6837
$t_{cl} = 0.20$s.	Unstable	Unstable	35.8159	18.8781

The results show that the peak values of sensitivities increase as the clearing time gets larger and the system becomes more in danger of losing synchronism. Because the sensitivity $\partial\delta_2/\partial P_2$ is larger at every case, machine two is more critical than machine three. Also, by comparing both cases at identical clearing times, it is observed that when the SVC is embedded in the system, the peak values of sensitivities do not increase as much as when the SVC is not included. This means that the SVC improves the transient stability of the system by adding reactive power during the disturbance. This statement is demonstrated in Figs. 5.6 and 5.7.

Figure 5.6 shows the swing curves for the rotors angles of machines 2 and 3, as well as their respective sensitivities for a clearing time of 20 ms when the SVC is not connected to the system. The same quantities are shown in Fig. 5.7 but with the SVC embedded to the system. The comparison of both sets of results shows that when the SVC is connected to the system, the machine angles do not lose synchronism, and the SVC helps to damp the oscillations. Furthermore, the sensitivity values remain within bounds, instead of having a continuous increment as a function of time. The reason for the higher sensitivity of P_2 is that the disturbance takes place in a node which is electrically closer to machine 2.

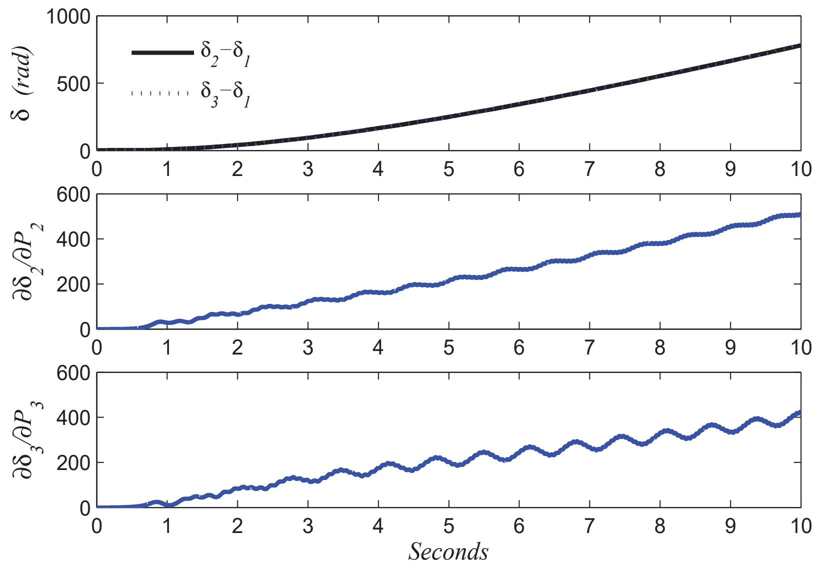

Figure 5.6: Rotor angles and sensitivities for $t_{cl} = 0.20$s without SVC.

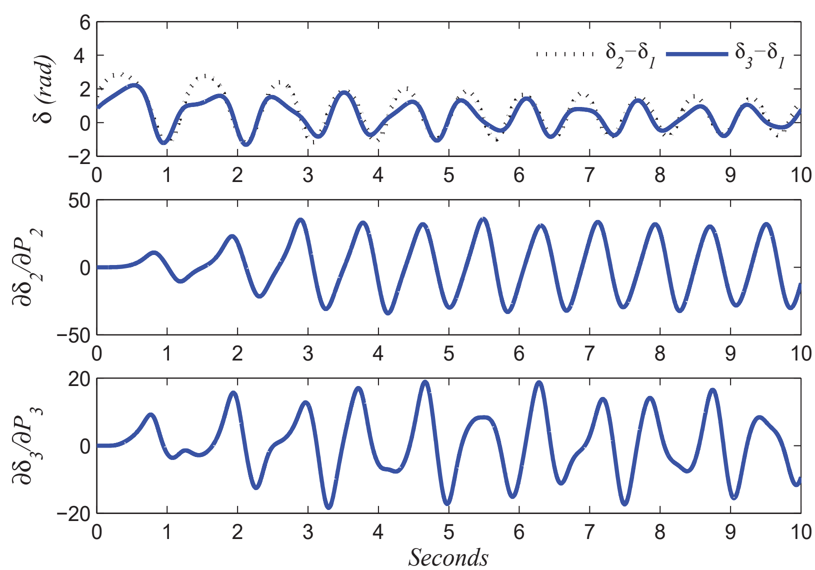

Figure 5.7: Rotor angles and sensitivities for $t_{cl} = 0.20$s with SVC.

Figure 5.8 shows the SVC state variables as a function of time for the case under analysis. At the pre-disturbance operation state, the variable x_1 has a value equal to the voltage magnitude measured at the SVC node. During the disturbance period, this value decreases due to the increment of load and absorption of reactive power. Hence, the variables x_2 and B_{SVC} begin to rise to supply more reactive power to the system. Once the load is disconnected, the SVC return to their initial values. It is important to observe in Figure 5.8, that at the pre-disturbance the SVC is connected to the system but without giving reactive support.

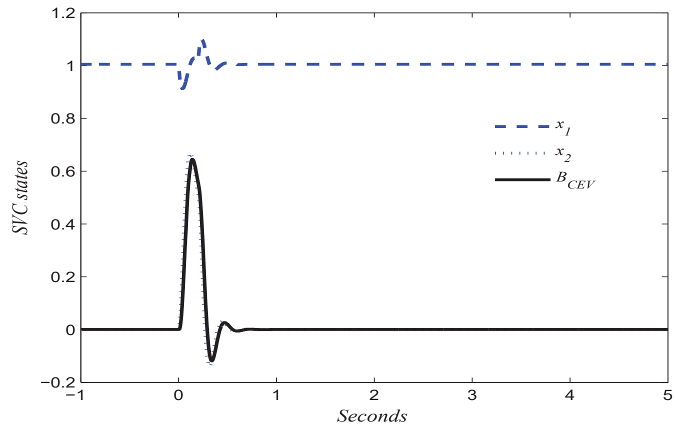

Figure 5.8: SVC state variables.

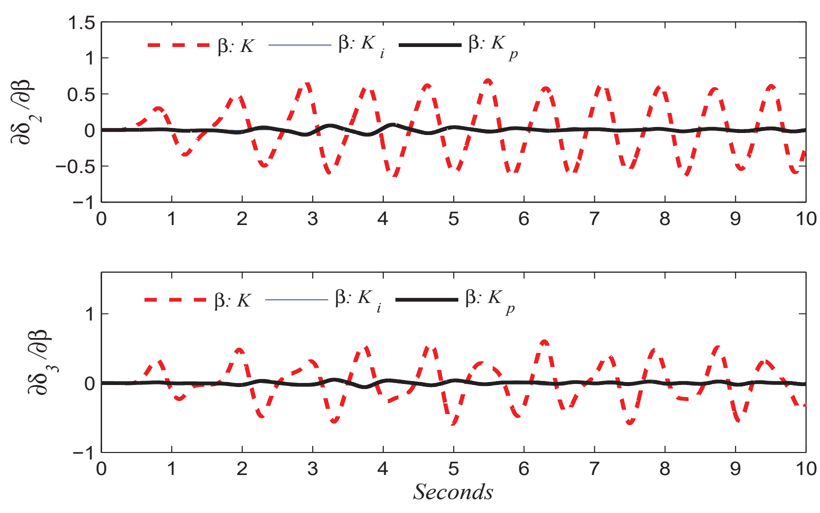

Figure 5.9: Rotor angle sensitivities w.r.t. SVC control gains.

Figure 5.9 shows the sensitivities of machine angles w.r.t. the SVC control gains. It is observed that the block K has the major impact on the system dynamic performance. This is because this block corresponds to the slope of the SVC control characteristic, which determines the amount of reactive power to be injected by the controller.

5.3.2 Effect of series compensation with TCSC

A TCSC is connected to the system in series with the transformer connected between the buses 2 and 7. The block diagram and the parameters of the TCSC are given in Appendix B.2. Similarly to the disturbance applied in the last section, a load of $P_{L7} = 1.0$pu and $Q_{L7} = 0.2$pu is connected at bus 7, and after a certain period of time it is disconnected from the system. For the study of dynamic sensitivities, the results obtained with a TCSC connected in the system are compared with those obtained when a fixed-series capacitor replaces the controller. In this case, the capacitor value corresponds to the TCSC's equivalent susceptance value when it is operating at the capacitive region in the pre-disturbance state. For the simulated case, the TCSC is operating in control mode of constant current. Sensitivity results for different load clearing times are presented in Table 5.6.

Table 5.6: Maximum sensitivities with series compensation.

Sensitivity	Fixed capacitor		TCSC	
	$\partial\delta_2/\partial P_2$	$\partial\delta_3/\partial P_3$	$\partial\delta_2/\partial P_2$	$\partial\delta_3/\partial P_3$
$t_{cl} = 0.01$s.	2.8972	0.5990	2.8775	0.5980
$t_{cl} = 0.10$s.	9.3752	0.8469	7.9871	0.7537
$t_{cl} = 0.15s$.	14.5048	1.1642	11.8364	0.9624
$t_{cl} = 0.20$s.	27.5641	1.9870	18.5321	1.3239
$t_{cl} = 0.25$s.	Unstable	11.4260	69.3096	4.6837

As observed in the last section, as the clearing time increases, the system approaches to its stability boundary, as indicated by the increment of the sensitivity peak value. Comparing results at identical clearing times, it is observed that the system is less stressed when the TCSC is connected in the system. For a clearing time of 0.25 seconds, the system loses synchronism when it is compensated with a fixed capacitor whilst the TCSC allows it to remain in synchronism. The observations based on the peak values of sensitivities are confirmed by analyzing the rotor angle profile of machines 2 and 3 as a function of time, for a clearing time of 0.25 seconds, shown in Figure 5.10 and their sensitivities shown in Figure 5.11.

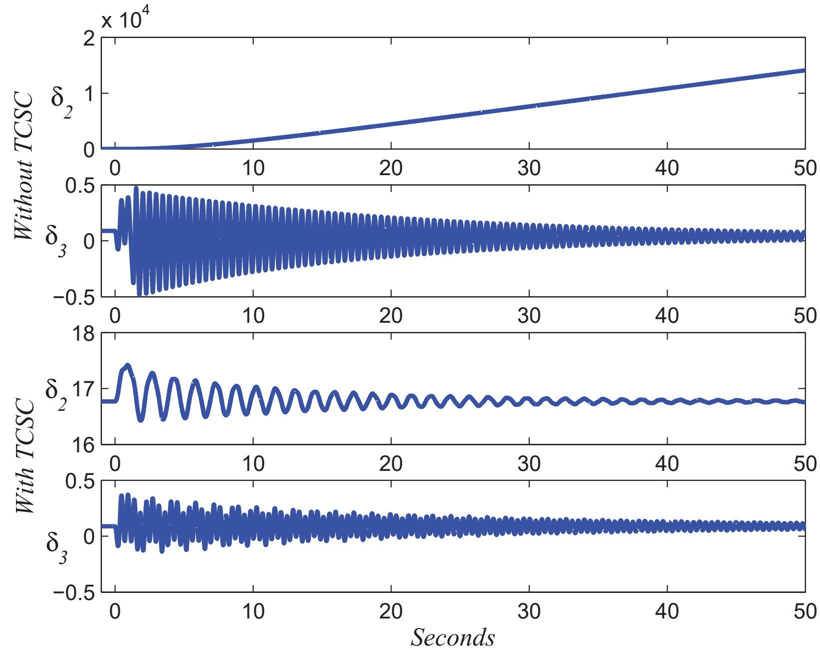

Figure 5.10: Rotor angle trajectories for $t_{cl} = 0.25$s. with series compensation.

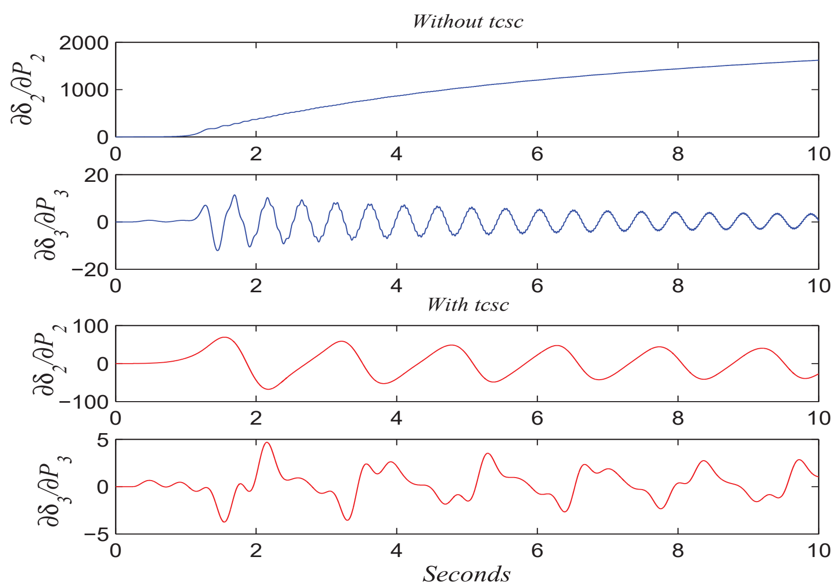

Figure 5.11: Sensitivities for $t_{cl} = 0.25$s. with series compensation.

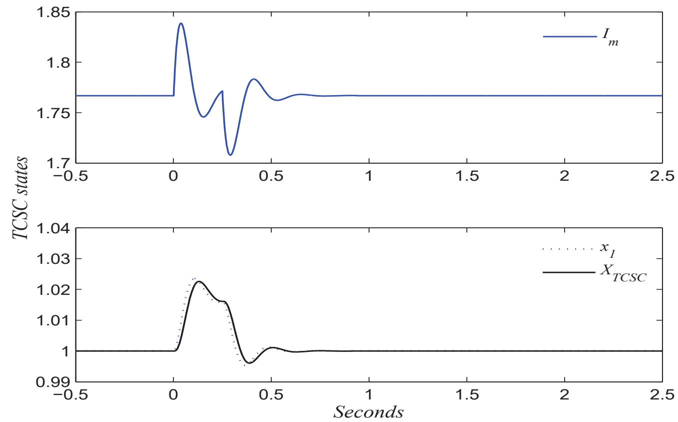

Figure 5.12: TCSC state variables.

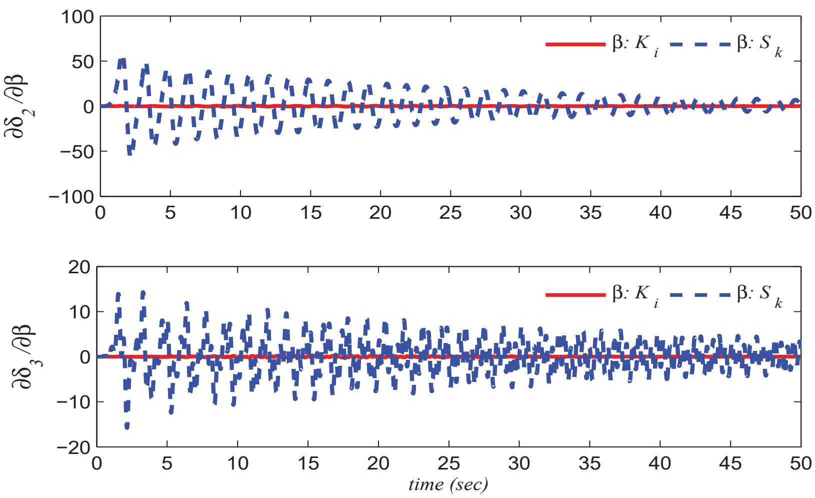

Figure 5.13: Rotor angle sensitivities w.r.t. TCSC control gains.

The dynamic performance of the TCSC control variables is shown in Fig. 5.12. At the time of the disturbance, the TCSC current increases its value and the controller modulates its equivalent reactance in order to adjust the current at the nominal value. This adjustment takes place during the disturbance and post-disturbance operating periods until the original TCSC control variable values are obtained because the system has returned to its original operating point. The sensitivities of machine angles w.r.t. the TCSC control gains are shown in Figure 5.13. It is observed that rotor angles are very sensitive w.r.t. the variable s_k, which determines the TCSC control operation mode.

5.4 Improvement of voltage profile by using a voltage sensitivity index

One of the worst disturbances considered on transient stability is the loss of generation. When a generator suddenly goes out of operation, the system suffers an unbalance between the total generated and demanded powers corresponding to the power generated by the generation unit out of operation. This contingency makes the rest of the generators connected in the system decrease their speeds starting the fall of system frequency [Poonam, 07]. The instantaneous change in power generation produces a sudden fall in the system voltage profile, such that there exists a decrease of the power demanded by loads [IEEE, 93]. Therefore, the generation requirements decrease and the rotor angles decrease in the new stated operating point. If the system is stable after this loss of generation, all variables in the system will reach a new EP [Sauer, 02]. However, sometimes the new voltage profile is too low from the operating point of view, i.e. some voltages violate their lower limits [IEEE, 02] [Poonam, 07] . In order to return the system voltages to acceptable values between operative limits, in this section we propose to use the trajectory sensitivities of the voltage magnitudes. Such sensitivities are computed w.r.t. the reactive powers in order to identify their influence on the voltage profile of the system.

In order to quantify the influence of system loads a sensitivity index is proposed and used to take corrective actions consisting of load shedding. Also, another index is proposed in order to calculate the proportional effect of each load in the voltage profile. Such an index assists on estimating the amount of total load that has to be shed to keep the voltages within the operation limits. In addition, this index allows the distribution of the total load shedding according to the influence of each load on the voltage profile.

5.4.1 Voltage sensitivity quantification

In order to quantify the loads effect we propose to use a voltage profile index based on the trajectory sensitivities of voltage magnitudes. Such a voltage profile index is calculated by the sum of all voltage sensitivities in the system as shown in Eq. (5.4). Larger deviations of voltages w.r.t. load parameters at the disturbance instant will provide larger indices. Therefore, the maximum index indicates that parameter (load) which has the most influential effect in the voltage profile of the system.

$$SV_i = \sum_{k=1}^{n_b} \frac{\partial V_k}{\partial \beta_i} \quad \forall i = 1, \ldots, N_P \tag{5.4}$$

Therefore, by using this index we can identify the most sensitive loads in the system, i.e. those loads that provide major changes in the transient voltage trajectories. It is then possible to rank for a specific location of disturbance the most critical and noncritical loads in the voltage profile.

5.4.2 Load effect assessment

The WSCC 9-bus, 3-generator system shown in Appendix C, was analyzed to assess the effectiveness of the proposed approach. The classical model was used to represent the system generators, whereas the constant impedance model is considered for the system loads. The generality of results provided by the proposed approach is not dependent of the load model considered. The disturbance analyzed in the test case is the loss of the generator embedded at node 2. The transient behavior of rotor angles and voltage magnitudes are shown in Figures 5.14 and 5.15, respectively. Figure 5.14 shows the relative rotor angle response after the disturbance. Figure 5.15 shows the voltage profile behavior after the loss of generator. Such a disturbance produces a power unbalance between generation and load power, and steers the system to another equilibrium point as can be observed in both figures after 50 seconds of simulation.

It is important to observe that the voltage profile conditions at the instant of disturbance are very close to those stated after 50 seconds of simulation shown in Figure 5.15. This feature in the voltage profile performance provides some advantages on identifying the most sensitive load. A numerical comparison of voltage profile at the instant of disturbance (3 seconds) and in the new stated equilibrium point (50 seconds) are presented in Table 5.7. In this way, the proposed indices of voltage sensitivities (5.4) can be calculated at the disturbance instant at 3 seconds, instead of waiting the establishment of the new system EP at 50 seconds.

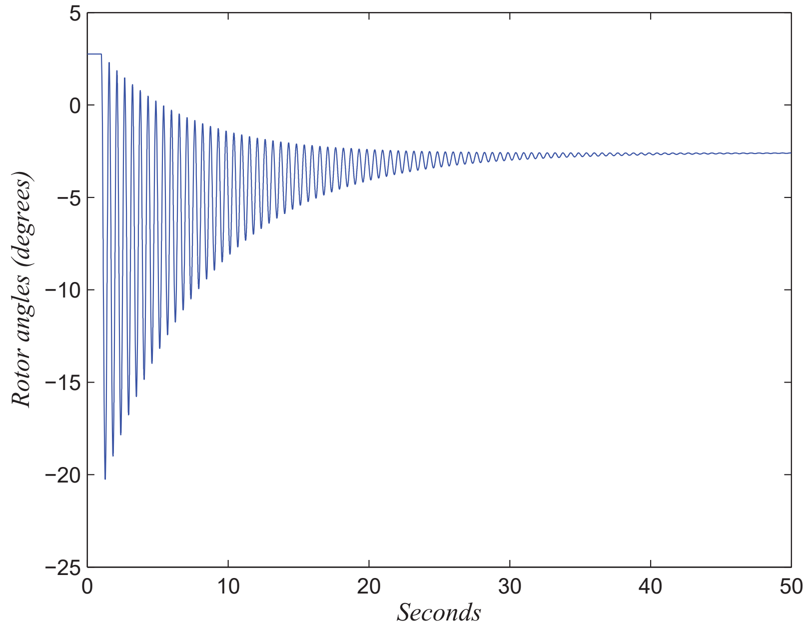

Figure 5.14: Relative rotor angle $\delta_3 - \delta_1$.

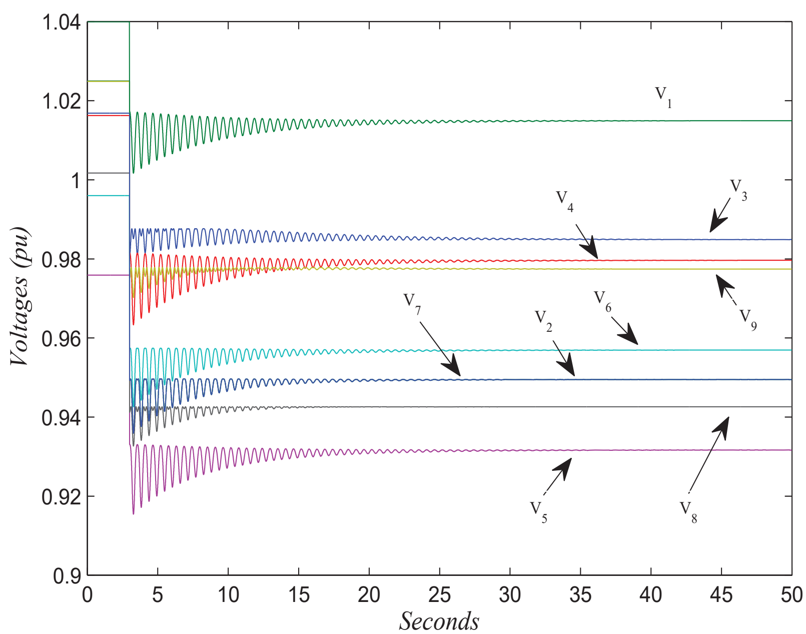

Figure 5.15: Voltage profile.

Table 5.7: Voltage profile at pre-contingency and post-contingency equilibrium points.

V(pu)	At 3 secs.	At 50 secs.	V(pu)	At 3 secs.	At 50 secs.
V_3	0.9806	0.9848	V_9	0.9750	0.9774
V_2	0.9493	0.9494	V_8	0.9411	0.9425
V_4	0.9815	0.9796	V_7	0.9493	0.9494
V_6	0.9573	0.9569	V_1	1.0172	1.0149
V_5	0.9330	0.9316			

It is clear from Figure 5.15 that the voltages decrease and reach a new equilibrium point. The new voltage profile is very similar to that observed at the disturbance instant as can be observed in Table 5.7. In order to find out the effect of the reactive loads we compute the index of voltage sensitivities (5.4) through the time during the transient, as shown in Figure 5.16.

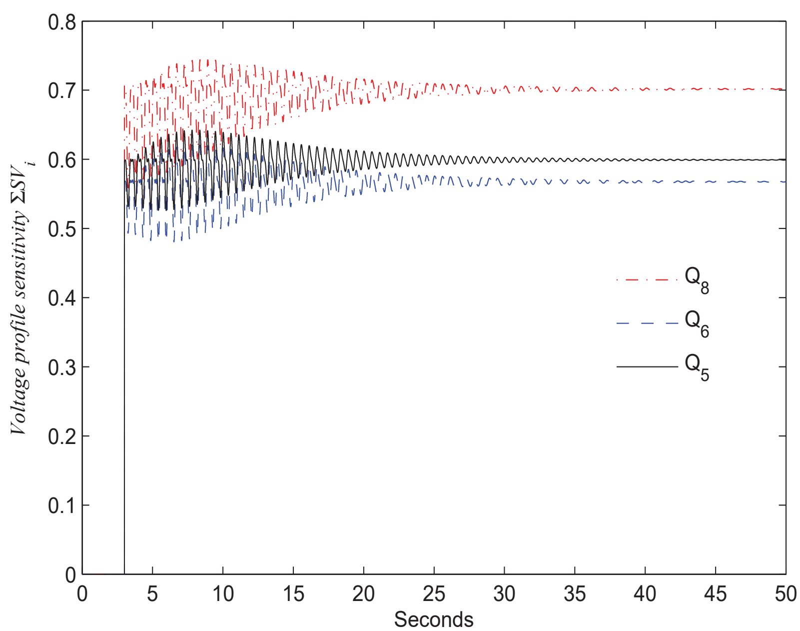

Figure 5.16: Voltage sensitivity index.

It is clear that the most sensitive reactive load is that connected to bus 8, i.e. any modulation of such a load during the transient will provide the most significant effect on the new voltage profile. Besides, by observing the figure it must be pointed out that the computed values of the voltage sensitivity indices at the instant of disturbance are also very close to those values computed at the new EP. Thus, the values of the sensitivity indices present the same characteristic observed in the voltage magnitudes as can be observed in Figure 5.15 and Table 5.7.

5.4.3 Voltage profile load shedding characteristic

The instantaneous change on the voltage profile due to loss of generation and the voltage sensitivity indices allow us to identify instantaneously the most sensitive load. Therefore, after the instant of disturbance it is possible to take any action in order to improve the voltage profile, i.e. either load shedding or reactive switching even at the moment of identification of the most sensitive load in the voltage profile.

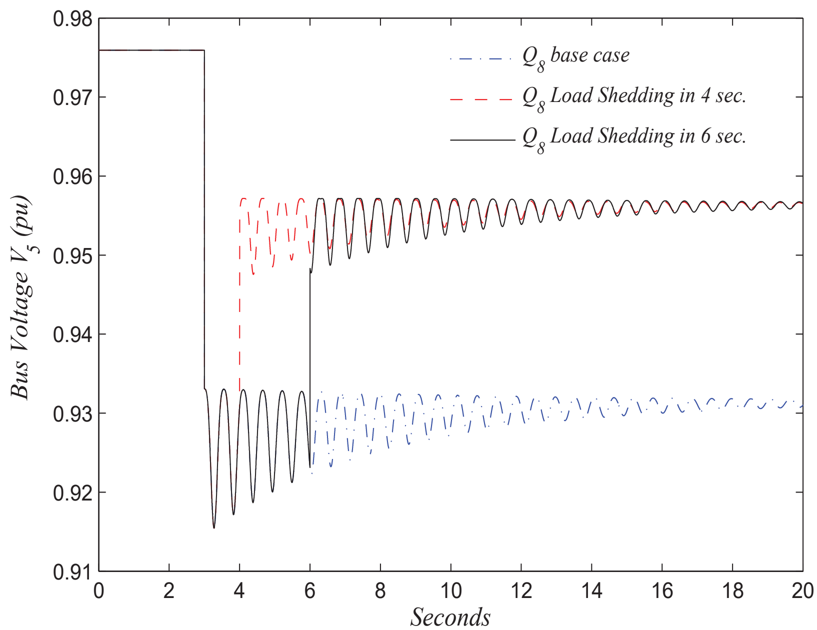

Figure 5.17: 10% load shedding in bus 8.

Figure 5.17 shows the transient behavior of voltage magnitude at bus 5. The loss of generator 2 takes place after 3 seconds of a pre-disturbance state operation. A 10% of the load at bus 8 (the most influential) is modulated (shed) in the second 4 and 6 of simulation, each one at a time. It must be observed from the figure that the voltage trajectories only depends on the location and the amount of load modulation, and there is not dependence at the execution time.

In order to assess the effectiveness of the voltage sensitivity index on the identification of the most influential load to the voltage profile, a gradual load shedding was obtained at each loading direction. The quantification of the voltage profile improvement by means of load shedding after the contingency is obtained by computing the average of voltages at the post-contingency equilibrium point. Figure 5.18 shows the change of the voltage average versus the percentage of total load shedding in the three different loading directions, each one at a time. It is clear that the voltage average has a linear characteristic, which can be obtained by extrapolation using only two points. Therefore, it is possible to estimate the amount of load modulation in order to improve the average of voltage profile close to the pre-disturbance value.

The average pre-disturbance voltage profile is 1.013 p.u. and is indicated in the figure via the horizontal line. At the moment of the disturbance, this value instantaneously decays to 0.965 p.u. The linear trajectories corresponding to the different loading directions facilitate estimating the required amount to be shed at each load in order to return the voltage average to the pre-disturbance value. According to the sensitivity indices shown in Figure 5.16, the load embedded at bus 8 was most sensitive to the generator outage. Hence, the amount of load to be shed at this bus is the least, in comparison to other load buses, to steer the average voltage magnitude at its pre-disturbance value. On the other hand, the load embedded at bus 6 is the least sensitive, and a greater amount of load shedding is required to achieve the same goal. To validate the above mentioned statement, the linear extrapolation was used to calculate the amount of load shedding required to obtain a post-disturbance average voltage magnitude equal to its value at the pre-disturbance value, resulting in 17.28%, 20.55% and 24.39% at nodes 8, 5 and 6, respectively. Despite the load model used, the generality of results is maintained in the proposed approach.

The line identified as distributed load shedding in Figure 5.18 represents the case where the percentage of the total load is shedding in a distributed way at all loading directions of the system at the same time. The distribution of the load shedding consists of quantifying the effects of each load on the voltage profile, by using the voltage sensitivity indices computed with Eq. (5.4) at the instant of disturbance. The amount of power to be shed at each load bus is known by calculating the percentages of participation of each load in the voltage profile transient. In this way, the most sensitive loads will have the highest percentages of

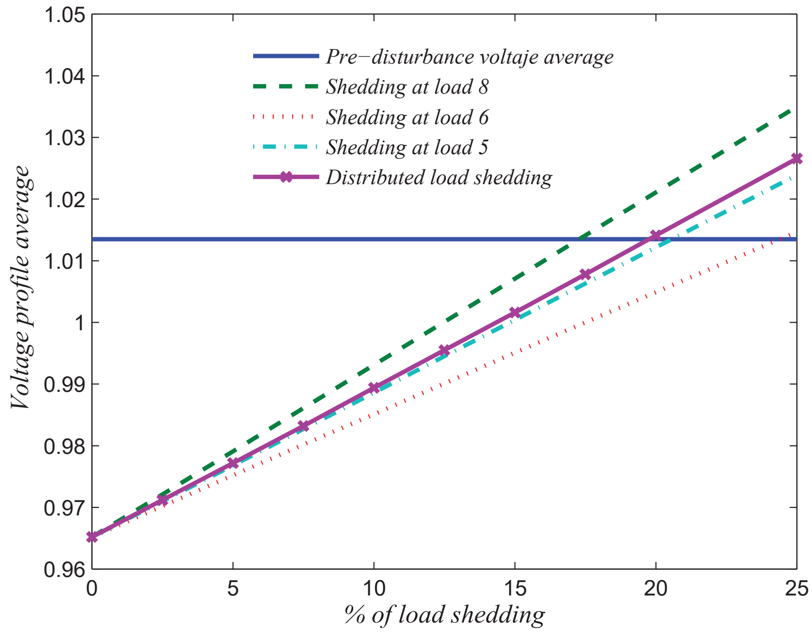

Figure 5.18: Voltage average versus load shedding.

participation, which are computed with (5.5), where each sensitivity index (5.4) is divided by the sum of all sensitivity indices w.r.t. N_P parameters. By applying (5.5) the load shedding is distributed in 37.74%, 31.93% and 30.33% in the loads embedded at buses 8, 5 and 6, respectively. Thus, from the extrapolation in Figure 5.18 an estimated 19.76% of the total load must be shed in such distribution percentages in order to return the average of voltage to the pre-disturbance value.

$$\%Part_i = \sum_{k=1}^{n_b} \frac{\partial V_k}{\partial \beta_i} / \sum_{i=1}^{N_P} \sum_{k=1}^{n_b} \frac{\partial V_k}{\partial \beta_i} \tag{5.5}$$

It is very important to mention that the line corresponding to the distributed load shedding in Figure 5.18 can be computed by performing only one time-domain simulation. The linear characteristic of the average voltage versus percentage of load shedding can be obtained by computing only two points, which can be computed in the same simulation. The first point is computed at the instant of disturbance, whereas the second point is computed at the post-contingency equilibrium point. Therefore, at the instant of disturbance the first point of average voltage as well as the participation percentages (5.5) are computed at the same time.

After this, a small percentage of load is shed in all loading directions of the system, with load distribution according to the computed participation percentages based on the sensitivity indices (5.5). At the instant of the load shedding the second point of average voltage is computed, which is closely the same as the newly established EP as shown in Figure 5.17.

Figure 5.19 shows the voltage profile after the distributed load shedding at 3 seconds of simulation. The voltages are not exactly the same as the pre-disturbance values; however, the average voltage is the same.

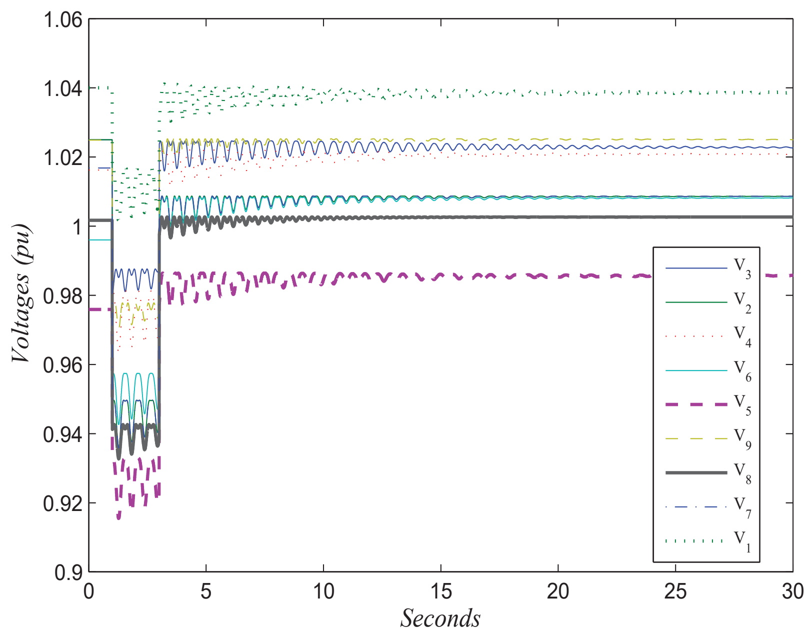

Figure 5.19: Voltage profile with distributed load shedding.

The same approach can be used in order to investigate the best place to locate shunt compensation. Figure 5.20 shows the average of voltage profile dependent on the shunt compensation. For this case, the average of 1 p.u. is considered as a set point to keep the voltage profile. It is clear from the figure that load 8 is the best candidate to be compensated after the loss of the generator 2. Furthermore, this information can be used for estimating the amount of shunt compensation required to keep the voltages within operating limits. Besides, this approach can be used to calculate the amount of reactive injection to be switched on at each point where shunt compensation is suitable. In this case the best location of shunt compensation is at bus 8, where less compensation level is required to keep a specific average voltage, as compared to the cases of loads 5 and 6.

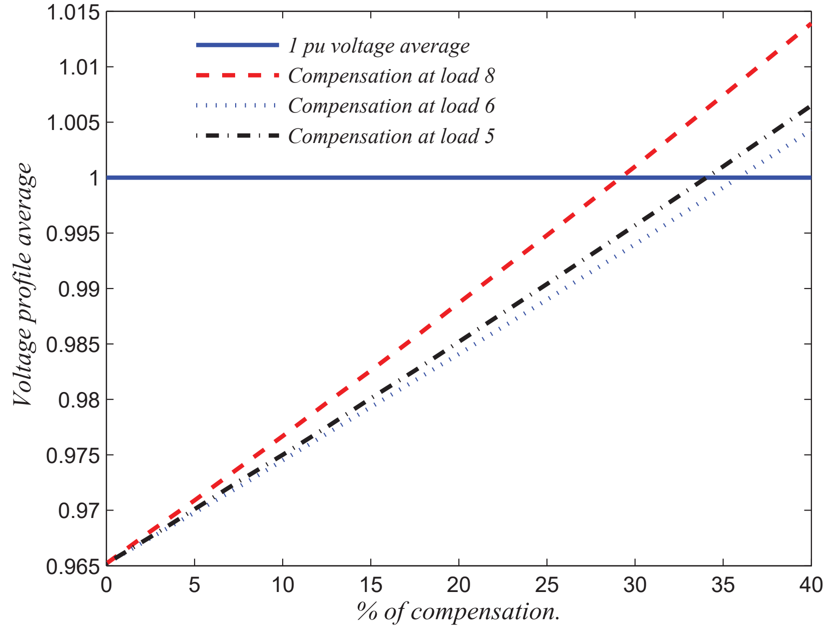

Figure 5.20: Voltage average versus shunt compensation.

5.5 Conclusions

In this chapter, a systematic multi-parameter trajectory sensitivity-based approach has been applied to determine the proper allocation of series-connected controllers in order to improve the transient stability margin of power systems. The approach is completely general, and its application does not depend on the kind of series controllers to be installed in the system. Guidelines to identify the most suitable location are given according to the relation between sensitivities of relative rotor angle with respect to line susceptances and an index of proximity to instability. Numerical examples on two benchmark power systems are provided and confirm the feasibility as well as the validity of the formulation. The proposed approach is an effective and practical method which could be used for large-scale power systems planning and operation studies.

We also described the application of the dynamic sensitivity theory to assess the effect of FACTS controllers on the transient stability condition of a power system. It has been observed that both SVC and TCSC help to stabilize the system in a transient stability sense. This effect has been quantified based on the peak values of sensitivities, as they decrease for identical clearing time when the controller is embedded in the system. It was also shown how the machine variables change with respect to the FACTS controller gains, so that it is possible to determine which control parameters have more effect on the system dynamics.

Lastly, in order to keep the voltage profile inside the system operative limits a load shedding approach from the transient stability viewpoint has been proposed. Such an approach is based on assessing the loads effect on the voltage profile of a power system by using multi-parameter trajectory sensitivities of voltage magnitudes with respect to the reactive loads. Voltage sensitivity indices have been proposed to estimate the amount of load that should be shed as well as its distribution to obtain a good voltage profile after a generator outage.

Chapter 6

APPLICATION OF TS TO SMALL SIGNAL STABILITY ANALYSIS

6.1 Introduction

Small signal stability is the ability of a power system to maintain synchronism when subjected to small disturbances such as small load and/or generation changes [IEEE, 04]. The analysis of SSS consists of assessing the stability of an EP, as well as determining the most influential state variables in the stability of the operating point. For small enough disturbances the system behavior can be studied via the theory of linear systems around an equilibrium point [Chen, 99]. The stability of an EP is assessed by eigenvalue analysis (eigen-analysis) according to the Lyapunov criterion [Lyapunov, 67], which states that an EP will be stable in the small signal sense, if all system eigenvalues of the system matrix are located on the left side of the complex plane. On the other hand, the EP will be unstable if at least one eigenvalue locates on the right side of the imaginary axis. In this context, the resulting dominant eigenvalue from the eigen-analysis is called the critical eigenvalue, and its association to the state variables is investigated by SMA [Pérez et al., 82] [Verghese et al., 82]. Based on the PFA, the SMA provides those state variables having the highest influence in the EP stability by means of their coupling to the critical eigenvalue [Kundur, 94] [Sauer and Pai, 98]. Since the system eigenvalues are directly related to its dynamic performance, different forms of instability in a power system can be studied by means of well-defined structures of eigenvalues which are called bifurcations.

The theory of bifurcations is a powerful mathematical tool based on eigen-analysis to assess the stability of EPs in nonlinear systems [Nayfeh and Balachandran, 95]. This theory consists of searching for specific eigenvalue structures associated to different instability forms that appear on power systems [Ajjarapu, 06]. One of the most common local bifurcations that can appear in the power system operation are the Hopf Bifurcation, which occurs when the system matrix contain a pair of purely imaginary eigenvalues causing undamped oscillatory behavior [Ajjarapu and Lee, 92] [Kwatny et al., 95] [Wen, 05]. Any parameter variation in the system may result in complicated behavior until the system stability changes. This point where the stability changes is defined as a bifurcation point. In this chapter the system loads are changed in order to analyze the stability of the EPs. The maximum load in a specific direction that a power system can provide before the appearance of a bifurcation point establishes the loading limit in that direction. Thus, the loading limit is directly associated with the stability margin of the system. The critical eigenvalue of an EP is used as an index of the stability margin. After a load change, an eigen-analysis permits us to assess the stability margin closeness. A small margin indicates closeness to a bifurcation point (instability).

SSS analysis is very important to determine the corresponding control strategies to improve security under stressed operating conditions of power systems. Control strategies employed in electric power systems are usually tested by means of an assessment of the stability improvement. Thus, the influence of parameters and components in the EP stability provides an insight to achieve the best control. In this context, the participation factors let us know the highest association between state variables and the critical eigenvalue dominating the EP stability [Kundur, 94] [Sauer and Pai, 98]. In this way, PFA allows the selection via the associated states to the critical eigenvalue of those components that will provide the best control in EP stability. Although, the PFA selects the most sensitive states in the EP stability, it is not possible to identify in a direct form the most influential parameters, e.g. those most sensitive loads influencing the stability. In order to achieve this, the PFA must be combined with other methods providing parameter sensitivity features. In [Joorabian et al, 08] the authors combined the PFA and modal controllability of the weak damping oscillatory modes to obtain an optimal location of SVCs. In [Sharma and Singh, 07] the authors presented an approach to examine the effect of loads in the system stability by using participation factors and mode shape analysis. In [Sauer and Pai, 98] both a voltage stability analysis and a low-frequency oscillations analysis were performed by using the SSS analysis in the EPs. As the system faces increased loading conditions, bifurcation points appear and the participating generators are identified by means of the most associated states obtained from the SMA.

This thesis proposes an alternative method based on the trajectory sensitivity theory [Frank, 78] [Tomovic and Vucobratovic, 72] to investigate the stability of the EPs by using a time-domain simulation. In this approach, the TS were computed w.r.t. the load parameters; therefore, besides the stability assessment and the participating states, the proposed approach also has the ability to identify those most sensitive load parameters influencing the critical states. The stability assessment consists of just examining the TS oscillations. In the proposed approach, the stability analysis of the EP is never perturbed. The TS oscillations required for the stability assessment are produced by means of the initial condition values selected for the sensitivity variables.

The proposed approach uses an index of sensitivity quantification, which facilitates identifying the influence of the system loads around the HB points. The index allows us to rank the power system loads in order to predict the most critical loading directions toward a HB point.

6.2 Sensitivity quantification

As the system approaches its stability boundary, the trajectory sensitivities approach infinity [Laufenberg and Pai, 98]. It is possible to associate the sensitivity information with the stability level of the system for a particular system parameter. The load power effect on the system small signal stability is measured by computing sensitivities of rotor angle and speed trajectories w.r.t. active power loads, and measuring the proximity to instability.

An index of proximity to transient instability is determined based on the sensitivity norm given in [Nguyen et al., 02], for a system of n_g-machines

$$SN_i = \sqrt{\sum_{k=1}^{n_g} \left(\left(\frac{\partial \delta_k}{\partial P_{Li}} - \frac{\partial \delta_j}{\partial P_{Li}} \right)^2 + \left(\frac{\partial \omega_k}{\partial P_{Li}} \right)^2 \right)} \qquad \forall i = 1, \ldots, N_p \tag{6.1}$$

where j denotes the reference machine.

The growth in peak values of trajectory sensitivities indicates an underlying stability problem, and ideally SN_i should be infinite at the point of the system transient instability. In this thesis (6.1) is used as an index to identify the loads influence in the stability of EPs, where the highest values of the sensitivity norms indicate the most sensitive loads.

6.3 Sensitivity initial conditions

In order to analyze an operating point with the proposed approach, the EP is kept constant $(X(t_0), Y(t_0))$ during the whole simulation. Thus, the matrices g_y, g_x, g_β and f_y, f_x, f_β are time-invariant in the linear sensitivity model (3.13), whereas the TS $\left(X_\beta^{k+1}, Y_\beta^{k+1}\right)$ are time-varying. As time tends to infinity $t_\infty = t \to \infty$, the TS tend to a stationary behavior established at nonzero constant values $X_\beta(t_\infty) \neq 0$ and $Y_\beta(t_\infty) \neq 0$. If we use these constant values $\left(X_\beta(t_\infty), Y_\beta(t_\infty)\right)$ as the sensitivity initial conditions in (3.13), we would not have a TS transient behavior (oscillations), and it would not be possible to obtain any sensitivity information. However, by using $X_\beta(t_0) = Y_\beta(t_0) = 0$ as the initial conditions of the sensitivity variables, a transient behavior on the TS will be induced and the oscillations during the transition period from the initial condition $X_\beta(t_0) = Y_\beta(t_0) = 0$ to the stationary final condition $\left(X_\beta(t_\infty), Y_\beta(t_\infty)\right)$. Such a transient behavior provides the necessary sensitivity information to assess the stability as well as the influence on the states and parameters in the analyzed EP.

6.4 Small Signal Stability Analysis

This section presents the analysis of the TS applied on assessing the SSS analysis. The effectiveness of the proposed approach is numerically tested by analyzing the WSCC 9-buses, 3-generators system [Sauer and Pai, 98] and a reduced equivalent system corresponding to the Mexican power system consisting of 190-buses with 46 embedded generators. The system diagrams and corresponding parameters are given in Appendixes C and E, respectively. For the purpose of the studies presented in this section, the system generators are represented by means of the Two-Axis model with a simple fast exciter loop containing max/min ceiling limits. For this case the system loads are represented by means of the constant power load model, however the generality of the method allows to consider any load model.

6.4.1 Modal analysis WSCC system

In this subsection the conventional modal analysis is employed in order to investigate the small signal stability of the WSCC power system. Table 6.1 presents the modal analysis for different EPs as the active power at bus 5 is increasing.

Table 6.1: Modal analysis of the WSCC system

P_5(pu)	λ_{crit}	Associated states	Participation factors
4.2	$-0.5085 \pm 7.3001i$	$\omega_2, \delta_2, E^{'}_{d2}, E^{'}_{q1}, E_{fd1}$	1.0,0.99,0.18,0.18,0.16
4.3	$-0.5395 \pm 6.8512i$	$\omega_2, \delta_2, E^{'}_{d2}, E^{'}_{q1}, E_{fd1}$	1.0,0.99,0.28,0.39,0.35
4.4	$-0.0305 \pm 6.1462i$	$\delta_2, \omega_2, E^{'}_{d2}, E^{'}_{q1}, E_{fd1}$	1.0,0.99,0.46,0.99,0.83
4.5	$0.7064 \pm 5.8935i$	$E^{'}_{q1}, \delta_2, \omega_2, E_{fd1}, E^{'}_{d2}$	1.0,0.85,0.85,0.79,0.38
4.6	$1.5118 \pm 5.7190i$	$E^{'}_{q1}, \delta_2, \omega_2, E_{fd1}, E^{'}_{d2}$	1.0,0.81,0.80,0.76,0.32
4.7	$2.6677 \pm 5.5020i$	$E^{'}_{q1}, \delta_2, \omega_2, E_{fd1}, E^{'}_{d2}$	1.0,0.79,0.78,0.74,0.28
4.8	$5.3798 \pm 4.5835i$	$E^{'}_{q1}, \delta_2, \omega_2, E_{fd1}, E^{'}_{d2}$	1.0,0.77,0.75,0.76,0.26

SSS and modal analysis were performed to investigate the different operating points corresponding to the different levels of loading. Eigen-analysis revealed the SSS of EPs, whereas participation factors were used to identify the most associated states to the critical eigenvalue at each EP, as given in Table 6.1. The first column represents the load changes at bus 5. The second column presents the critical eigenvalue for the EP. The third column presents the most associated states to the critical mode (eigenvalue), obtained by selecting the highest magnitudes of participation factors, which are given in the fourth column in the table.

As the load embedded at bus 5 increased, the stability of the new EP decreased with respect to the previous one. The power system oscillatory instability called the HB was detected when the load changed from 4.4 p.u. to 4.5 p.u. The modal analysis around the HB revealed machine 2 as the most participative in the unstable EP. It is important to observe in Table (6.1) that machine 2 is the most associated with the critical eigenvalues for all analyzed EPs.

6.5 Trajectory Sensitivity Analysis - WSCC system

In order to test the proposed method based on TS to assess the EPs stability, operating points before and after the HB point were investigated. As the active power increases at bus 5, as was performed in [Sauer and Pai, 98], the system proximity to the bifurcation points is assessed by using the analysis of TS. The rotor angle and speed sensitivities w.r.t the load active powers were traced and observed through the time. The TS oscillations provide qualitative information used to investigate the proximity to bifurcations points. Such sensitivity oscillations agree with the critical eigenvalues obtained by the modal analysis approach at each EP, as reported in Table 6.1. Thus, the oscillatory behavior in the TS indicates that the EP is around the HB point and the critical eigenvalue of the EP is complex. The proximity to the HB point is qualitatively assessed by observing the damping of the TS oscillation, i.e. if the TS oscillation is positively damped, the system is operating before the HB (stable EP); however, if the TS oscillation is undamped the system operates after the HB (unstable EP).

Multi-parameter sensitivity is used to assess the loads influence around the HB. Such an assessment requires only one simulation to identify the critical loading direction on approaching HB. The TS computation in all cases started from second one onwards.

6.5.1 Stability around the Hopf Bifurcation

Figure 6.1 shows the TS w.r.t. $P_5 = 4.3$pu where the sensitivity oscillations are damped. This agrees with the corresponding critical eigenvalue $\lambda_{crit} = -0.5395 \pm 6.8512i$ which indicates that the system is not too close to the HB point. However, Figure 6.2 shows sensitivity oscillations with a very small damping when $P_5 = 4.4$pu, where the critical eigenvalue $\lambda_{crit} = -0.0305 \pm 6.1462i$ it is very close to the imaginary axis in the complex plane, and hence close to a HB point. This means that a very small variation in the load parameter could steer the system to operate in an unstable EP. Figure 6.3 shows the TS behavior when $P_5 = 4.41$pu, which corresponds to an unstable EP after a HB point. From Figure 6.1 to Figure 6.3, it is clear that the highest peaks of the TS oscillations in all cases correspond to machine 2. Therefore, such a machine is the most influential in the EP stability according to the most associated states reported in Table 6.1. However, this correspondence between associated states and TS is not always kept as will be shown in the upcoming sections.

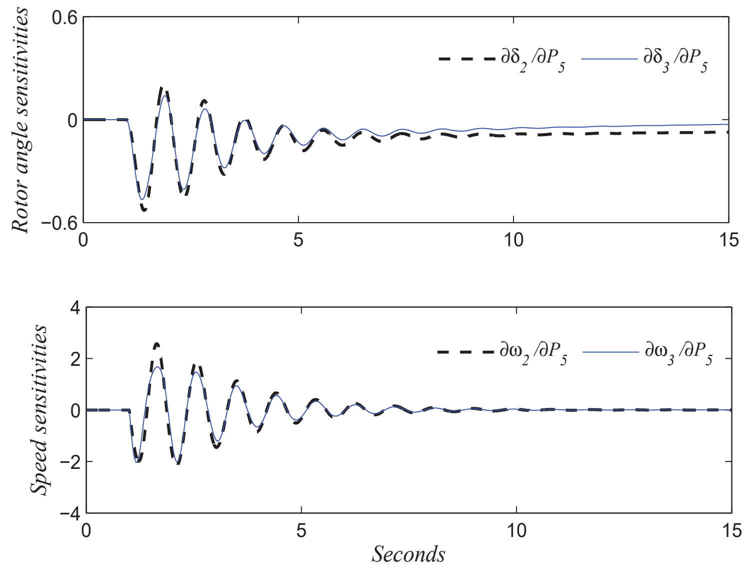

Figure 6.1: TS w.r.t. $P_5 = 4.3$pu, $\lambda_{crit} = -0.5395 \pm 6.8512i$.

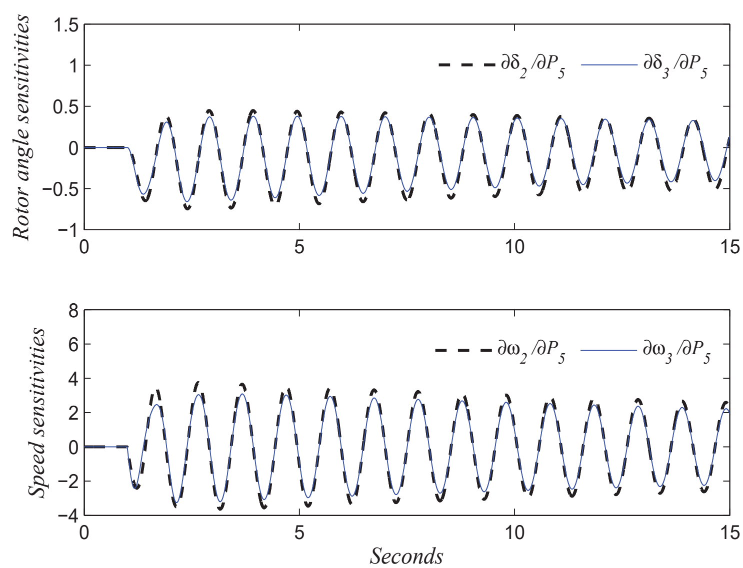

Figure 6.2: TS w.r.t. $P_5 = 4.4$pu, $\lambda_{crit} = -0.0305 \pm 6.1462i$.

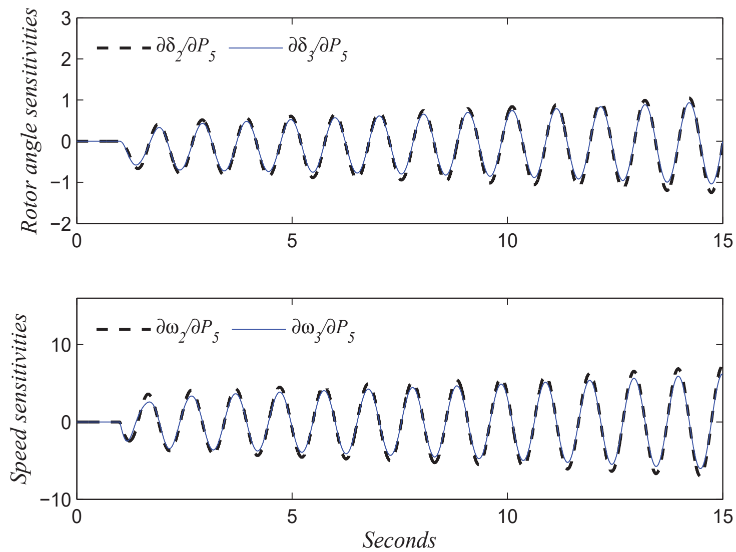

Figure 6.3: TS w.r.t. $P_5 = 4.41$pu, $\lambda_{crit} = 0.0462 \pm 6.1105i$.

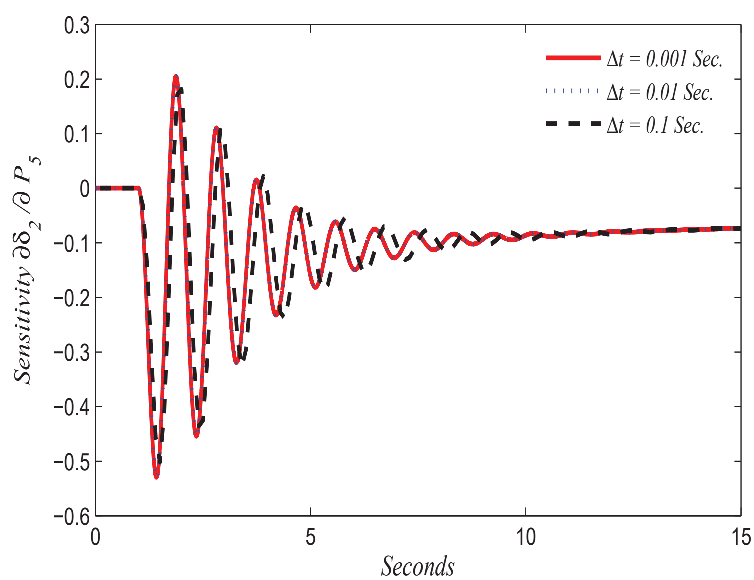

Figure 6.4: Effect of the integration time-step on trajectory sensitivities.

In order to observe the effect of the time-step integration $\triangle t$ in the computational burden, Figure 6.4 shows the rotor angle sensitivity of machine 2 w.r.t. the active power embedded at bus 5. Such a trajectory was computed using three different time-step values, as shown in the figure. The figure shows sensitivity oscillations considering a period of 14 seconds.

It is important to observe that the big difference between $\triangle t = 0.001$sec and $\triangle t = 0.01$sec results in negligible differences in the resulting trajectory sensitivities. For the two cases, the TS calculation required to compute 14000 and 1400 forward/backward substitutions, respectively. Such a difference is equivalent to reduce in 90% the number of sensitivity solutions. For the case with $\triangle t = 0.1$sec. 140 forward/backward substitutions were required, which represents a reduction of 99% of such solutions required to assess the transient. Although for this case, a small difference between trajectory sensitivities results, this is still negligible. This TS-based method can assess at the same time the effect of N_P parameters in the EP stability, whereas in the method of eigenvalues and modal analysis it is not possible.

6.5.2 Most sensitive loads to Hopf bifurcation

The participation factors provide the change of critical eigenvalues to the change of the states of critical machines $(\partial\lambda/\partial x)$, which establishes the modal analysis. However, this analysis does not provide information about the critical parameter (critical load in this case) influencing the EP stability, but only the critical machine and its most participative states. Thus, the modal analysis does not allow the direct identification of the most sensitive loading directions in the stability of the EPs around a HB point. In practice, load increments have not a unique loading direction as in the previous study, which results in a valid consideration only for academic interest. All loads are then constantly varying in N_p-dimensional directions, so that it is very important to have a general tool to assess the stability of the EPs, especially operating under stressed conditions of loading. In this context, besides identifying the critical machines (states), the proposed approach based on TS identifies the loading directions which are most sensitive to oscillatory instabilities.

Multi-parameter analysis of TS allows computing trajectory sensitivities w.r.t. N_p parameters in a power system [Hiskens and Pai, 00] at the same time, as explained in Chapter 3, and can be used to find out the influence of the different loading directions on the SSS around a HB point.

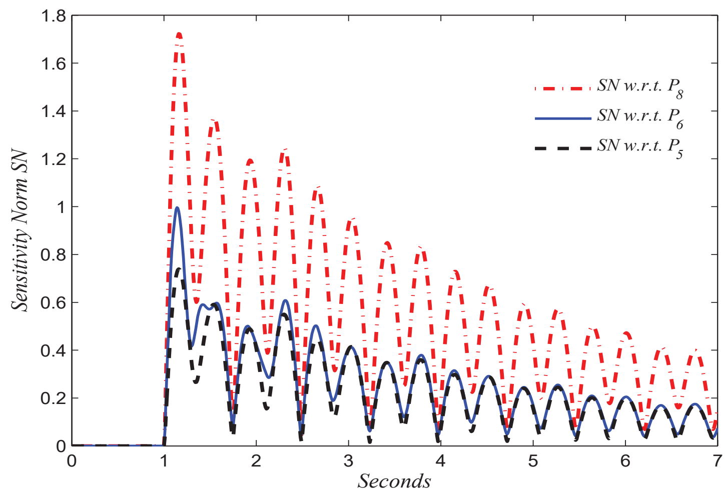

Figure 6.5: Loads' effect on the equilibrium point stability.

Figure 6.5 shows the sensitivity norm (*SN*) through the time w.r.t. the three embedded loads in the system. The load demand corresponds to the base case as provided in Appendix C. The oscillation of *SNs* shows that the load embedded at bus 8 (P_8) is the most sensitive for the EP. The load at bus 6 (P_6) is the next most sensitive and finally the load P_5. In order to validate the information provided by the *SNs* in Figure 6.5, one parametric study at a time was carried out for the active powers P_8 and P_6 as was performed in Table 6.1 for the load P_5. The results are reported in Table 6.2 as follows: the first column indicates the load nodes, columns 2 and 3 present the obtained values of *SNs* and measured powers in the base case, the fourth column provides the active power magnitude at which a HB point occurs and lastly, the fifth column indicates the active power increment from the base case to the HB point to each loading direction. It is important to observe in Table 6.2 that the increment $\Delta P_8 = 299$MW takes the system to the HB faster than $\Delta P_6 = 314$MW, and this in turn faster than $\Delta P_5 = 316$MW. This agrees with the *SNs* reported in Figure 6.5.

Table 6.2: Loads' sensitivity to Hopf Bifurcation in the WSCC system.

Node	*SN*	P_{base}(MW)	P_{HB}(MW)	ΔP_{HB}(MW)
8	1.723	100.0	399	299
6	0.997	90.0	404	314
5	0.739	125.0	441	316

6.6 Trajectory Sensitivity Analysis - Mexican system

In this section, the study consisted of computing the TS norm for 91 loads embedded in a reduced equivalent of the Mexican energy system, which consists of 190 nodes and 46 generators. The transmission components are divided into 180 transmission lines and 83 power transformers. Lastly, the system contains 26 capacitive compensators in shunt connection. The schematic and unifilar diagrams of the power system are given in Appendix E.

Via the sensitivity norm, Figure 6.6 shows the effect of the 91 system loads on a critically stable EP. It is observed that the active power of loads connected at buses from 150 to 152 are the most sensitive in the EP stability. Therefore, the loading increase in such directions will steer in a faster way the system to a HB than the rest of the system loads.

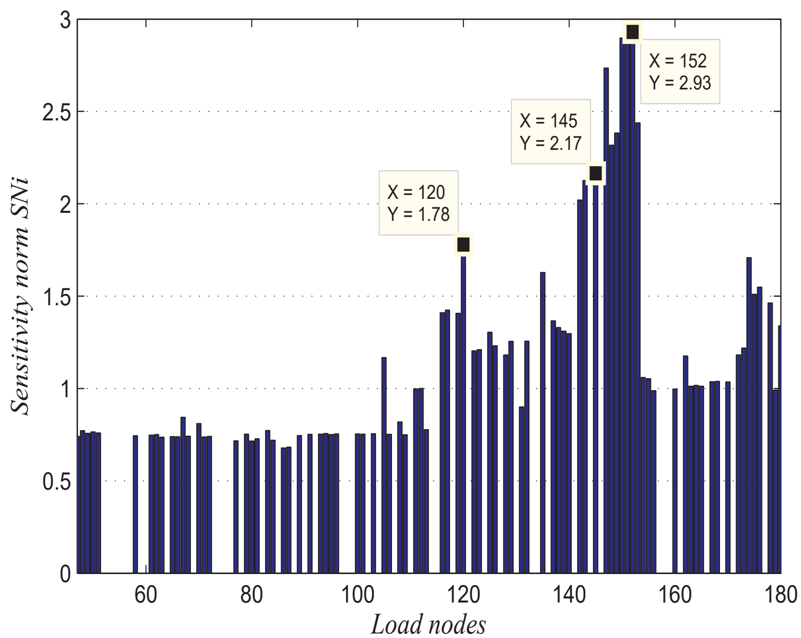

Figure 6.6: Loads' effect on the equilibrium point.

It must be pointed out that the computation of the sensitivity norms for the 91 system loads were carried out by using one sole time-domain simulation, which corresponds to solving 91 sensitivity DAE systems, with each one consisting of 702 equations and variables. Thus, the assessment of the 91 loads is equivalent to solving 63882 equations in the same simulation at the same time. However, considering the linearity of the sensitivity systems, the same time-invariant Jacobian matrix is used during the whole time-domain simulation, which considerably reduces the computational burden.

Once the critical loads have been identified from Figure 6.6, it is possible to know the most affected generators by the most sensitive loads. Figure 6.7 shows the TS w.r.t. the active power at bus 152, which resulted as the most sensitive in the sensitivity norm assessment. The damped oscillations in the TS indicate that the EP is stable, and the operation point is not at a HB, which agrees with the corresponding critical eigenvalue of the EP $\lambda = -0.0501 \pm 7.8518i$. It must be observed from Figure 6.7 that the highest rotor angle sensitivities have identified generators 32 and 33 as the most influenced by the active power embedded at bus 152.

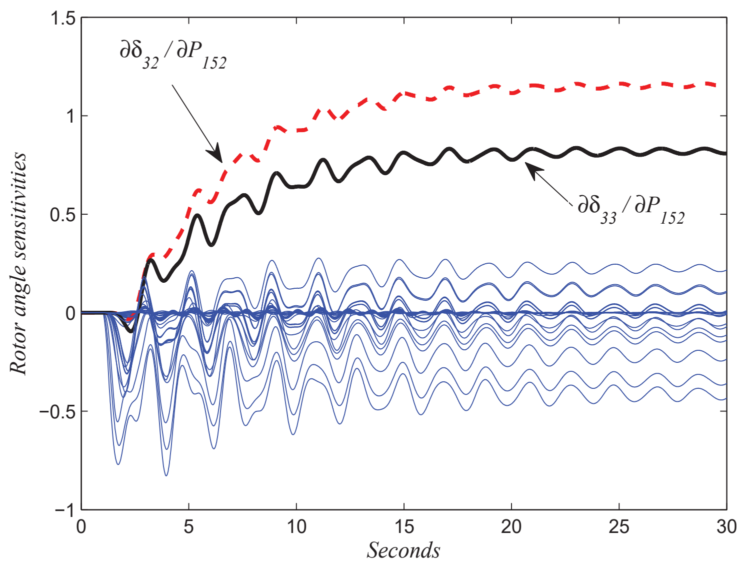

Figure 6.7: Trajectory sensitivities w.r.t. P_{152} with $\lambda = -0.0501 \pm 7.8518i$.

In order to validate the loads ranking influence via the sensitivity norm, Table 6.3 shows how the increments in the most sensitive loading directions influence the SSS, as well as the proximity to the HB point. Column 1 indicates the most sensitive loads resulted from the TS analysis shown in Figure 6.6. Column 2 shows the measured value of active power in the analyzed base case (P_{base}) corresponding to Figure 6.7. In columns 3 and 4 (ΔP(60MW)) and (λ_{crit}) represent the increment in the specified loading direction and the critical eigenvalue for the new EP resulting from such an increment, respectively. Lastly, in columns 5 and 6 (P_{HB})

and (ΔP_{HB}) indicate the value and increased amount of the active power where the system crosses a HB point by following the corresponding loading directions.

Table 6.3: Loads' sensitivity to Hopf Bifurcation in the Mexican system.

Node	P_{base} (MW)	$\Delta P(60\text{MW})$	λ_{crit}	P_{HB}(MW)	ΔP_{HB}(MW)
152	172.64	232.64	$0.0219 \pm 5.0272i$	225.64	53.0
150	188.24	248.64	$0.0187 \pm 5.0308i$	242.24	54.0
151	18.72	78.72	$0.0159 \pm 5.0344i$	72.72	54.0
147	104.00	164.00	$0.0122 \pm 5.0522i$	160.00	56.0
153	78.00	138.00	$-0.0113 \pm 8.8336i$	141.00	63.0
145	83.20	143.20	$-0.0154 \pm 5.1393i$	155.20	72.0
120	308.88	368.88	$-0.0501 \pm 7.8519i$	497.88	189.0

It is important to outline that the load effect in the EP stability is not only dependent on the magnitude, but also on the topologic location of loads. For example, the power demand embedded at bus 120 is 17 times larger than the load at bus 151; however, the load at 151 resulted in being more sensitive that the load embedded at bus 120, as shown in Table 6.3, column 2. It must be observed that the most sensitive loads (loads 152-147) provided a major change in the critical eigenvalue and thus in the SSS. The same increment in the most sensitive loading directions (buses 152-147) led the system to oscillatory instability due to a HB point, whereas with the increment in the least sensitive loading directions the system remained stable. Then, the stability margins in the most sensitive loading directions become more reduced; therefore, according to the sensitivity ranking in Table 6.3, as the most sensitive loads were increased the appearance of the HB was found faster as can be observed in column 6.

6.7 Conclusions

In this chapter we proposed an alternative method for monitoring the Hopf Bifurcations along variations in multidimensional loading directions by using a time domain method, which is based on trajectory sensitivities. This method is general and flexible, i.e. the size of the power systems, as well as the complexity of their mathematical modeling do not represent any restriction.

The proposed method allowed to identify the critical loading directions that steer the system to Hopf Bifurcation points. Such a method was tested in the 9-buses, 3-generators system as well as in a 190-buses, 46-generators system. Regardless of the number of sensitivity parameters and system dimensions the proposed method requires only one simulation. Such a method keeps constant the Jacobian matrix of the system, requiring only one evaluation and factorization during the whole simulation. The computational effort then, consists of performing just one forward/backward substitution at each time step. Furthermore, the method can handle a very large integration step to drastically reduce the computational effort.

Chapter 7

GENERAL CONCLUSIONS AND SUGGESTIONS FOR FUTURE RESEARCH WORK

7.1 General conclusions

This research has been focused on developing trajectory sensitivity-based approaches for improving the security of electric power systems. In general, these approaches were especially developed in order to increase the angular stability of power systems. For these purposes, a transient stability digital program was developed considering the power balance formulation and the implementation of an efficient methodology to compute TS w.r.t. multiple parameters of the power systems, at the same time. The transient stability time domain-solution of the DAE systems under a single frame of reference is obtained by using simultaneous implicit integration. In this thesis, the implementation of the trajectory sensitivity theory was done by means of the programming of the SDM. It is important to point out that this methodology has been proposed in several research works in the open literature; however, it had been never reported as implemented and used on power system stability assessment. In this thesis, such a methodology was implemented in C++ programming language under an object oriented programming philosophy, by considering sparsity and pre-ordering techniques to improve the computational efficiency. The methodology efficiency, programming philosophy as well as computational efficiency allowed us to develop efficient approaches in order to improve the angular stability of the power systems.

The developed digital program was used on locating series-connected controllers to improve the power system security from the transient stability point of view. This approach allowed us to improve the transient stability from a global viewpoint by compensating the most sensitive transmission line in geographical area of a power system. The compensation of the most sensitive line, which is located in a critical region, allowed us to improve the critical clearing times of all considered faults. The proposed approach based on the multi-parameter trajectory sensitivity method has proved to be much more efficient with respect to the numerical approach, from the computational effort point of view, because of the huge reduction of the number of simulations required to assess the critical component of the power system.

Owing to the fact that the trajectory sensitivities model is derived from the set of DAE associated with the power system, it was also possible to extended the proposed approach to compute TS of nodal voltage magnitudes with respect to all reactive power demanded by loads. Such sensitivities were used to assess the effect of a generator outage in the system voltage profile. Hence, indices based on voltage magnitude sensitivities were proposed in order to estimate the total load to be shed, as well as its distribution percentages to improve the voltage profile of power systems.

Finally, the digital program developed in this thesis was utilized to assess and improve the small signal stability of equilibrium points. Based on trajectory sensitivities w.r.t. all system loads, an approach was proposed to identify the most influential loads in the stability of an equilibrium point. The approach is capable to assess all system loading directions and identify the most critical, at the same time. From the operation point of view, this information is of paramount importance because allows to detect those likely loads that could steer the system toward a Hopf bifurcation point. It must be pointed out that if the numerical approach is used to assess the effect of parameters variation, one solution is required for each perturbed parameter, such that it is necessary to perform n simulations for the n parameters assessment. However, the proposed approach requires one sole solution (1-simulation) for the assessment of n parameters. The approach efficiency was tested in a 190-bus, 46-generators system where 91 loads were assessed at same time.

The computational implementation of the analytical method to calculate multi-parameter trajectory sensitivities represents an new contribution to the state of art. The features of such an implementation allowed to develop the proposed approaches in this thesis in order to improve the transient stability and assessing the small signal stability of power systems. Hence, these proposals based on multi-parameter sensitivities computation and sensitivity indices represent new and important contributions to the state of art in the trajectory sensitivity topic, employed to improve the power system security. Lastly, in addition to the benefits provided by this implementation, new and attractive ideas have emerged, which could be developed in a future research work as suggested in the following section.

7.2 Suggestions for future research work

Trajectory sensitivity theory has demonstrated to be a powerful tool in power systems stability. In order to extend the research reported in this thesis, an interesting suggestion for future research work is to use trajectory sensitivities to estimate the amount of series compensation required to obtain the maximum improvement of the transient stability. In this case, besides to identify the best line to improve the transient stability from a global point of view, we will be able to calculate the optimal amount of such a compensation to obtain the best improvement of the power system security.

Another interesting application is to compute trajectory sensitivities on-line together with dynamic state estimation. Considering the linear computation of the trajectory sensitivities after one dynamic state estimation, the trajectory sensitivities could be computed, and the assessment of the parameters influence in the voltage stability could be performed on-line.

On the other hand, an easy and fast modification of the developed digital program will allow us to investigate the most influential system parameter for the equilibrium points in small signal stability. The sensitivity and selective modal analyses could be integrated in a general approach suitable to identify the most associated system parameter to the critical eigenvalue. Such an approach could use the sensitivities with respect to line susceptances to allocate series and shunt compensation in order to improve the stability of equilibrium points.

The most of the computational effort required to perform a transient stability analysis preserving the network structure is spent during the Jacobian matrix computation. An increase in the computational efficiency in the security assessment could be attained if a current injections formulation is employed to assess the transient stability instead of the power flow formulation. In this case, the majority of the Jacobian elements are constant during the whole simulation. In this context, we propose to combine the current injections formulation for transient stability and the power flow formulation for the trajectory sensitivity model. The time of simulation should be reduced more as the size of the power systems increase.

Bibliography

[Acha et al., 02] E. Acha, V. G. Angelidis, O. Anaya-Lara, and T.J.E Miller, "Power Electronic Control in Electrical Systems", Plan and Tree, 2002.

[Acha et al., 04] E. Acha, C.R. Fuerte-Esquivel, H. Ambriz-Perez and C. Angeles-Camacho, FACTS: Modelling and Simulation in Power Networks, John Wiley & Sons, 2004.

[Ajjarapu and Lee, 92] V. Ajjarapu, B. Lee, Bifurcation, "Theory and its application to nonlinear dynamical phenomena in an electrical power system", *IEEE Trans. On Power Syst.* 7 (1) pp. 424-431, 1992.

[Ajjarapu, 06] V. Ajjarapu, "Computational Techniques for Voltage Stability Assessment and Control", Springer, 2006.

[Alvarado et al., 83] F. L. Alvarado, R. H. Lasseter and J. J. Sanchez, 'Testing of trapezoidal integration with damping for the solution of power transient problems', *IEEE Transactions On Power Apparatus and Systems*, Dec. 1983, Vol. PAS-102, pp. 3783-3790.

[Anderson and Fouad, 94] M. P. Anderson and A. A. Fouad, "Power System Control and Stability," IEEE Press, 1994.

[Barlow and Bernat, 94] M. J. Barlow and P. Z. Bernat: "The Practicalities of Implementing On-Line Network Analysis and Data Management," IEE Colloquium on 'Developments with Interfacing of Power System Analysis Software with SCADA and Data Management Systems', London, UK, 15 Nov. 1994.

[Beardmore and Laister, 78] R. E. Beardmore and R. Laister, "The flow of a differential-algebraic equation near a singular equilibrium", SIAM J. Matrix Anal. Vol. 4, no. 1, pp. 106-120, 2002.

[Benchluch and Chow, 93] S.M. Benchluch and J.H. Chow, A trajectory sensitivity method for the identification of nonlinear excitation system models, *IEEE Trans. Energy Convers.*, Vol. 8, No. 2, (June) (1993), pp. 159-165.

[Bikhovsky, 58] M. L. Bikhovsky, "Dynamic Accuracy of Electrical and Mechanical Circuits." Akademia Nauk USSR, Moscow, 1958.

[Bikhovsky, 64] M. L. Bikhovsky, Sensitivity and Dynamic Accuracy of Control Systems, Eng. Cibern. (USSR), 121-134 (1964).

[Bode, 45] H. W. Bode, "Network Analysis and Feedback Amplifier Design." Van Nostrand-Reinhold, Princeton, New Jersey, 1945.

[Brogan, 74] W. L. Brogan, "Modern Control Theory." Quantum Publ, Inc., 1974.

[Buzzi-Ferraris, 94] G. Buzzi-Ferraris: 'Scientific C++, Building Numerical Libraries the Object Oriented Way', Ed. Addison-Wesley, 1994, ISBN 0-201-63192-X.

[Campbell and Marszalek, 99] S. L. Campbell and W. Marszalek, "Index of infinite dimensional differential algebraic equations", Mathemat. Comput. Modeling of Dynamical Syst., vol. 5, pp. 18-42, 1999.

[Capper, 94] D.M. Capper: 'C++ for Scientists, Engineers and Mathematicians', Springer-Verlag, 1994, ISBN 0-387-19847-4.

[Cañizares and Faur, 99] C.A. Cañizares, and Z.T. Faur, Analysis of SVC and TCSC controllers in voltage collapse, *IEEE Trans. Power Syst.* Vol. 14, (Feb.) (1999), pp. 158-165.

[Chatterjee and Ghosh, 07] D. Chatterjee and A. Ghosh, Transient stability assessment of power system containing series and shunt compensators, *IEEE Trans. on Power Syst.*, Vol. 22, No. 3, (Aug.) (2007), pp.1210-1220.

[Chatterjee and Ghosh, 07-1] D. Chatterjee and A. Ghosh, Application of the Trajectory Sensitivity for the Evaluation of the Effect of TCSC Placement on Transient Stability, *International Journal of Emerging Electric Power Systems*, Vol. 8, No. 1. 2007.

[Chatterjee and Ghosh, 07-2] D. Chatterjee and A. Ghosh, TCSC control design for transient stability improvement of a multi-machine power system using trajectory sensitivity, *Electric Power System Research* 77, (June) (2007), 470-483.

[Chatterjee et al., 08] D. Chatterjee, A. Ghosh and M. A. Pai, Trajectory Sensitivity Analysis in Distributed Generation Systems, *International conference on Power Electronics*, Drives and Energy Systems, PEDES 06, p. 1-6, 12 to 15 December 2008.

[Chen, 99] C. T. Chen, "Linear System Theory and Design," 1999.

[Chiang et al., 95] H. D. Chiang, C. C. Chu, and G. Cauley, "Direct stability analysis of electric power system using energy functions: Theory, applications, and perspective," *Proceedings of the IEEE*, Vol. 83, No. 11, pp. 1497-1529, Nov. 1995.

[Cruz and Perkins, 64] J. B. Cruz and W. R. Perkins, A New Approach to the Sensitivity Problem in Multivariable Feedback System Design, *IEEE Trans. Autom. Contr.* 9, 216.223 (1964).

[Cruz and Perkins, 65] J. B. Cruz and W. R. Perkins, Sensitivity Comparison of Open-Loop and Closed- Loop Systems, Proc. Ann. Allerton Conf., 3rd, October 1965.

[Cruz and Perkins, 66] J. B. Cruz and W. R. Perkins, Criteria for System Sensitivity to Parameter Variations, IFAC Cong., 3rd, London, 1966, Paper 18C.

[EPRI, 77] "Power System Dynamic Analysis-Phase I," EPRI Report EL-484, Electric Power Research Institute, July 1977.

[Fang and Ngan, 99] W.L. Fang, and H.W. Ngan, "Optimising location of unified power flow controllers using the method of augmented Lagrange multipliers," *IEE Proc.-Gener. Transm. Distrib*, Vol. 146, (September) (1999), pp. 428-434.

[Foley et al., 93] M. Foley, A. Bose, W. Mitchell and A. Faustini: "An Object Based Graphical User Interface for Power Systems," *IEEE Trans. on Power Systems*, Vol. 8, No. 1, pp. 97-104, Feb. 1993.

[Foley and Bose, 95] M. Foley and A. Bose: "Object-Oriented On-Line Network Analysis," *IEEE Trans. on Power Systems*, Vol. 10, No. 1, pp. 125-132, Feb. 1995.

[Fouad and Vittal, 92] A.A. Fouad and V. Vittal, Power System Transient Stability Analysis using the Transient Energy Function Method, Prentice Hall, Englewood Cliffs, New Jersey, 1992.

[Frank, 78] Paul M. Frank, "Introduction to System Sensitivity Theory", Academic Press, 1978.

[Fuerte and Acha, 97] C.R. Fuerte-Esquivel and E. Acha, "A Newton-type Algorithm for the Control of Power Flow in Electrical Power Networks," *IEEE Trans. on Power Syst.*, Vol. 12, No. 4, Nov 1997.

[Fuerte et al., 98] C.R. Fuerte-Esquivel, E. Acha, S. G. Tan and J.J. Rico, "Efficient Object Oriented Power Systems Software for the Analysis of Large-Scale Networks Containing FACTS-Controlled Branches," *IEEE Trans. on Power Syst.*, Vol. 13, No. 2, May 1998.

[Gamm and Golub, 98] A.Z. Gamm, and I.I. Golub, "Determination of locations for FACTS and energy storage by the singular analysis," in: *Proceedings of International Conference on Power System Technology*, Powercon '98., pp. 411-414.

[Gerbex et al., 03] S. Gerbex, R. Cherkaoui, and A.J. Germond, Optimal location of FACTS devices to enhance power system security, in: *Proceedings IEEE Bologna Power Tech Conf.*, (2003) 7 pages.

[Hakavik and Holen, 94] B. Hakavik and A.T. Holen, "Power System Modelling and Sparse Matrix Operations Using Object Oriented Programming," *IEEE Trans. on Power Systems*, Vol. 9, No. 2, pp. 1045-1051, May 1994.

[Hill and Mareels, 90] D. J. Hill and M. Y. Mareels, “Stability theory for differential/algebraic systems with application to power system”, *IEEE Trans. Circuits Syst.*, vol. 37, no. 11, pp. 1416-1423, Nov. 1990.

[Hiskens and Pai, 00] I. A. Hiskens and M. A. Pai, “Trajectory sensitivity analysis of hybrid systems,” *IEEE Trans. on Circ. and Syst.*-I, Vol. 47, No. 2, pp. 204-220, Feb. 2000.

[Hiskens et al., 00-1] I.A. Hiskens, M.A. Pai, and T.B. Nguyen, “Bounding uncertainty in power system dynamic simulations,” in: *Proceedings IEEE PES Winter Meeting*, 2000, pp. 1533-1537.

[Hiskens and Pai, 00-2] I. A. Hiskens and M. A. Pai, “Power system application of trajectory sensitivities,” in: *Proceedings IEEE PES Winter Meeting*, 2000, pp. 1200-1205.

[Hiskens, 01] I. Hiskens, Nonlinear dynamic model evaluation from disturbance measurements, *IEEE Trans. Power Syst.* Vol. 16, No. 4, (Nov.) (2001), pp. 702-710.

[Hiskens and Alseddiqui, 06] I.A. Hiskens and J. Alseddiqui, Sensitivity, approximation, and uncertainty in power system dynamic simulation, *IEEE Trans. Power Syst.*, Vol. 21, No. 4, (Nov.) (2006), pp. 1808-1820.

[Hiskens and Akke, 99] I. A. Hiskens and M. Akke, Analysis of the Nordel power grid disturbance of January 1, 1997 using trajectory sensitivities, *IEEE Trans. on Power Syst.*, Vol.14, No.3, (Aug.) (1999), pp. 987-994.

[Horowitz, 63] I. M. Horowitz, “Synthesis of Feedback Systems.” Academic Press, New York, 1963.

[Horowitz and Shaked, 75] I. M. Horowitz and U. Shaked, Superiority of Transfer Function over State Variable Methods in Linear Time-Invariant Feedback System Design, *IEEE Trans. Autom. Contr*. 84-97 (1975).

[Huneault and Galiana, 91] M. Huneault and F. D. Galiana, “A survey of the optimal power flow literature,” *IEEE Trans. On Power Syst.*, Vol. 6, No. 2, pp. 762-770, May 1991.

[IEEE, 02] C. A. Cañizares, "Voltage stability assessment: concepts, practices and tools", Tech. rep., IEEE/PES Power System Stability Subcommitee, Final Document, available at http://www.power.uwaterloo.ca (Aug. 2002).

[IEEE, 04] IEEE/CIGRE Joint Task Force on Stability Terms and Definitions, "Definition and Classification of Power System Stability", *IEEE Trans. On Power Syst.*, Vol. 19, No. 2, May 2004.

[IEEE, 73] IEEE Working group on power plant response to load changes: 'MW response of fossil fueled steam units', *IEEE Trans.*, 1973, PAS-92, pp. 455-463.

[IEEE, 93] IEEE Task force on load representation for dynamic performance, Load Representation for Dynamic Performance Analysis, *IEEE Trans. On Power Systems*, Vol. 8, No. 2, May 1993.

[Joorabian et al, 08] M. Joorabian, N. F. Ramandi, and M. Ebadi, "Optimal Location of Static VAR Compensator (SVC) Based on Small Signal Stability of Power System", 2nd IEEE International Conference on Power and Energy (PECon 08), Dec. 1-3, 2008, Johor Baharu, Malaysia.

[Kokotovic, 64] P. V. Kokotovic, Method of Sensitivity Points in the Investigation and Optimization of Linear Control Systems, Autom. Remote Control (USSR) 1512-1518, (1964).

[Kokotovic and Rutman, 65] P. V. Kokotovic and R. S. Rutman, Sensitivity of Automatic Control Systems (Surver), Autom. Remote Control (USSR) 26. 727-749 (1965).

[Kokotovic and Rutman, 66] P. Kokotovic and R. S. Rutman, On the Determination of Sensitivity Functions with Respect to the Change of System Order, Proc. Int. Symp. Sensitivity, Dubrovnik, Yugoslavia, 1964, pp. 131-137, Pergamon Press, Oxford, 1966.

[Kokotovic and Sannuti, 68] P. Kokotovic and P. Sannuti, Singular Perturbation Method for Reducing the Model Order in Optimal Control Design, *IEEE Trans. Autom. Contr*. 13, 377-384 (1968).

[Kokotovic et al., 69] P. Kokotovic, J. Heller and P. Sannuti, Sensitivity Comparison of Optimal Controls, Int. J. Contr. 111-117 (1969).

[Kreindler, 68] E. Kreindler, On the Definition and Application of the Sensitivity Function, J. Franklin Inst. 285, 26-36 (1968).

[Kreindler, 68-1] E. Kreindler, Closed-Loop Sensitivity Reduction of Linear Optimal Control Systems, *IEEE Trans. Autom. Contr.* 13, 254-262, (1968).

[Kreindler, 69] E. Kreindler, Formulation of the Minimum Trajectory Sensitivity Problem, *IEEE Trans. Autom. Contr*. 14, 206-207 (1969).

[Kundur, 94] P. Kundur, “Power System Stability and Control,” McGraw Hill, 1994.

[Kwatny et al., 95] H. G. Kwatny, R. F. Fischl, and C. O. Nwankpa, “Local bifurcation in power systems: Theory, computation and applications”, *Proc. IEEE*, vol. 83, no. 11, pp. 1456-1483, Nov. 1995.

[Laufenberg and Pai, 98] M. J. Laufenberg and M. A Pai., “A new approach to dynamic security assessment using trajectory sensitivities,” *IEEE Trans. Power Syst.*, Vol. 13, No. 3, pp. 953-958, Aug. 1998.

[Lima et al., 03] F.G.M. Lima, F.D. Galiana, I. Kockar, and J. Munoz, “Phase shifter placement in large-scale systems via mixed integer linear programming,” *IEEE Trans. Power Syst.* Vol. 18, (Aug.) (2003), pp. 1029-1034.

[Lyapunov, 67] A. M. Lyapunov, Stability of Motion, English translation, Academic Press, Inc., 1967.

[Magaji and Mustafa, 08] N. Magaji and M.W. Mustafa, Optimal location of FACTS devices for damping oscillations using residue factor, in: *Proceedings 2nd Int. Conf. on Power and Energy*, 2008 pp. 1339-1344.

[Mansour et al., 94] Y. Mansour, W. Xu, F. Alvarado, and C. Rinzin, SVC placement using critical modes of voltage stability, *IEEE Trans. Power Syst.* Vol. 9, (May) (1994), pp. 757-762.

[Manzoni et al., 97] A. Manzoni, E. Silveira, A. Silva and I.C. Decker: 'Power Systems Dynamics Simulation Using Object-Oriented Programming', accepted for its publication in *IEEE Trans. on Power Systems*, 1997.

[Martins and Lima, 90] N. Martins, and L. Lima, Determination of suitable location for power systems stabilizers and static VAR compensators for damping electromechanical oscillations in large power systems, *IEEE Trans. Power Syst.* Vol. 5, No. 4, (Nov.) (1990), pp. 1455-1469.

[Messina et al., 02] A.R. Messina, H. Hernández, E. Barocio, M. Ochoa, J. Arroyo "Coordinated application of FACTS controllers to damp out interarea oscillations," *Electric Power Systems Research* 62 (2002) 43-53.

[Nayfeh and Balachandran, 95] A. H. Nayfeh and B. Balachandran, "Applied Nonlinear Dynamics", John Wiley & Sons,1995.

[Neyer et al., 90] A. F. Neyer, F. F. Wu and K. Imhof: 'Object Oriented Programming for Flexible Software: Example of a Load Flow', *IEEE Trans. on Power Systems*, Vol. 5, No. 3, pp. 689-696, Aug. 1990.

[Nguyen et al., 02] T. B. Nguyen, M. A. Pai and I. A. Hiskens, Sensitivity approaches for direct computation of critical parameters in a power system, *Electric Power & Energy Systems* 24 (2002) 337-343.

[Nguyen, 02-1] T. B. Nguyen, Dynamic Security Assessment of Power Systems using Trajectory Sensitivity Approach, Ph. D. Thesis, University of Illinois, Urbana-Champaign 2002, Illinois, USA.

[Nguyen and Pai, 03] T.B. Nguyen and M.A. Pai, Dynamic security-constrained rescheduling of power systems using trajectory sensitivities, IEEE *Trans. on Power Syst.*, Vol.18, No.2, (May) (2003), pp. 848-854.

[Nguyen and Pai, 08] T. Nguyen and M. Pai, A sensitivity-based approach for studying stability impact of distributed generation, *International Journal of Electrical Power & Energy Systems*, Vol. 30, No. 8, 2008.

[Nuguyen, 71] Thuong Ngo Nuguyen, Sensitivity of Automatic Control Systems (Survey), Autom. Remote Control (USSR) 32, 735-762 (1971).

[Okamoto et al., 95] H. Okamoto, A. Kurita and Y. Sekine, A method for identification of effective locations of variable impedance apparatus on enhancement of steady-state stability in large scale power systems, *IEEE Trans. Power Syst.* Vol. 10, No. 3, (Aug.) (1995), pp. 1401-1407.

[Padiyar and Ghosh, 89] K. R. Padiyar and K. K. Ghosh, "Direct stability evaluation of power systems with detailed generator models using structure preserving energy functions," *International Journal of Electrical Power and Energy Systems*, Vol. 11, No. 1, pp. 47-56, Jan. 1989.

[Padiyar and Varma, 91] K.R. Padiyar and R.K. Varma, "Damping torque analysis of static var system controllers," *IEEE Transactions on Power System*, Vol. 6, No. 2, May 1991, pp. 458-465.

[Padiyar and Rao, 95] K. Padiyar and K. Uma Rao, "Investigations of power flow control schemes with controlled series compensator," presented at *EHV Technology Conference*, Bangalore, India, August 1995.

[Pai, 89] M. A. Pai, Energy Function Analysis for Power System Stability. Kluwer, 1989.

[Paterni et al, 99] P. Paterni, S. Vitet, M. Bena, and A. Yokoyama, Optimal location of phase shifters in the French network by genetic algorithm, *IEEE Trans. Power Syst.* Vol. 14, (Feb.) (1999) pp. 37-42.

[Perkins and Cruz, 65] W. R. Perkins and J. B. Cruz, The Parameter Variation Problem in State Feedback Control Systems, Trans. ASME 87, 120-124 (1965).

[Perkins and Cruz, 66] W. R. Perkins and J. B. Cruz, Sensitivity Operators for Linear Time-Varying Systems, Proc. Int. Symp. Sensitivity, Dubrovnik, Yugoslavia, 1964, pp. 67-77, Pergamon Press, Oxford, 1966. Symp.

[Perkins, 71] W. R. Perkins, Sensitivity Models for Discrete-Time Linear Systems, 2nd, Proc. IFAC Symp. On Multivariable Technical Control Systems, Düsseldorf, 1971, pp. 1-9, Paper 1.5.3.

[Perkins et al., 72] W. R. Perkins and J. B. Cruz and P. Kokotovic, The Sensitivity Techniques for Adaptive Control, Proc. Int. Conf. Cybern. Soc., Washington, D.C., October 1972, pp. 396-400.

[Poonam, 07] M. J. Poonam, Load shedding algorithm using voltage and frequency data, M.Sc. Thesis, Clemson University, December 2007.

[Pérez et al., 82] I. J. Pérez-Arriaga, G. C. Verghese, and F. C. Schweppe, "Selective Modal Analysis with Applications to Electric Power Systems, Part I: The Dynamic Stability Problem", *IEEE Trans. On Power Apparatus and Syst.*, Vol PAS-101, No. 9, Sept. 1982.

[Sadikovic et al., 06] R. Sadikovic, G. Andersson and P. Korba, Method for Location of FACTS for Multiple Control Objectives, X SEPOPE, Brasil, May 2006.

[Sanchez et al., 88] J. J. Sanchez-Gasca, C. J. Bridenbaugh, C. E. J. Bowler, and J. S. Edmonds, Trajectory sensitivity based identification of synchronous generator and excitation system parameters, *IEEE Trans. Power Syst.*, Vol. 3, No. 4, (Nov.) (1988), pp. 1814-1822.

[Sauer, 02] P. W. Sauer, "Post-contingency equilibrium analysis of power systems," in *Proceedings of the 35th Annual Hawaii International Conference, 2002*.

[Sauer et al., 89] P. W. Sauer, A. K. Behera, M A. Pai, J. R. Winkelman and J. H. Chow, Trajectory approximations for direct energy methods that use sustained faults with detailed power system models, *IEEE Trans. on Power Syst.*, Vol. 4, No. 2, (May) (1989), pp. 499-506.

[Sauer and Pai, 98] P. W. Sauer and M. A. Pai, "Power System Dynamics and Stability", Prentice Hall, 1998.

[Shackshaft et al., 77] G. Shackshaft, O. C. Symons, and J. G. Hadwick, : 'General-purpose model of power system loads', *Proc. IEE*, 1977, 124, (8), pp. 715-723.

[Sharma and Singh, 07] C. Sharma and P. Singh, "Contribution of Loads to Low Frequency in Power System Operation", iREP Symposium-Bulk Power System Dynamics and Control-VII, Revitalizing Operational Reliability, Aug. 19-24, Charleston, SC, USA, 2007.

[Shubhanga and Kulkarni, 02] K.N. Shubhanga, and A.M. Kulkarni, Application of structure preserving energy margin sensitivity to determine the effectiveness of shunt and series FACTS devices, *IEEE Trans. on Power Syst.*, Vol. 17, No. 3, (Aug.)(2002), pp.730-738.

[Shubhanga and Kulkarni, 04] K. N. Shubhanga and A. M. Kulkarni, "Determination of Effectiveness of Transient Stability Controls Using Reduced Number of Trajectory Sensitivity Computations", *IEEE Trans. on Power Systems*, Vol 19, No. 1, Feb. 2004.

[Singh and David, 01] S.N. Singh, and A.K. David, Optimal location of FACTS devices for congestion management, Elect. Power Syst. Res., Vol. 58, (Jun.) (2001), pp. 71-79.

[Song and Johns, 99] Y.H. Song and A.T. Johns (Editors), Flexible AC Transmission Systems (FACTS), *IEE Power and Energy series* 30, 1999.

[Stagg and El-Abiad, 68] Stagg and El-Abiad, "Computer Methods in Power System Analysis," McGraw-Hill, 1968.

[Tinney and Walke, 67] W.F. Tinney and J.M. Walke: 'Direct Solutions of Sparse Network Equations by Optimally Ordered Triangular Factorization', *Proc. of IEEE*, vol. 55, pp. 1801-1809, Nov. 1967.

[Tomovic and Vucobratovic, 72] R. Tomovic and M. Vucobratovic, "General Sensitivity Theory." Amer, Elsevier, New York, 1972.

[Venkatasubramanian et al., 92] V. Venkatasubramanian, H. Schattler and J. Zaborszky, "A Stability Theory of large differential Algebraic Systems: A Taxonomy," Dept. Systems Sci. and Mathemat., Washington Univ., St. Louis, MS, Report SSM 9201-Part I, 1992.

[Verghese et al., 82] G. C. Verghese , I. J. Pérez-Arriaga, and F. C. Schweppe , "Selective Modal Analysis with Applications to Electric Power Systems, Part II: Heuristic Introduction", *IEEE Trans. On Power Apparatus and Syst.*, Vol PAS-101, No. 9, Sept. 1982.

[Vittal, 00] V. Vittal, "Consequence and impact of electric utility industry restructuring on transient stability and small signal stability analysis," *Proc. of IEEE*, Vol. 88, No. 2, pp. 196-207, Feb. 2000.

[Vittal et al., 89] V. Vittal, E-Z. Zhou, C. Hwang, and A.A. Fouad, Derivation of stability limits using analytical sensitivity of the transient energy margin, *IEEE Trans. on Power Syst.*, Vol. 4, No. 4, (Oct.)(1989), pp.1363-1372.

[Wang, 99] H.F. Wang, Selection of robust installing locations and feedback signals of FACTS-based stabilizers in multi-machine power systems, *IEEE Trans. Power Syst.* Vol. 14, No. 2, (May.) (1999), pp. 569-574.

[Wen, 05] Wen Xiaoyu, "A Novel Approach for identification and Tracing of Oscillatory Stability and Damping Ratio Margin Boundaries", A dissertation for PhD degree, Iowa State University, 2005.

[Zhao et al., 94] J. Zhao, A. Ishigame, S. Kawamoto, and T. Taniguchi, Structural control of electric power networks for transient stability, *IEEE Trans. on Power Syst.*, Vol. 9, No. 3, (Aug.)(1994), pp.1575-1581.

Appendix A

GENERATOR MODEL

A.1 Linear magnetic circuit model

The generator model in the frame of reference rotating synchronously is [Sauer and Pai, 98],

$$\frac{1}{\omega_0}\frac{d\psi_{Di}}{dt} = R_{si}I_{Di} + \psi_{Qi} + V_{Di} \tag{A.1}$$

$$\frac{1}{\omega_0}\frac{d\psi_{Qi}}{dt} = R_{si}I_{Qi} - \psi_{Di} + V_{Qi} \tag{A.2}$$

$$\frac{1}{\omega_0}\frac{d\psi_{0i}}{dt} = R_{si}I_{0i} + V_{0i} \tag{A.3}$$

$$T'_{d0i}\frac{dE'_{qi}}{dt} = -E'_{qi} - (X_{di} - X'_{di})\left[I_{di} - \frac{(X'_{di} - X''_{di})}{(X'_{di} - X_{lsi})^2}\left(\psi_{1di} + (X'_{di} - X_{lsi})I_{di} - E'_{qi}\right)\right] + E_{fdi} \tag{A.4}$$

$$T''_{d0i}\frac{d\psi_{1di}}{dt} = -\psi_{1di} + E'_{qi} - (X'_{di} - X_{lsi})I_{di} \tag{A.5}$$

$$T'_{q0i}\frac{dE'_{di}}{dt} = -E'_{di} - (X_{qi} - X'_{qi})\left[I_{qi} - \frac{(X'_{qi} - X''_{qi})}{(X'_{qi} - X_{lsi})^2}\left(\psi_{2qi} + (X'_{qi} - X_{lsi})I_{qi} + E'_{di}\right)\right] \tag{A.6}$$

$$T''_{q0i}\frac{d\psi_{2qi}}{dt} = -\psi_{2qi} - E'_{di} - (X'_{qi} - X_{lsi})I_{qi} \tag{A.7}$$

$$\frac{d\delta_i}{dt} = \omega_i - \omega_0 \tag{A.8}$$

$$\frac{2H}{\omega_0}\frac{d\omega_i}{dt} = P_{Mi} - (\psi_{di}I_{qi} - \psi_{qi}I_{di}) - D_i(\omega_i - \omega_0) \tag{A.9}$$

$$\psi_{di} = -X''_{di}I_{di} + \frac{(X''_{di} - X_{lsi})}{(X'_{di} - X_{lsi})}E'_{qi} + \frac{(X'_{di} - X''_{di})}{(X'_{di} - X_{lsi})}\psi_{1di} \tag{A.10}$$

$$\psi_{qi} = -X''_{qi}I_{qi} - \frac{(X''_{qi} - X_{lsi})}{(X'_{qi} - X_{lsi})}E'_{di} + \frac{(X'_{qi} - X''_{qi})}{(X'_{qi} - X_{lsi})}\psi_{2qi} \tag{A.11}$$

$$\psi_{oi} = -X_{lsi}I_{0i} \tag{A.12}$$

where

$$(V_{Di} + jV_{Qi}) = (V_{di} + jV_{qi})e^{j(\delta_i - \pi/2)} \tag{A.13}$$

$$(I_{Di} + jI_{Qi}) = (I_{di} + jI_{qi})e^{j(\delta_i - \pi/2)} \tag{A.14}$$

$$(\psi_{Di} + j\psi_{Qi}) = (\psi_{di} + j\psi_{qi})e^{j(\delta_i - \pi/2)} \tag{A.15}$$

If T''_{d0i} and T''_{q0i} are sufficiently small, the first approximation of the fast damper windings is found by setting them equal to zero. In this way it is possible to eliminate the damper winding dynamics ψ_{1di} and ψ_{2qi} from the complete model. By doing this in (A.5) and (A.7) we have

$$0 = -\psi_{1di} + E'_{qi} - (X'_{di} - X_{lsi})I_{di} \tag{A.16}$$

$$0 = -\psi_{2qi} - E'_{di} - (X'_{qi} - X_{lsi})I_{qi} \tag{A.17}$$

Substituting (A.16) and (A.17) in (A.10) and (A.11), respectively, results in

$$\psi_{di} = E'_{qi} - X'_{di} I_{di} \tag{A.18}$$

$$\psi_{qi} = -E'_{di} - X'_{qi} I_{qi} \tag{A.19}$$

By substituting (A.16) and (A.17) in (A.4) and (A.6), respectively the internal voltages equations (2.2) and (2.3) are obtained. Besides, by using (A.18) and (A.19) in (A.9) Eq. (2.5) is obtained. Thus, the Two-Axis generator model without controls is determined by the equations (2.2)-(2.5).

Now by neglecting the stator transients, the equations (A.1) and (A.2) are

$$0 = R_{si} I_{Di} + \psi_{Qi} + V_{Di} \tag{A.20}$$

$$0 = R_{si} I_{Qi} - \psi_{Di} + V_{Qi} \tag{A.21}$$

By using the expressions (A.13)-(A.15) in (A.20) and (A.21) and converting to the complex form, we obtain the expression (2.8) associated with the dynamic circuit of the Two-Axis generator model shown in Figure 2.2.

A.2 Stator voltages and currents in coordinates $dq0$

The balanced set of scaled sinusoidal voltages and currents of the stator are [Sauer and Pai, 98]

$$V_a = \sqrt{2} V_s cos(\omega_0 t + \theta_s) \tag{A.22}$$

$$V_b = \sqrt{2} V_s cos(\omega_0 t + \theta_s - 2\pi/3) \tag{A.23}$$

$$V_c = \sqrt{2} V_s cos(\omega_0 t + \theta_s + 2\pi/3) \tag{A.24}$$

$$I_a = \sqrt{2} I_s cos(\omega_0 t + \phi_s) \tag{A.25}$$

$$I_b = \sqrt{2} I_s cos(\omega_0 t + \phi_s - 2\pi/3) \tag{A.26}$$

$$I_c = \sqrt{2} I_s cos(\omega_0 t + \phi_s + 2\pi/3) \tag{A.27}$$

By applying the Park's transformation to the sinusoidal voltages and currents (A.22)-(A.27), we have

$$V_d = V_s sin\left(\frac{P}{2}\theta_{shaft} - \omega_0 t - \theta_s\right) \tag{A.28}$$

$$V_q = V_s cos\left(\frac{P}{2}\theta_{shaft} - \omega_0 t - \theta_s\right) \tag{A.29}$$

$$V_0 = 0 \tag{A.30}$$

$$I_d = I_s sin\left(\frac{P}{2}\theta_{shaft} - \omega_0 t - \phi_s\right) \tag{A.31}$$

$$I_q = I_s cos\left(\frac{P}{2}\theta_{shaft} - \omega_0 t - \phi_s\right) \tag{A.32}$$

$$I_0 = 0 \tag{A.33}$$

where $\theta_{shaft}$is the mechanical angle between the magnetic $q-$axis and one stator phase used as reference. The rotor angle in electrical radians is defined as $\delta = \frac{p}{2}\theta_{shaft} - \omega_0 t$, which is constant for constant shaft speed.

Substituting the defined rotor angle δ in the expressions (A.28)-(A.29) and (A.31)-(A.32) results in

$$V_d = V_s sin(\delta - \theta_s) \tag{A.34}$$

$$V_q = V_s cos(\delta - \theta_s) \tag{A.35}$$

$$I_d = I_s sin(\delta - \phi_s) \tag{A.36}$$

$$I_q = I_s cos(\delta - \phi_s) \tag{A.37}$$

Expressing (A.34) and (A.35) in complex form we obtain the following expressions for the voltages terminals:

$$(V_d + jV_q) = V_s\left(sin(\delta - \theta_s) + jcos(\delta - \theta_s)\right) \tag{A.38}$$

$$(V_d + jV_q)e^{j(\delta - \pi/2)} = V_s e^{j\theta_s} \tag{A.39}$$

In the same way (A.36) and (A.37) converted to complex form, the expressions for the current injections at terminals are

$$(I_d + jI_q) = I_s\left(sin(\delta - \phi_s) + jcos(\delta - \phi_s)\right) \tag{A.40}$$

$$(I_d + jI_q)e^{j(\delta - \pi/2)} = I_s e^{j\phi_s} \tag{A.41}$$

The complex power injection at generator terminals is as follows

$$P_{Gi} + jQ_{Gi} = V_s e^{j\theta_s}(I_{di} - jI_{qi})e^{-j(\delta_i - \pi/2)} \tag{A.42}$$

Separating in two real equations we have

$$P_{Gi} = I_{di}V_i sin(\delta_i - \theta_i) + I_{qi}V_i cos(\delta_i - \theta_i) \tag{A.43}$$

$$Q_{Gi} = I_{di}V_i cos(\delta_i - \theta_i) - I_{qi}V_i sin(\delta_i - \theta_i) \tag{A.44}$$

Appendix B

FACTS MODELS

B.1 Static Var Compensator

The block diagram of the SVC controller [Padiyar and Varma, 91] is as follows:

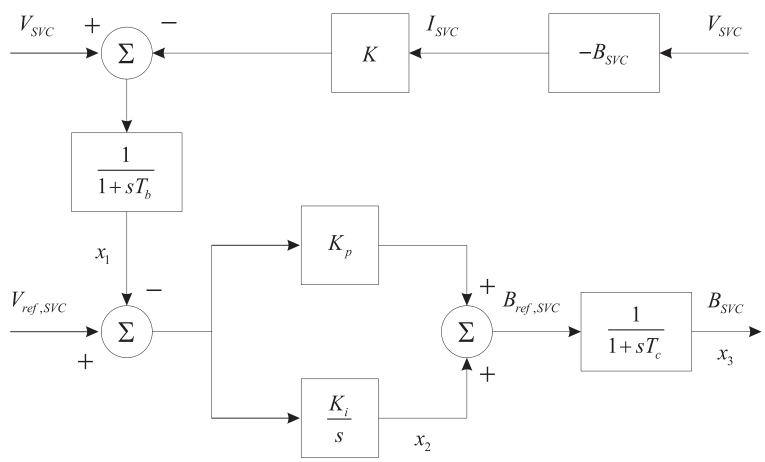

Figure B.1: SVC block diagram.

The nonlinear state equations of the SVC [Padiyar and Varma, 91] are

$$\dot{x}_1 = \frac{1}{T_b}\left(V_{SVC}(1 - Kx_3) - x_1\right) \tag{B.1}$$

$$\dot{x}_2 = K_i(V_{ref,SVC} - x_1) \tag{B.2}$$

$$\dot{x}_3 = \frac{1}{T_c}\left(x_2 + K_p(V_{ref,SVC} - x_1) - x_3\right) \tag{B.3}$$

$$Q_{SVC} = V_{SVC}^2 x_3 \tag{B.4}$$

B.2 Thyristor-Controlled Series Compensator

The block diagram of the TCSC controller [Padiyar and Rao, 95] is as follows:

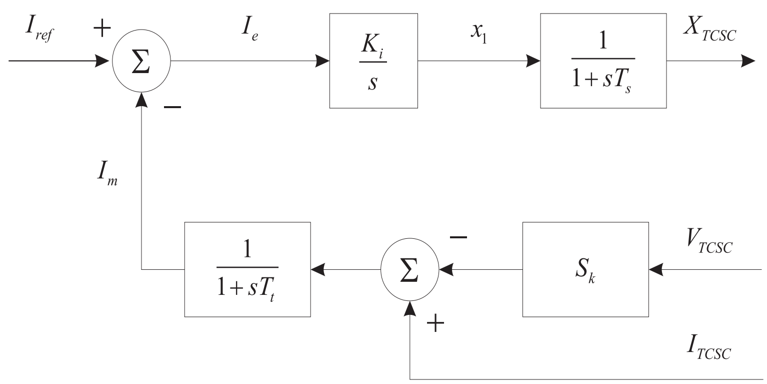

Figure B.2: TCSC block diagram.

The nonlinear state equations of the TCSC [Padiyar and Rao, 95] are

$$\dot{I}_m = \frac{1}{T_t}\left[\sqrt{V_i^2 + V_j^2 - 2V_iV_jcos(\theta_i - \theta_j)}\left(\frac{1}{|X_{TCSC}|} - S_k\right) - I_m\right] \tag{B.5}$$

$$\dot{x_1} = K_i(I_{ref} - I_m) \tag{B.6}$$

$$\dot{X}_{TCSC} = \frac{1}{T_s}(x_1 - X_{TCSC}) \tag{B.7}$$

Appendix C

WSCC SYSTEM DATA (9-buses, 3-generators)

The diagram and data of the WSCC power system were taken from [Sauer and Pai, 98].

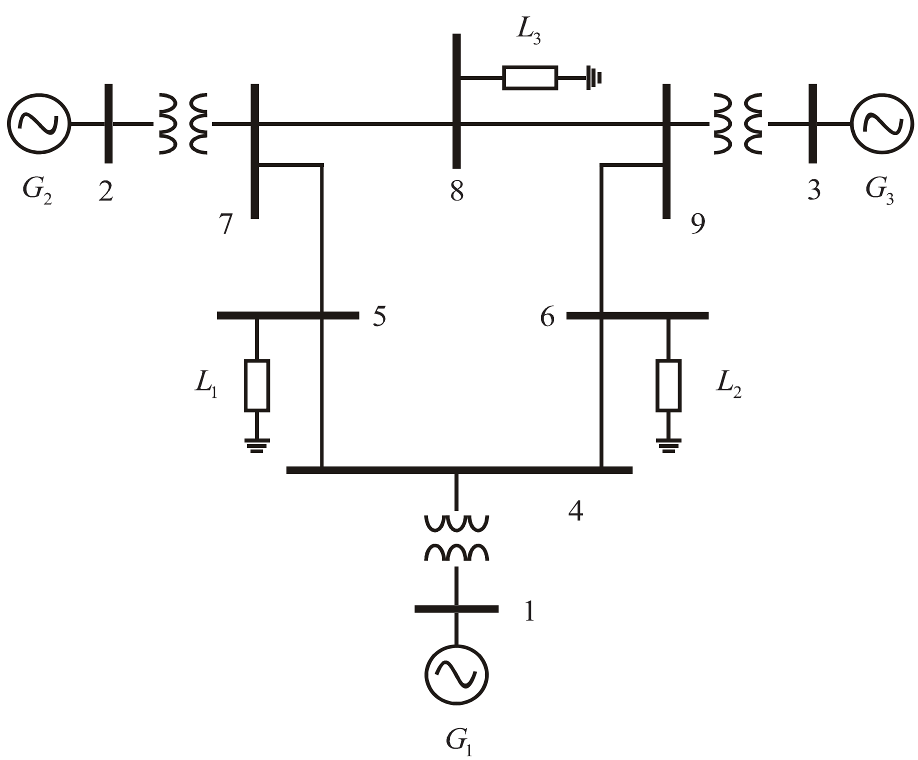

Figure C.1: WSCC power system.

Table C.1: Line parameters.

Nodes		$\boldsymbol{R}$(pu)	$\boldsymbol{X}$(pu)	$\boldsymbol{B}/2$(pu)	Nodes		$\boldsymbol{R}$(pu)	$\boldsymbol{X}$(pu)	$\boldsymbol{B}/2$(pu)
7	8	0.0085	0.0720	0.149	9	6	0.039	0.1700	0.358
8	9	0.0119	0.1008	0.209	5	4	0.010	0.085	0.176
7	5	0.032	0.161	0.306	6	4	0.017	0.092	0.158

Table C.2: Transformer parameters.

Nodes		$\boldsymbol{R}_s$(pu)	$\boldsymbol{X}_s$(pu)	*Tap:* T_v	*Tap:* U_v
2	7	0.0	0.0625	1.0	1.0
1	4	0.0	0.0576	1.0	1.0
3	9	0.0	0.0586	1.0	1.0

Table C.3: Load parameters.

Nodes	$\boldsymbol{P}$(Mw)	$\boldsymbol{Q}$(Mw)
8	100	35
6	90	30
5	125	50

Table C.4: Generator parameters.

Node	$\boldsymbol{X}_d$ (pu)	$\boldsymbol{X}_d^{'}$ (pu)	$\boldsymbol{T}_{d0}^{'}$ (s)	$\boldsymbol{X}_q$ (pu)	$\boldsymbol{X}_q^{'}$ (pu)	$\boldsymbol{T}_{q0}^{'}$ (s)	$\boldsymbol{H}$ (Mw·s)	$\boldsymbol{D}$ (pu)
2	0.8958	0.1198	6.0	0.8645	0.1969	0.535	640	0.0068
3	1.3125	0.1813	5.89	1.2578	0.2500	0.6	301	0.0048
1	0.1460	0.0608	8.96	0.0969	0.0969	0.31	2364	0.01254

Table C.5: Exciter parameters.

Node	$\boldsymbol{K}_A$	$\boldsymbol{T}_A$(s)
2	20	0.2
3	20	0.2
1	20	0.2

Appendix D

NEW ENGLAND SYSTEM DATA (39-buses, 10-generators)

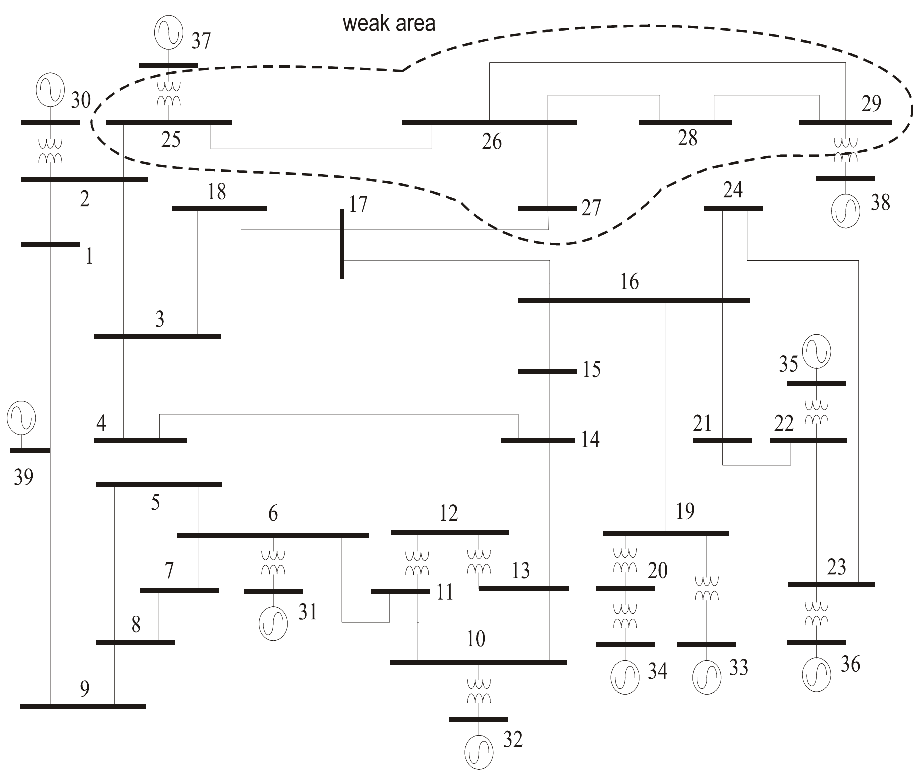

Figure D.1: New England power system.

Table D.1: Transmission line parameters.

Nodes		$\boldsymbol{R}$(pu)	$\boldsymbol{X}$(pu)	$\boldsymbol{B}/2$(pu)	Nodes		$\boldsymbol{R}$(pu)	$\boldsymbol{X}$(pu)	$\boldsymbol{B}/2$(pu)
1	2	0.0035	0.0411	0.6987	13	14	0.0009	0.0101	0.1723
1	39	0.0010	0.0250	0.7500	14	15	0.0018	0.0217	0.3660
2	3	0.0013	0.0151	0.2572	15	16	0.0009	0.0094	0.1710
2	25	0.0070	0.0086	0.1460	16	17	0.0007	0.0089	0.1342
3	4	0.0013	0.0213	0.2214	16	19	0.0016	0.0195	0.3040
3	18	0.0011	0.0133	0.2138	16	21	0.0008	0.0135	0.2548
4	5	0.0008	0.0128	0.1342	16	24	0.0003	0.0059	0.0680
4	14	0.0008	0.0129	0.1382	17	18	0.0007	0.0082	0.1319
5	8	0.0008	0.0112	0.1476	17	27	0.0013	0.0173	0.3216
6	5	0.0002	0.0026	0.0434	21	22	0.0008	0.0140	0.2565
6	7	0.0006	0.0092	0.1130	22	23	0.0006	0.0096	0.1846
6	11	0.0007	0.0082	0.1389	23	24	0.0022	0.0350	0.3610
7	8	0.0004	0.0046	0.0780	25	26	0.0032	0.0323	0.5130
8	9	0.0023	0.0363	0.3804	26	27	0.0014	0.0147	0.2396
9	39	0.0010	0.0250	1.2000	26	28	0.0043	0.0474	0.7802
10	11	0.0004	0.0043	0.0729	26	29	0.0057	0.0625	1.0290
10	13	0.0004	0.0043	0.0729	28	29	0.0014	0.0151	0.2490

Table D.2: Transformer parameters.

Nodes		$\boldsymbol{R}_s$(pu)	$\boldsymbol{X}_s$(pu)	*Tap* T_v	*Tap* U_v	Nodes		$\boldsymbol{R}_s$(pu)	$\boldsymbol{X}_s$(pu)	*Tap* T_v	*Tap* U_v
2	30	0.0	0.0181	1.025	1.0	19	33	0.0007	0.0142	1.070	1.0
6	31	0.0	0.0250	1.070	1.0	20	34	0.0009	0.0180	1.009	1.0
10	32	0.0	0.0200	1.070	1.0	22	35	0.0	0.0143	1.025	1.0
12	11	0.0016	0.0435	1.006	1.0	23	36	0.0005	0.0272	1.0	1.0
12	13	0.0016	0.0435	1.006	1.0	25	37	0.0006	0.0232	1.025	1.0
19	20	0.0007	0.0138	1.060	1.0	29	38	0.0008	0.0156	1.025	1.0

Table D.3: Load parameters.

Node	***P***(Mw)	***Q***(Mw)	**Node**	***P***(Mw)	***Q***(Mw)	**Node**	***P***(Mw)	***Q***(Mw)
3	322.0	2.4	16	329.0	32.3	25	224.0	47.2
4	500.0	184.0	18	158.0	30.0	26	139.0	17.0
7	233.8	84.0	20	628.0	103.0	27	281.0	75.5
8	522.0	176.0	21	274.0	115.0	28	206.0	27.6
12	8.5	88.0	23	247.5	84.6	29	283.5	26.9
15	320.0	153.0	24	308.6	-92.2	39	1104.0	250.0

Table D.4: Generator parameters.

Node	$\boldsymbol{X}_d$ (pu)	$\boldsymbol{X}_d^{'}$ (pu)	$\boldsymbol{T}_{d0}^{'}$ (s)	$\boldsymbol{X}_q$ (pu)	$\boldsymbol{X}_q^{'}$ (pu)	$\boldsymbol{T}_{q0}^{'}$ (s)	$\boldsymbol{H}$ (Mw·s)	$\boldsymbol{D}$ (pu)
32	0.2495	0.0531	5.7	0.2370	0.0531	1.50	7060	0.0
33	0.2620	0.0436	5.69	0.2580	0.0436	1.50	5720	0.0
34	0.6700	0.1320	5.4	0.6200	0.1320	0.44	5200	0.0
35	0.2540	0.0500	7.3	0.2410	0.0500	0.40	6960	0.0
36	0.2950	0.0490	5.66	0.2920	0.0490	1.5	5280	0.0
37	0.2900	0.0570	6.7	0.2800	0.0570	0.41	4860	0.0
38	0.2106	0.0570	4.79	0.2050	0.0570	1.96	6900	0.0
30	0.1000	0.0310	10.2	0.0690	0.0310	1.50	8400	0.0
31	0.2950	0.0697	6.56	0.2820	0.1700	1.50	6060	0.0
39	0.0200	0.0060	7.0	0.0190	0.0080	0.70	100000	0.0

Table D.5: Exciter parameters.

Node	$\boldsymbol{K}_A$	$\boldsymbol{T}_A$(s)	**Node**	$\boldsymbol{K}_A$	$\boldsymbol{T}_A$(s)
32	5	0.06	37	5	0.02
33	5	0.06	38	5	0.02
34	40	0.02	30	5	0.06
35	5	0.02	31	6.2	0.05
36	40	0.02	39	40	0.02

Appendix E

MEXICAN SYSTEM DATA (190-buses, 46-generators)

The Mexican Interconnected System (MIS) covers a vast geographical area stretching interconnections from the southern border with Central America to its northern border with the USA. The MIS consists of eight operating regions, where 7 of these regional systems, referred to as north-western (NW), northern (N),north-eastern (NE), western (W), central (C), south-eastern (SE) and peninsular (P) systems, are interconnected to operate as a multi-area system as shown in the schematic diagram Figure E.1 [Messina et al., 02], and the system components are interconnected as shown in the unifilar diagram Figure E.2. Main loads are located in the largest metropolitan areas of the country, namely Mexico City in the central system, Guadalajara city in the western system, and Monterrey city in the north-eastern system. Under normal operating conditions, the power flows from the north to the south systems, from the peninsular to the south-eastern system and from the south to the central system, respectively. However, given the longitudinal structure of these sparsely connected transmission paths, voltage and transient stability problems are acute and of prime importance.

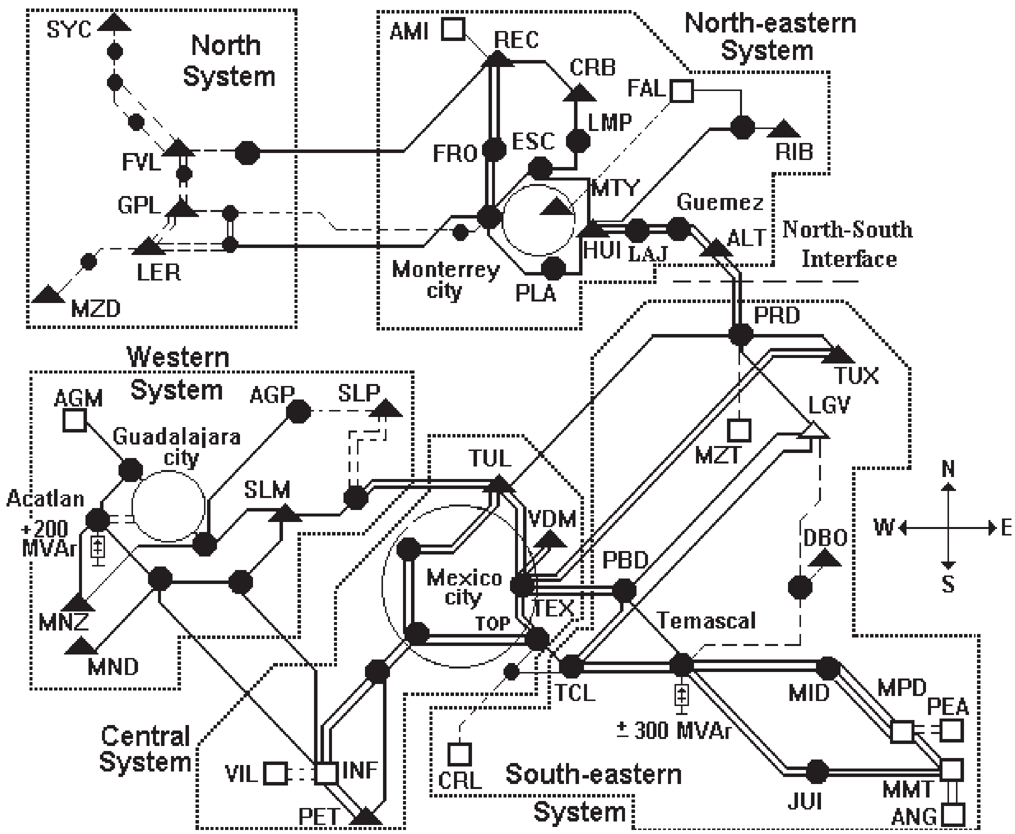

Figure E.1: Schematic diagram of the Mexican interconnected power system.

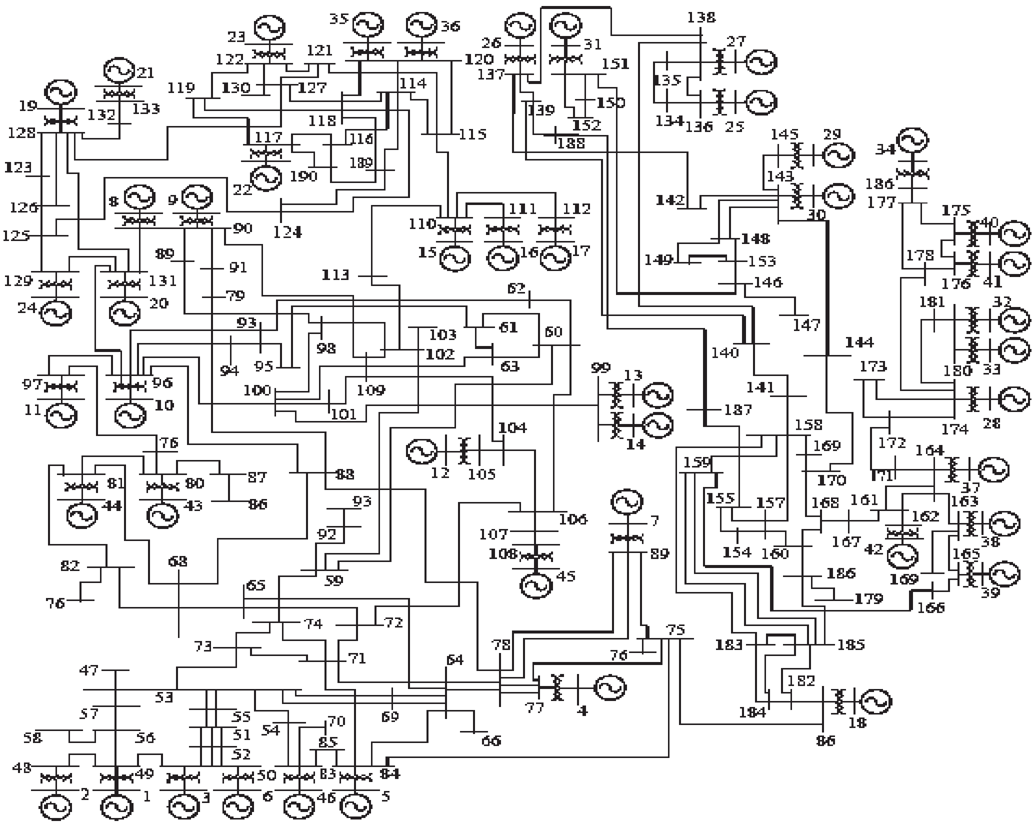

Figure E.2: Mexican power system.